MANDELA MINING PRECINCT
MINDS FOR MINES

# TECHNICAL SERVICES OPTIMISATION

## MMS22WP1: Rock Engineering Pillar Design Phase III

### Optimised K-values for the Hedley and Grant pillar strength formula

**Final Report**

ENTERPRISES
University of Pretoria


| | |
|---|---|
| Research agency: | Enterprises University of Pretoria |
| Project Lead: | Dr. Francois Malan |
| Programme Manager: | Martin Pretorius |
| Date: | March 2024 |

# TABLE OF CONTENTS

# 1 EXECUTIVE SUMMARY

Based on the previous pillar study (MMS22WP1 - Phase II), it was concluded that significant uncertainty exists in terms of the best equation to describe pillar strength behaviour in hard rock bord and pillar mines. This can only be resolved by conducting additional laboratory testing and underground observations of pillar behaviour. Both the power-law and linear formulae, and variations of these, are widely used in other countries. It appears that the problem of finding a "universal" strength equation is caused by the variability in the measured strength of pillars, both in the laboratory and in actual mines. It is difficult to fit strength equations to the measured results because of the wide scatter of the data. Also, of concern is that a different formula is typically developed for every new study on pillar strength. This was highlighted by a re-analysis of the PlatMine pillar database done for this project and a new formula was proposed by the sub-contractor. In this case the problem is most likely caused by the limited range of pillar heights in the database. Based on these considerations, a different approach in terms of future research was proposed. To make a meaningful contribution in a short period of time, Phase III of the project focussed on historic and new back analyses of bord and pillar layouts in South Africa to obtain improved estimates of pillar strength. Based on the Phase II project, the exponents of the Hedley and Grant formula appears to be a reasonable approximation to account for variations in pillar width and height and this formula was retained for this study. This somewhat crude approach can be critised, but no alternative strength formula exists that is well proven. Although advocated by some consultants and researchers, numerical modelling approaches are also considered problematic owing to the many assumptions made in these codes and the difficulty to select and calibrate an appropriate constitutive failure model.

A review of historic studies available to the project team members were conducted. New pillar back analyses were also done to expand the database compiled from the historic data. Sites were selected that added the most value to the project within the constraints imposed by the allocated budget. A further back-analysis of the Merensky Reef pillar strength at Styldrift Mine was conducted. As a second case study, a LG6/LG6A bord and pillar section was also analysed as little historic data is available on this reef type. Additional work was done on a UG2 site were pillar sliping was done to determine pillar strength. Manganese pillars were also studied as it proved to be valuable to illustrate the effect of rock mass rating on pillar strength.

The following are the key findings from the study:

- The pillars are typically substantially stronger than the historic assumption when using $\boldsymbol{K} = \frac{1}{3}\boldsymbol{UCS}$ in the Hedley and Grant pillar strength formulation (but only if there are no weak clay layers and the rock is competent). This conservative assumption should therefore not be used for new projects unless there is convincing evidence that this approach will indeed predict the actual pillar strength.
- From the case studies conducted in the Rustenburg area, it was found that the strength of Merensky Reef pillars can be approximated by the Hedley and Grant formulation with a K-value of 90 MPa.
- For the UG2 pillars studied in the Eastern Bushveld, the strength can be approximated by the Hedley and Grant formulation with a K-value of 75 MPa.
- The strength of the LG6/LG6a pillars can be approximated by using at least K = 70 MPa in the Hedley and Grant formulation.

- The rock mass rating affects the pillar strength and the strengths given above cannot be used for pillars in areas with poor ground conditions.
- If there is a weak clay layer in the pillars, this substantially reduces the pillar strength and a realistic value for the strength, when using the Hedley and Grant formula, will be obtained for a K-value of 6 to 10 MPa.

A key finding of this study is that the rock mass rating and the nature of the joint sets affect the pillar strength. Although this was already published in the 1990s with the proposal to use the design rock mass strength (DRMS) as the K-value, evidence of different pillar strengths in different geotechnical areas in a particular mine was never published. The current study highlighted this aspect from back analyses done at Styldrift Mine. A study of manganese pillars in areas with different rock mass ratings also supported this finding. A discussion on the use of a "modified" DRMS as an estimate of the K-value in the Hedley and Grant formula is included in the report. The original assumptions made by Laubscher (1990) need to be carefully assessed to ensure that the estimated K-value is not too conservative. Another key finding from this study is that the back-calculated K-values should be used with caution in areas with distinctly different rock mass ratings. A K-value determined for one area may not guarantee stable pillars in another area where the rock mass rating is much lower. A new approach to pillar design is required as historically only one pillar design, using a constant K-value, was typically adopted for an entire mine.

Revised pillar strength calibrations should be tested in trial sections with suitable instrumentation and monitoring before it is adopted at any mine. The site of a trial site needs to be carefully selected. Ideally it should be in an isolated area, or between regional pillars, that can arrest a potential collapse.

One method to test the estimated pillar strength is to mine a new mining section with the experimental pillar dimensions. Numerical modelling is described in the report that gives an indication of the size of the trial section required. For the example given in the report of a square geometry containing 100 pillars, the peak stress in the centre of the layout is only 93% of the tributary area theory value.

A second viable option for a trial area is to do pillar sliping in an old bord and pillar mining section. A key question to address is what reduction in pillar size is required to test for a particular K-value when doing the subsequent back analysis of the area. A mathematical and numerical analysis is described in the report to assist in calculating the required pillar size reduction. Pillar sliping will be associated with an increase in bord spans and work should be done to ensure that the larger spans can be safely supported and that it will remain stable during the duration of the trial.

# 2 AIM OF RESEARCH PROGRAMME

This work is an extension of the project *MMS22WP1 Developing an effective pillar design methodology for mechanised mining*. The objective of this previous study was to determine the most appropriate type of pillar strength formula to use when designing bord and pillar layouts. A key aspect to clarify before commencing with the expensive laboratory and underground experimental work was to determine the most appropriate type of pillar strength formula to use. The type of formula needs to be decided upon before it can be calibrated for different areas.

It was concluded from the previous study that significant uncertainty still exists in terms of the best equation to predict pillar strength and this can only be resolved by conducting further laboratory testing and underground observations of pillar behaviour. Both the power-law and linear formulae, and variations of these, are widely used. It appears that the problem of finding a “universal” strength equation is caused by the variability in the measured strength of pillars, both in the laboratory and in actual mines. It is difficult to fit strength equations to the results because of the wide scatter of the data. This is a significant finding and this improved understanding must guide future research. Based on these many considerations, a different approach in terms of future research was proposed. To make a meaningful contribution in a short period of time, it is proposed that the work focus on back analyses of carefully selected bord and pillar layouts to estimate pillar strength. This data was used to calibrate the K-value for the Hedley and Grant strength formula for different reef types. The use of this formula is motivated in Section 4.1.

# 3 METHODOLOGY USED

The methodology of the project consisted of several components. The first step was to collate all the historic information on pillar strength in the South African mines available to the project team members. A limited number of additional new sites were analysed as a second step and additional pillar strength values were calculated. A summary of the estimated pillar strengths, based on these two steps, was compiled for this project. Some work was also done to give guidelines in terms of establishing trial mining sites to test the revised pillar strength. The historic PlatMine pillar database was re-analysed to study the question regarding the volumetric strengthening effect of pillars predicted by the original PlatMine formulae.

# 4 RESEARCH FINDINGS

The following sections give an overview of the important information collected during this project. All relevant material and many photographs were included in the text to ensure that the information is preserved in a reference document that can be easily accessed.

## 4.1 *Use of the Hedley and Grant pillar strength formula*

This report should be read in conjunction with the 2023 report (*MMS22WP1: Developing an effective pillar design methodology for mechanised mining, 13 March 2023*). This gives an extensive overview why it was decided to proceed with calibration of the Hedley and Grant power-law strength formula. Without this background, it may be argued that a linear formula or a power-law formula with different exponents, or even a completely different equation, should be used. Some consultants and researchers also favour a numerical modelling approach rather than the empirical pillar strength equations. It should, however, be considered that numerical modelling approaches are potentially flawed as it is not always known what the most appropriate constitutive failure law is to use for the type of pillar material encountered. Calibration of the complex constitutive models is extremely difficult and perhaps even impossible. Ironically, to calibrate the parameters of the constitutive models, such as the Hoek and Brown failure model, empirical equations are often used. These empirical equations may not be applicable to all rock types and this negates the value of numerical modelling. The complexity of the numerical models is sometimes used to motivate this "superior" approach of designing pillars. This is not the approach followed in this current study and a short summary of the 2023 report is given below to motivate the use of a simple empirical power-law formula.

The objective of the 2023 study was to determine the most appropriate type of pillar strength formula to use when designing bord and pillar layouts. A careful study of the historical motivation for the different types of pillar strength formulae was conducted. The power-law strength formulae, made famous by Salamon and Munro (1967), were inspired by laboratory and underground experiments in the 1940s and 1950s. These indicated that the strengths, or "resistance to crush", of square pillars of the same height vary as the square root of their widths. The strengths of pillars of the same width also vary in inverse ratio to their height. This was generalised by Salamon in a power-law formula with the familiar exponents $\alpha$ and $\beta$. These exponents were calibrated using a database of failed and intact pillars. For the hard rock strength formula, Hedley and Grant (1972) used the same coal work in the 1940s and 1950s, as well as Salamon's paper to motivate the use of a power-law equation. Bieniawski (1968) conducted extensive underground experiments on different-sized coal specimens. An important finding of this study was that there was no change in strength once a specimen size of 1.5 m was reached. Based on this work, he proposed the simpler linear pillar strength formula. Martin and Maybee (2000) list the hard rock pillar formulae that were developed in later years based on observed pillar failures. Of significance is that these take the form of either a power- or linear-type equation and that both equations have been used to predict the pillar strength for a wide range of pillar shapes and rock mass strengths. No conclusive evidence could be found in this previous study that indicate which type of formula is more applicable. Laboratory experiments on different sizes cubes of Merensky Reef, UG2 and other chromitites will have to be done to determine if the pillar strength is better approximated by a linear or a power-law formulation. As a cautionary note, however, these experiments are notoriously difficult to conduct and the typical variability in strength results may not provide a clear answer.

A literature study of the effect of cube specimen size on the compressive strength of rock in the laboratory was conducted. All the studies indicated that laboratory rock strength decreases with increasing specimen size. This behaviour can be best described with a power-law, which includes the cube length as the controlling parameter. The exponent of this law has the typical value of ≈ -½. The drawback of this model is that it predicts that the pillar strength will eventually completely vanish for very large cube sizes. This is considered unreasonable and the model is probably only relevant to laboratory-sized specimens. Bieniawski (1968) attempted to circumvent this problem by describing the strength after a critical size with a linear strength function.

In summary, it was found that there is still uncertainty in terms of the most appropriate formula and both the power-law and linear formulae, and variations of these, are widely used. Based on this uncertainty and the knowledge that a power-law strength formula has been successfully used in the coal industry for decades, a simplified approach for the research for Phase III of the project was proposed. This was to focus on the back analyses of carefully selected bord and pillar layouts to calibrate the Hedley and Grant formula.

## 4.2 *Historic pillar back-analyses*

Several case studies analysed by members of the project team are described below. Some of these were done more than 15 years ago. As some of the mines changed owners, and the original persons who commissioned this work are no longer available, the mines are kept anonymous. As mentioned above, the work is replicated below as it is not easily accessible as a single source document.

### 4.2.1 Mine A - A study of the Merensky pillar strength at Styldrift Mine

An earlier report (Malan, 2021) describes a numerical modelling study of the pillar layout at Styldrift Mine. The mine is a mechanised operation using a bord and pillar layout to exploit the Merensky Reef horizon. Significant spalling of the in-panel pillars occurs and it was therefore a good case study to examine pillar strength. The regional layout of mine at the time of the study is illustrated in Figure 1.

Laboratory testing of the rock strengths were conducted by earlier workers and the results are presented in Table 1 (Le Bron and Malan, 2011). Reef samples were tested to verify the pillar strength assumptions made for the Styldrift layout. Note that for the Merensky Reef samples, UCS values of 99 MPa, 145 MPa, 127 MPa, 153 MPa, 159 MPa were obtained. This is an average of 137 MPa. Typically, very conservative pillar designs used a third of this value (46 MPa) for the K-value in the pillar strength formula. This is far too conservative. Interestingly, the 90 MPa derived below through back analysis is two-thirds of the average laboratory strength.

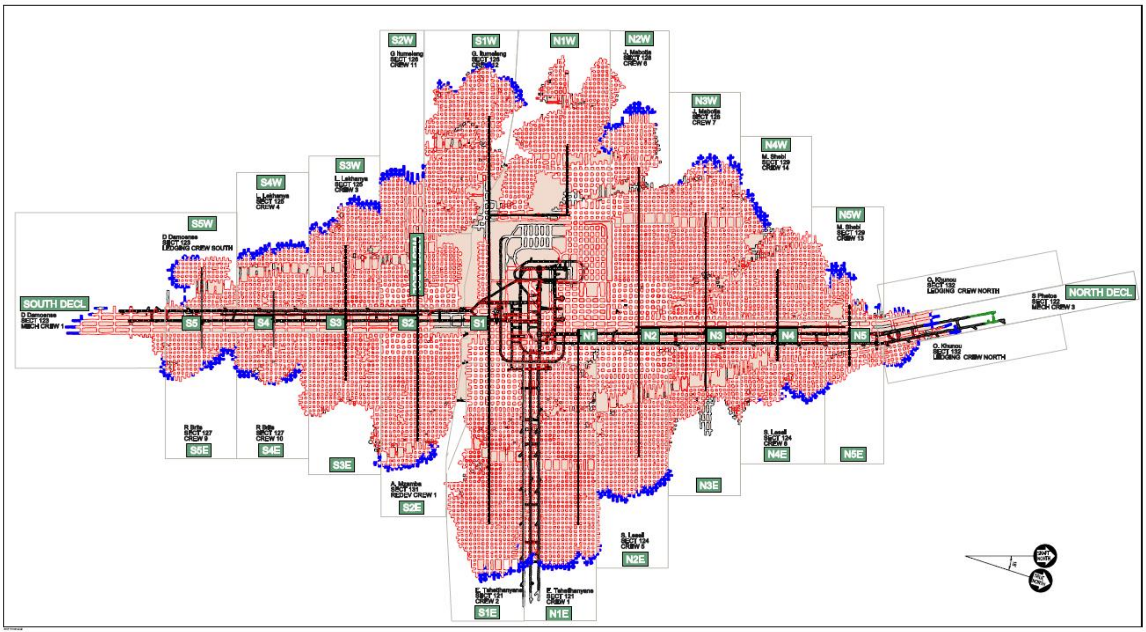


**Figure 1. Bord and pillar layout at Styldrift Mine in 2021**

**Table 1. Uniaxial compressive test results (after Le Bron and Malan, 2011)**

19-Jul-11

| SPECIMEN PARTICULARS | | | | SPECIMEN DIMENSIONS | | | | | SPECIMEN TEST RESULTS | | | | | | | | | |
|---|---|---|---|---|---|---|---|---|---|---|---|---|---|---|---|---|---|---|
| Rocklab Specimen No 4380- | Sample ID | Horizon & Position | Rock Type | Diameter mm | Height mm | Ratio of Height to Diameter | Mass g | Density g/cm³ | Failure Load kN | Strength (UCS) MPa | Tangent Elastic Modulus @ 50% UCS GPa | Secant Elastic Modulus @ 50% UCS GPa | Poisson's Ratio Tangent @ 50% UCS | Poisson's Ratio Secant @ 50% UCS | Linear Axial Strain at Failure mm/mm | Failure Code | Note |
| UCM-21 | 21 | | | 36.26 | 92.1 | 2.5 | 302.1 | 3.18 | 102.3 | 99.1 | 82.6 | 75.0 | 0.35 | 0.22 | 0.001380 | 2B | |
| UCM-22 | 22 | | | 47.30 | 84.0 | 1.8 | 466.8 | 3.16 | 254.0 | 144.6 | 104.0 | 100.0 | 0.28 | 0.23 | 0.001605 | XB | |
| UCM-23 | 23 | Merensky Reef | | 47.37 | 100.8 | 2.1 | 566.5 | 3.19 | 224.6 | 127.4 | 118.0 | 113.0 | 0.25 | 0.21 | 0.001219 | XA | |
| UCM-24 | 24 | | | 47.37 | 128.1 | 2.7 | 718.9 | 3.18 | 270.1 | 153.3 | 116.0 | 106.0 | 0.26 | 0.20 | 0.001679 | XA | |
| UCM-25 | 25 | | | 47.40 | 111.2 | 2.3 | 628.4 | 3.20 | 280.5 | 159.0 | 133.0 | 135.0 | 0.24 | 0.23 | 0.001230 | XB | |
| UCM-26 | 26 | | | 47.19 | 127.7 | 2.7 | 708.3 | 3.17 | 238.2 | 136.2 | 106.0 | 99.8 | 0.26 | 0.21 | 0.001562 | YA | |
| UCM-27 | 27 | | | 47.19 | 125.7 | 2.7 | 699.0 | 3.18 | 147.1 | 84.1 | 116.0 | 109.0 | 0.23 | 0.21 | 0.000745 | 2B | |
| UCM-28 | 28 | M Reef HW | | 47.17 | 127.7 | 2.7 | 710.9 | 3.19 | 271.5 | 155.4 | 124.0 | 122.0 | 0.28 | 0.23 | 0.001515 | XA | |
| UCM-29 | 29 | | | 47.38 | 128.3 | 2.7 | 689.5 | 3.05 | 296.1 | 167.9 | 84.1 | 58.9 | 0.40 | 0.18 | 0.002976 | XB | |
| UCM-30 | 30 | | | 47.37 | 126.0 | 2.7 | 671.9 | 3.03 | 275.0 | 156.0 | 86.3 | 68.2 | 0.40 | 0.19 | 0.002508 | XB | |
| UCM-31 | 31 | | | 47.78 | 109.9 | 2.3 | 797.4 | 4.05 | 89.2 | 49.8 | 66.3 | 51.6 | 0.21 | 0.16 | 0.001015 | 1B | |
| UCM-32 | 32 | | | 47.26 | 126.0 | 2.7 | 708.6 | 3.20 | 160.2 | 91.3 | 99.1 | 74.7 | 0.27 | 0.15 | 0.001175 | XA | |
| UCM-33 | 33 | UG2 | | 36.02 | 98.4 | 2.7 | 389.9 | 3.89 | 99.4 | 97.5 | 74.6 | 54.8 | 0.42 | 0.24 | 0.002006 | XA | |
| UCM-34 | 34 | | | 36.20 | 89.4 | 2.5 | 373.7 | 4.06 | 69.8 | 67.8 | 64.4 | 43.6 | 0.37 | 0.22 | 0.001375 | 1B | |
| UCM-35 | 35 | | | 36.05 | 100.0 | 2.8 | 356.4 | 3.49 | 124.5 | 122.0 | 78.5 | 64.3 | 0.45 | 0.23 | 0.002010 | XB | |
| UCM-36 | 36 | | | 47.68 | 126.0 | 2.6 | 745.6 | 3.31 | 143.7 | 80.5 | 70.0 | 58.7 | 0.27 | 0.17 | 0.001257 | 1B | |
| UCM-37 | 37 | | | 47.65 | 126.8 | 2.7 | 726.6 | 3.21 | 197.4 | 110.7 | 128.0 | 115.0 | 0.25 | 0.22 | 0.000930 | 2B | |
| UCM-38 | 38 | UG2 HW | | 47.63 | 123.7 | 2.6 | 703.0 | 3.19 | 187.2 | 105.1 | 109.0 | 104.0 | 0.27 | 0.23 | 0.001019 | 1B | |
| UCM-39 | 39 | | | 47.39 | 127.6 | 2.7 | 717.0 | 3.19 | 214.4 | 121.6 | 88.9 | 57.0 | 0.32 | 0.13 | 0.001944 | XB | |
| UCM-40 | 40 | | | 47.54 | 127.3 | 2.7 | 719.0 | 3.18 | 234.6 | 132.2 | 82.2 | 42.0 | 0.25 | 0.13 | 0.002783 | XB | |

The two areas used for the back analysis are shown in Figures 2 and 3. Six pillars were photographed in detail in this area and simulated in the models. These are numbered in red in Figures 2 and 3. As an example, photographs taken of pillar 1 are illustrated in Figure 4. From the underground visit, it was obvious that some of the smaller pillars are subjected to spalling (Figure 5).

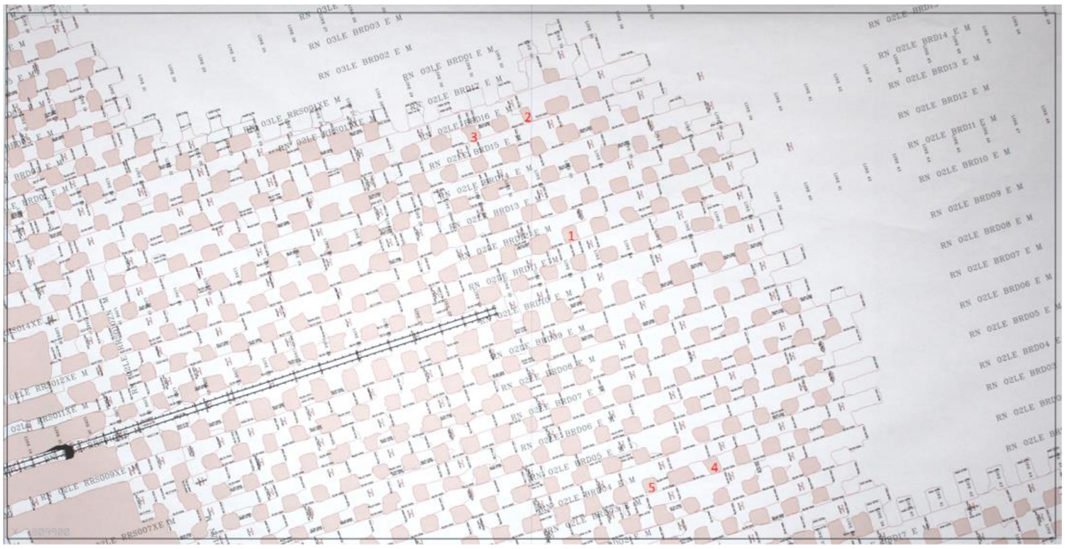


**Figure 2. Area (N2E) simulated at Styldrift Mine. The pillars numbered in red were studied in the numerical model**

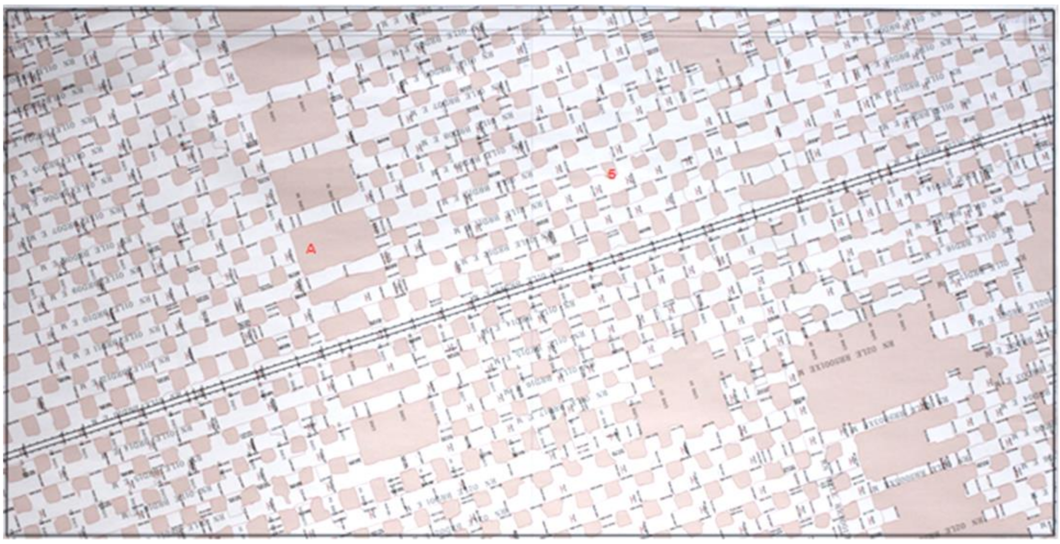

**Figure 3. Area (N1E) simulated at Styldrift Mine. The pillars labelled in red were studied in the numerical model**

**Figure 4. Photographs of Pillar 1 (see Figure 2 for the position of this pillar)**

**Figure 5. Extensive spalling seen for some of the pillars in Section N1E**

The TEXAN code was used to back analyse the layouts. To simplify the digitising of the outlines and the meshing procedure, the pillar outlines were approximated with straight line segments as illustrated in Figures 6 and 7.

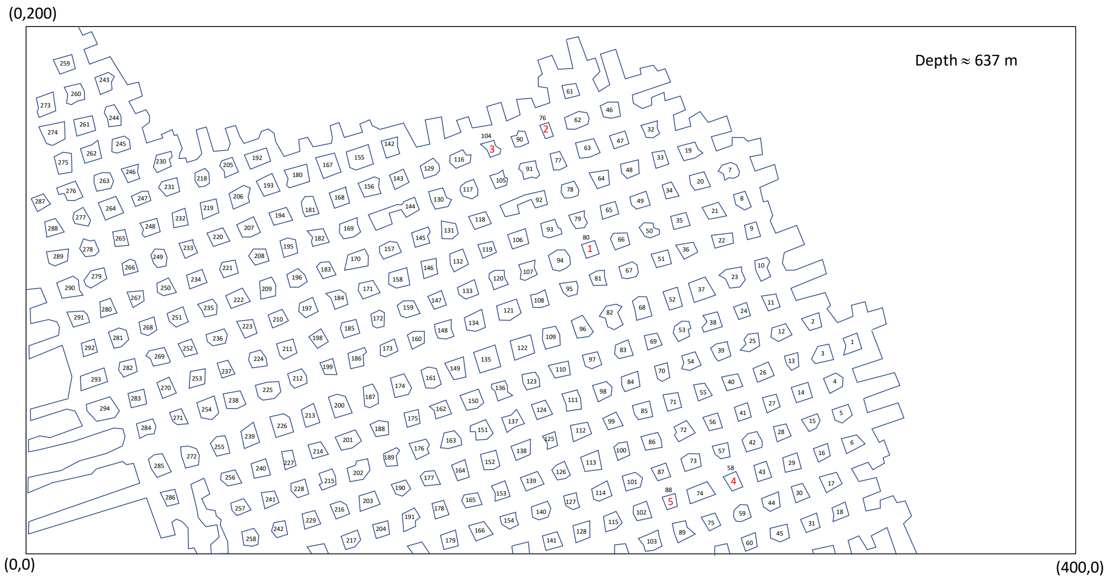


**Figure 6. Diagram illustrating the straight-line segments used to digitise the actual mining layout of N2E**

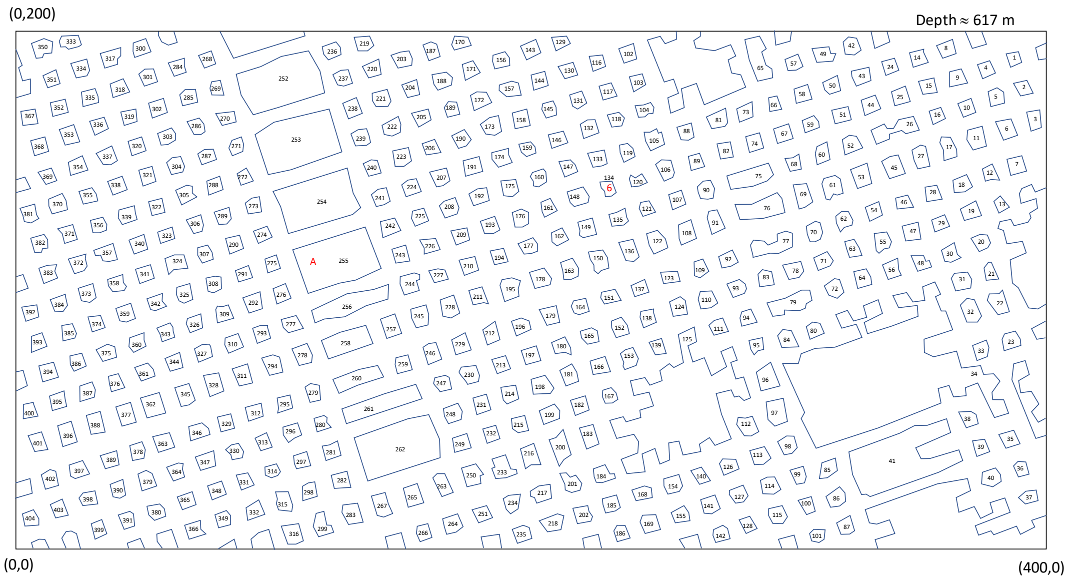


**Figure 7. Diagram illustrating the straight-line segments used to digitise the actual mining layout of N2E**

Although the problems with empirical strength formulae (such as Hedley and Grant) are well known, the simulated APS results were used to back-calculate K-values. This is done on the basis that the pillars simulated are still considered to be intact and have not failed. The spalling is nevertheless extensive for some of the pillars and the factor of safety is therefore probably close to 1 on these pillars. When substituting the simulated stress for the strength value in the Hedley and Grant formula, the K-value can be back calculated. This is illustrated in Table 2.

**Table 2. Back-calculation of K-values. This is done based on the assumption that the pillars are close to failure and therefore have a factor of safety of 1**

| Pillar number | Simulated APS (MPa) | Area ($m^2$) | Circum-ference (m) | Effective width (m) | Height (m) | K-value (MPa) |
|---|---|---|---|---|---|---|
| **Area N2E** | | | | | | |
| P58 (red 4) | 99.9 | 27.3 | 21.2 | 5.2 | 2.3 | 82.2 |
| P76 (red 2) | 114.4 | 16.9 | 17.0 | 4.0 | 2.3 | 107.1 |
| P80 (red 1) | 101.9 | 26.7 | 20.7 | 5.2 | 2.3 | 83.8 |
| P88 (red 5) | 100.5 | 22.4 | 19.0 | 4.7 | 2.3 | 86.4 |
| P104 (red 3) | 98.1 | 25.4 | 22.0 | 4.6 | 2.3 | 85.3 |
| **Area N1E** | | | | | | |
| P120 | 106.9 | 25.7 | 21.6 | 4.8 | 2.3 | 91.5 |
| P133 | 95.6 | 35.2 | 23.4 | 6.0 | 2.3 | 72.8 |
| P134 (red 6) | 110.9 | 26.8 | 21.3 | 5.0 | 2.3 | 92.3 |
| P135 | 98.8 | 34.2 | 21.3 | 6.4 | 2.3 | 72.8 |
| P136 | 89.6 | 43.2 | 25.8 | 6.7 | 2.3 | 64.7 |

From Table 2 it follows that a value of K = 90 MPa may be a good approximation of the strength for the Merensky Reef pillars in areas N1E and N2E at Styldrift Mine.

### 4.2.2 Mine B - A study of the Merensky pillar strength at a Rustenburg mine

This study was done in a mechanised mining area at a shaft in the Rustenburg area. Figure 8 illustrates the layout of the area visited. The in-panel pillars are designed as 6 m × 6 m pillars at a typical mining height of 2 m. The pillars were carefully scrutinised to ensure that the plan agrees with the shape of the pillars observed underground. Pillars A, B, C, D, E and F were measured (Figure 9) and photographed for use in a numerical modelling back analysis.

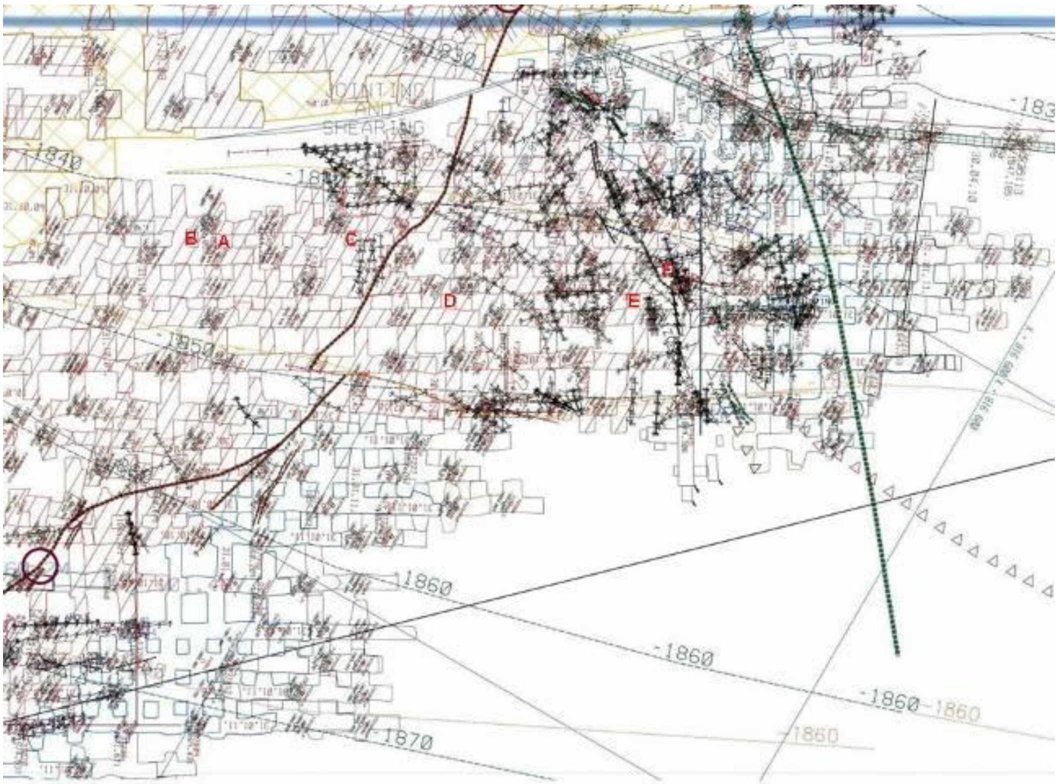


**Figure 8. Area used for the back-analysis. The pillars indicated with the red letters were chosen randomly and were studied in detail**

Despite the mining depth of approximately 1100 m, the pillars appeared to be in a reasonably good condition. Some spalling of the sidewalls could be observed on some of the pillars (but not all pillars) and this may be an indication that these pillars are loaded close to their peak strength. Examples of the pillar conditions are given in the Figures 10 to 21 below.

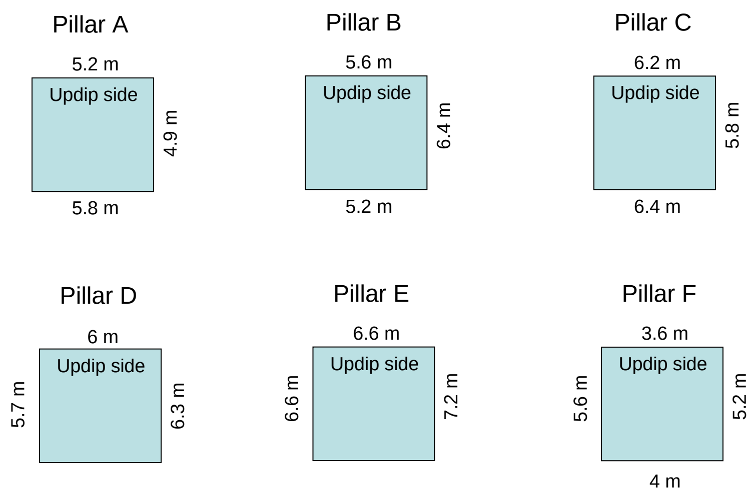


**Figure 9. Sizes of the pillars as measured underground. Note that pillars A and F are undersized**

**Figure 10. Spalling on the edge of pillar A**

**Figure 11. View of the other edges of pillar A. Less spalling was seen on these sides of the pillar**

**Figure 12. Views of the sides of pillar B. Less spalling was seen on this pillar compared to pillar A**

**Figure 13. View of one of the corners of pillar B. Some spalling could be seen in this corner and it appears to be caused by the opening of pre-existing joints**

**Figure 14. View of one of the corners of pillar C. Some minor spalling could be seen on this corner**

**Figure 15. View of the sidewalls of pillar C**

**Figure 16. View of the sidewalls of pillar D**

**Figure 17. View of the sidewalls of pillar D**

**Figure 18. View of the sidewalls of pillar E**

**Figure 19. View of the sidewalls of pillar E**

**Figure 20. View of the sidewalls of pillar F**

**Figure 21. View of a sidewalls of pillar F. One of the corners is shown on the right**

Owing to the distribution of the PGM metals, the pillars are cut in such a way that the upper 300 mm of the pillar comprises pyroxenite (Merensky Reef), below it is a prominent chrome stringer and the rest of the pillar consists of anorthosite. The pillar therefore has a multi-material composition. It was observed that the contact with the chrome stringer is a weak parting and this contributes to the spalling.

An examination of newly cut pillars close to the working faces indicates that the amount of spalling is low on these pillars (Figure 22) owing to the lower stresses (proximity to the abutment). The spalling seen in the back area is therefore stress induced and not caused by blast damage. There is a visual indication of stress increase on the pillars as they move into the back area. The weak parting caused by the chrome layer facilitates the spalling process (Figures 23 and 24) and if it was not for this layer, the pillars would have been stronger.

**Figure 22. Examples of pillars adjacent to the face. Very little spalling was seen on these pillars**

**Figure 23. A photograph illustrating the chrome stringer at the bottom of the pyroxenite. Note the weak parting between the pyroxenite and chrome**

**Figure 24. Signs of possible time-dependent spalling. Note the original position of the edge of the pillar and by how much the anorthosite and chrome stringer has scaled out**

To back-calculate the pillar strength at the mine, numerical modelling was conducted. As there are large barrier pillars to protect the conveyer belts, tributary area theory (TAT) will overestimate the stresses on the pillars. For the sake of interest, the TAT value on the 6 m x 6 m pillars for the 75% extraction ratio is given by

$$APS = \frac{\rho g h}{1-e} = \frac{2800 \times 10 \times 1100}{1-0.75} Pa = 132.2\ MPa \quad (1)$$

where $\rho$ is the density of the rock, $h$ is the depth, $g$ is gravitational acceleration and $e$ is the extraction ratio (a conservative density was used to ensure a conservative pillar strength is calculated).

The Merensky Reef pillars were digitised. This is shown in Figures 25 and 26. The parameters used for the modelling study are given in Table 3.

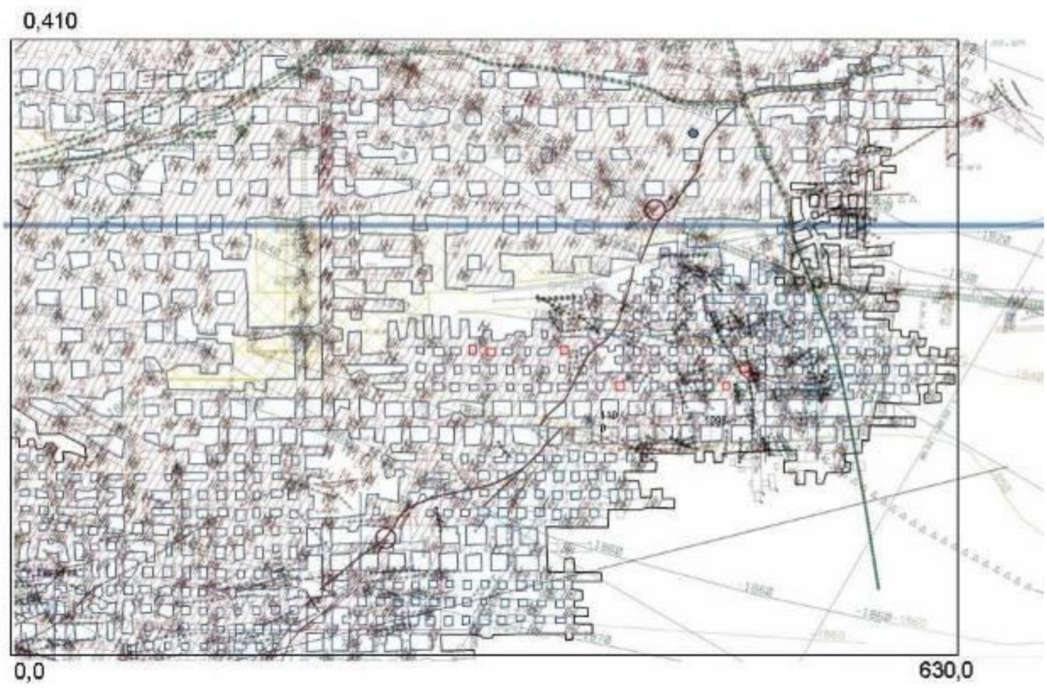


**Figure 25. Extent of the layout digitised**

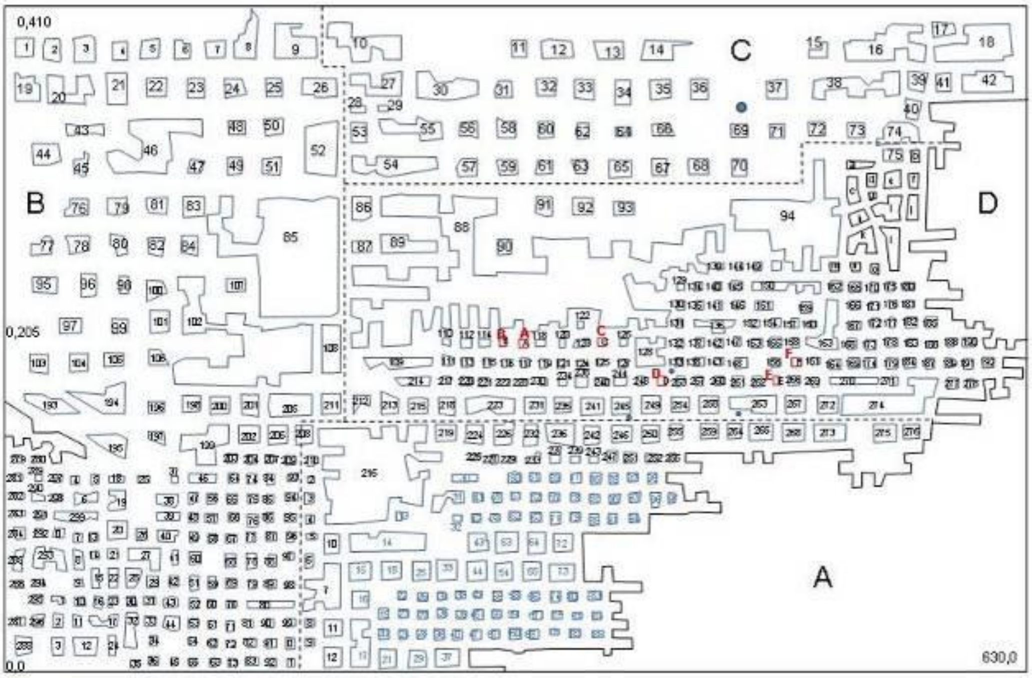


**Figure 26. Illustration of the digitised pillars**

**Table 3. Parameters used in the numerical model**

| Parameter | Value |
|---|---|
| Young's Modulus | 70 GPa |
| Poisson's ratio | 0.28 |
| k-ratio | 1.5 (strike)<br>1 (dip) |
| Average overburden density | 2800 kg/m$^3$ |

An average overburden density of 2800 kg/m$^3$ was used. Although this value might seem low, this value was adopted owing to the following reasons:

1. Mine personnel suggested the use of k-ratio's of 1.5 on strike and 1 on dip as well as a vertical stress gradient of 28 MPa/1000 m for modelling purposes at this mine.
2. Discussions with Mr Paul van der Heever indicated that an average overburden density of 2900 kg/m$^3$ would be a reasonable approximation if the density of all the different layers to surface is considered.
3. A higher value for the stress gradient might lead to an overestimation of the average pillar stress and the strengths of the pillars. It is therefore considered prudent to assume a lower stress gradient and this will result in more conservative pillar strengths.

The simulated APS values for the selected pillars are given below in Figure 27. Two values are shown for each pillar, namely the simulated values if only the smaller region D is simulated and the simulated values if the surrounding mining areas A, B and C are included. Note that the APS values are slightly larger with the surrounding areas included as the extraction ratio is high in these areas. The APS values of some of these pillars are also larger than the TAT value as some of these pillars are smaller than the specified 36 m$^2$.

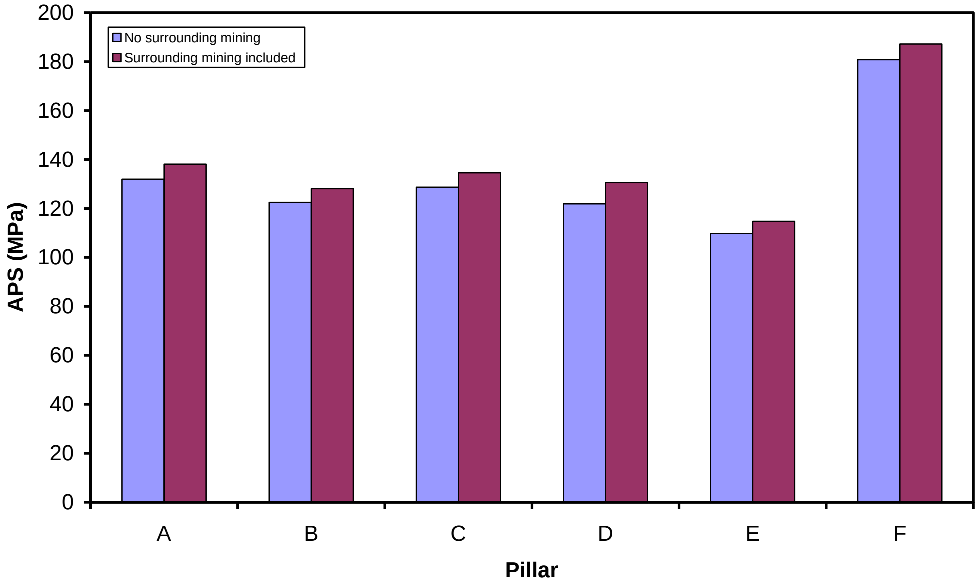


**Figure 27. Simulated APS values for the pillars of interest**

Some stress induced spalling could be seen on all pillars, but extensive damage was seen for pillar F and some prominent damage on one side of pillar A. These two pillars were undersized at 26.9 $m^2$ (A) and 20.1 $m^2$ (F). It therefore seems as if the strength of these pillars lies somewhere between 140 MPa and 180 MPa.

From the numerical modelling study, the classical Hedley and Grant approach with a K-value of 45 MPa for Merensky Reef is a too conservative approach of pillar strength. This is shown in Table 4. The simulated stress values as well as the Factors of Safety (FOS) for two pillar strength formulas are given. The Watson formula is the PlatMine formulation. Note that the FOS values for Hedley and Grant is less than 0.3, implying that all these pillars should have failed completely. This is not the case as seen during the underground visit.

The study illustrated that the pillars appears to be stronger than originally estimated. From the values given in Table 4, revised K-values for the Hedley and Grant formula were calculated (Table 5).

**Table 4. Simulated factor of safety (FOS) values.**

| Pillar | Area ($m^2$) | Perimeter (m) | Effective width (m) | Heigth (m) | APS (MPa) (no surrounding mining) | APS (MPa) (surrounding mining included) | Strength (Watson) | Strength (Hedley & Grant) K = 45 MPa | FOS (Watson) | FOS (Hedley & Grant) K = 45 MPa |
|---|---|---|---|---|---|---|---|---|---|---|
| A | 26.9 | 20.8 | 5.2 | 2.0 | 132.0 | 138.1 | 233.7 | 60.9 | 1.69 | 0.26 |
| B | 34.9 | 23.6 | 5.9 | 2.0 | 122.5 | 128.1 | 258.7 | 65.1 | 2.02 | 0.25 |
| C | 37.0 | 24.2 | 6.1 | 2.0 | 128.7 | 134.6 | 265.4 | 66.2 | 1.97 | 0.25 |
| D | 36.3 | 24.0 | 6.1 | 2.0 | 121.9 | 130.6 | 263.2 | 65.8 | 2.02 | 0.25 |
| E | 45.9 | 27.0 | 6.8 | 2.0 | 109.8 | 114.8 | 287.6 | 69.8 | 2.51 | 0.24 |
| F | 20.1 | 18.4 | 4.4 | 2.0 | 180.8 | 187.2 | 205.5 | 55.9 | 1.10 | 0.27 |

**Table 5. Calculated minimum K-values for the Hedley and Grant formula**

| Pillar | Area ($m^2$) | Perimeter (m) | Effective width (m) | Heigth (m) | APS (MPa) (surrounding mining included) | Minimum K-value (Hedley & Grant) |
|---|---|---|---|---|---|---|
| A | 26.9 | 20.8 | 5.2 | 2.0 | 138.1 | 102.1 |
| B | 34.9 | 23.6 | 5.9 | 2.0 | 128.1 | 88.6 |
| C | 37.0 | 24.2 | 6.1 | 2.0 | 134.6 | 91.5 |
| D | 36.3 | 24.0 | 6.1 | 2.0 | 130.6 | 89.3 |
| E | 45.9 | 27.0 | 6.8 | 2.0 | 114.8 | 74.0 |
| F | 20.1 | 18.4 | 4.4 | 2.0 | 187.2 | 150.6 |

If the average of the first 5 K-values (pillar F shows excessive spalling) in Table 5 is calculated, a value of 89.1 MPa is obtained. It therefore appears that a K-value of 90 MPa can be assumed as a reasonable estimate to calculate the strength of the Merensky pillars. This analysis seems to confirm the K-value back calculated at Styldrift Mine.

### 4.2.3 Mine C - A study of the UG2 pillar strength at a mine in the Eastern Bushveld

The work in this section is described in more detail in the paper by Oates and Malan (2023). A recent experimental pillar extraction project in a UG2 bord and pillar section at this mine presented a unique opportunity to compile a new pillar database. The experimental pillar mining area is illustrated in Figure 28. The site is described in Watson et al. (2021). The mine established this experimental section in an attempt determine the strength of UG2 chromitite pillars. A central pillar (pillar A in Figure 28) was instrumented, and the surrounding pillars were progressively mined until failure of the central pillar occurred. The central pillar showed signs of limited spalling, whilst the small neighbouring pillars were severely fractured and are considered to be in a failed state. As can be seen in Figure 28, the experiment resulted in pillars of different sizes and the observations indicated these are at varying degrees of stability. This is particularly valuable to estimate pillar strength as it is in the same area and therefore in the same geotechnical area.

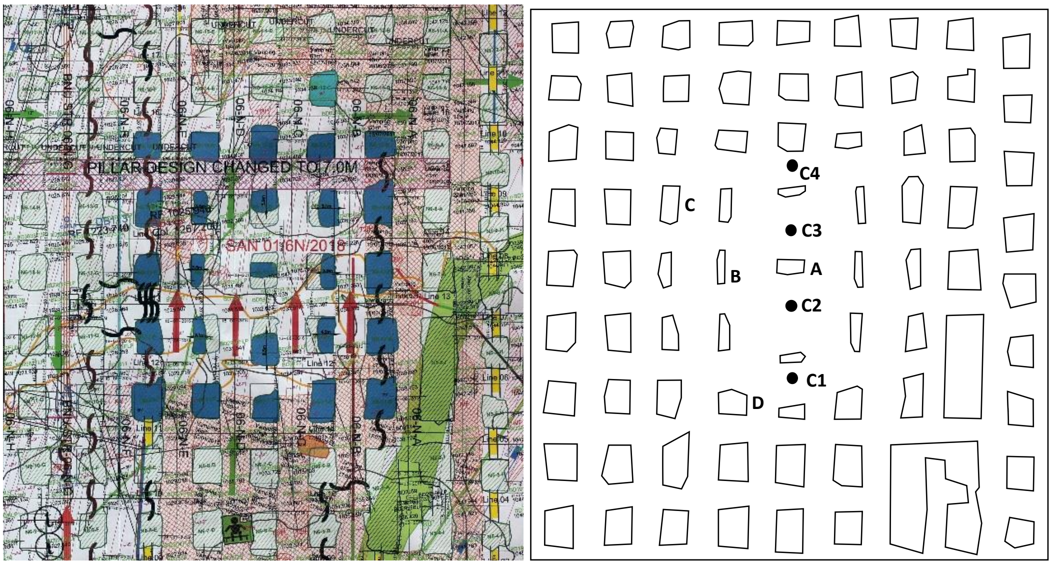


**Figure 28. Layout of the experimental pillar mining area where pillars in blue were gradually reduced in size to increase the load on the central pillar. The final geometry of the experimental area when the experiment was terminated is shown on the right (after Napier and Malan, 2021)**

In June 2021 several underground visits were conducted at the mine, as described in Oates and Malan (2023), to assess the pillar condition. A total of 66 pillars in 6 different areas (Figure 29) were selected for detailed observations and for populating the database.

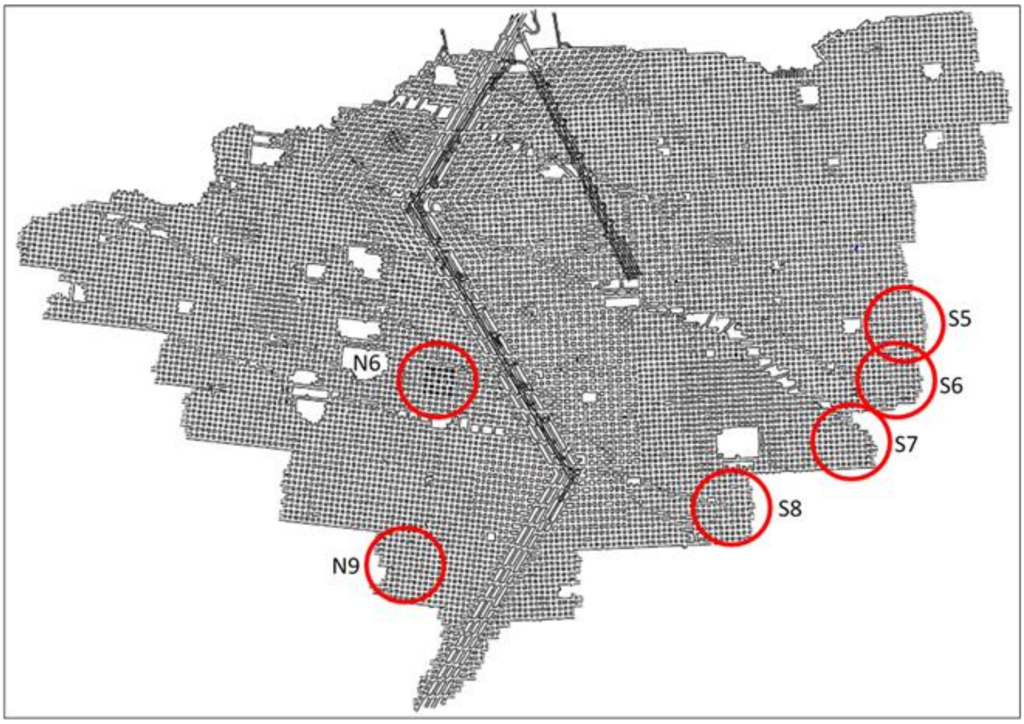


**Figure 29. Areas of the mine where the pillar data was collected**

The pillar classification proposed by Esterhuizen et al. (2006) was used to categorise the pillars. The experimental pillar project area (Figure 28) was the only area in the mine where pillars, in each of the categories, could be found. It should be noted that all the failed and unstable pillars in the database are from the pillars in the experimental pillar project area. A total of 7 of the 25 pillars in the experimental pillar project area were classified as failed. An example of a so-called "Class 5" failed pillar is shown in Figure 30.

**Figure 30. A "Class 5" failed pillar in the pillar project area**

A preliminary calibration of the Hedley and Grant (1972) formula was done by the authors by adjusting the K-value to obtain a reasonable fit to the data. The Hedley and Grant (1972) formula is well established in the design of hard rock pillars in South Africa and, as no suitable alternative was available to the authors, a recalibration of this formula by using this new dataset was done.

The estimated value of K was 75 MPa. The fitted curve is illustrated on Figure 31. This calibration seems to give reasonable failure envelope to separate the failed and stable pillars with all the intact pillars below the envelope. Note that this line is only a first trial and error estimate done by hand. Additional data will be required to verify the most appropriate failure envelope as there are one failed pillar data point far below the line. This may be an outlier, but further work needs to be done in future to refine this calibration with a larger database.

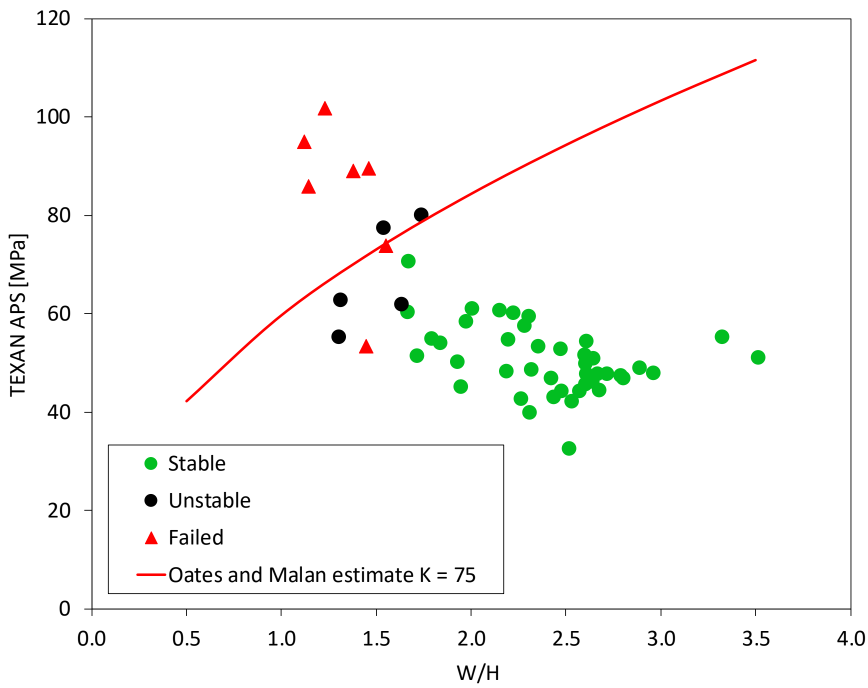


**Figure 31. A preliminary calibration of the Hedley and Grant formula for the UG2 pillar data collected (after Oates and Malan, 2023)**

### 4.2.4 Mine D - A study of the UG2 pillar strength at Everest Platinum Mine

Couto and Malan (2023) studied the large-scale collapse of the UG2 pillars at the Everest Platinum Mine. A major contributing factor to the collapse was the presence of weak alteration layers (weak partings with infilling) in the pillars. Figure 32 illustrates this alteration zone at the contact between the pillar and the hangingwall. This seems to reduce the pillar strength substantially and the typical pillar failure is shown in Figure 33. The authors conduced a back analysis of two areas and the so-called "collapsed area" is of interest to estimate the pillar strength (see Figure 34).

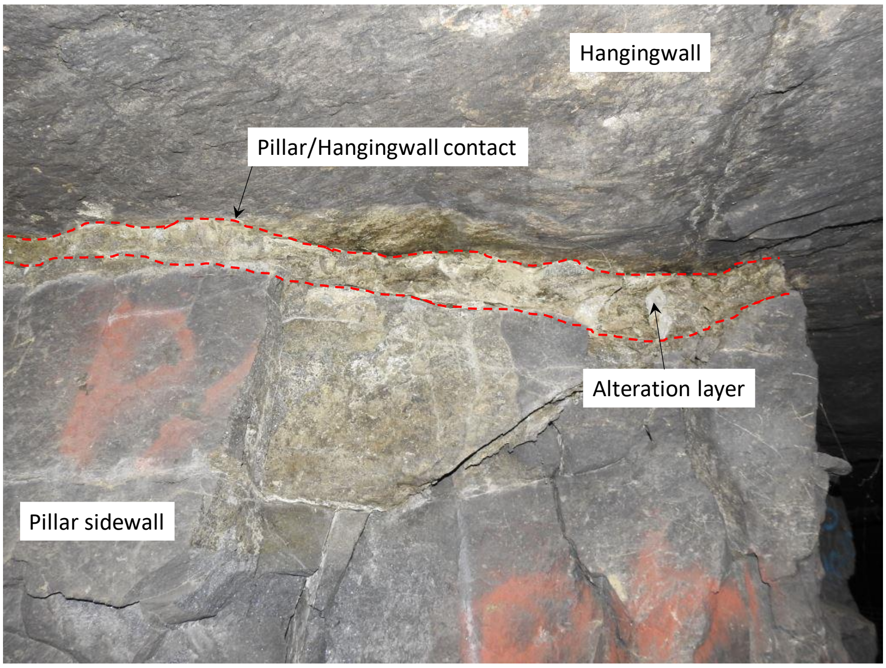


**Figure 32. A weak alteration layer is present at the contact between the pillar and the hangingwall at the Everest Platinum Mine (after Couto and Malan, 2023)**

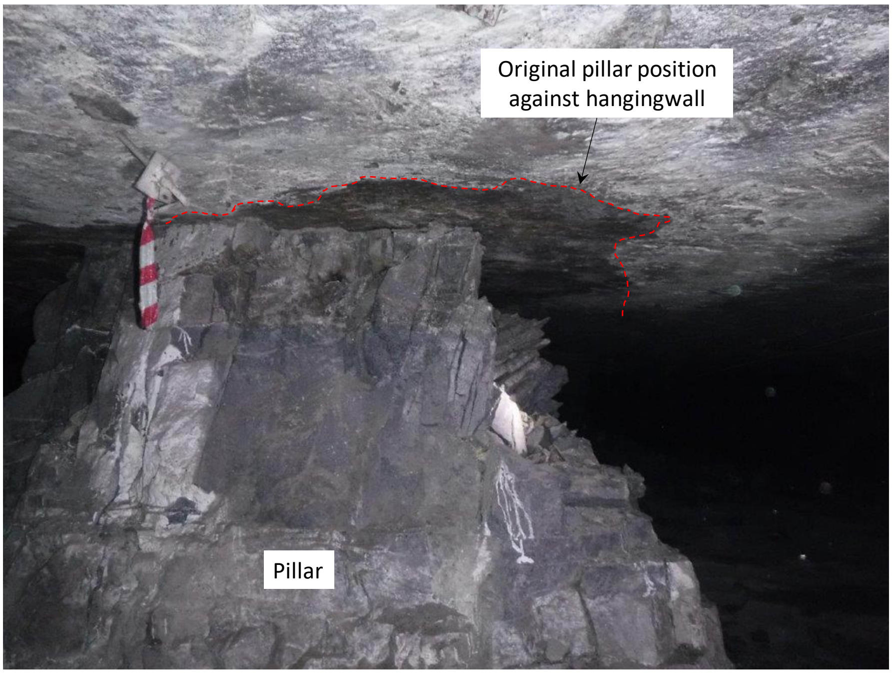


**Figure 33. Typical pillar failure in areas where weak alteration zones are present. Note the original size of the pillar against the hangingwall as indicated by the red dotted line (after Couto and Malan, 2023)**

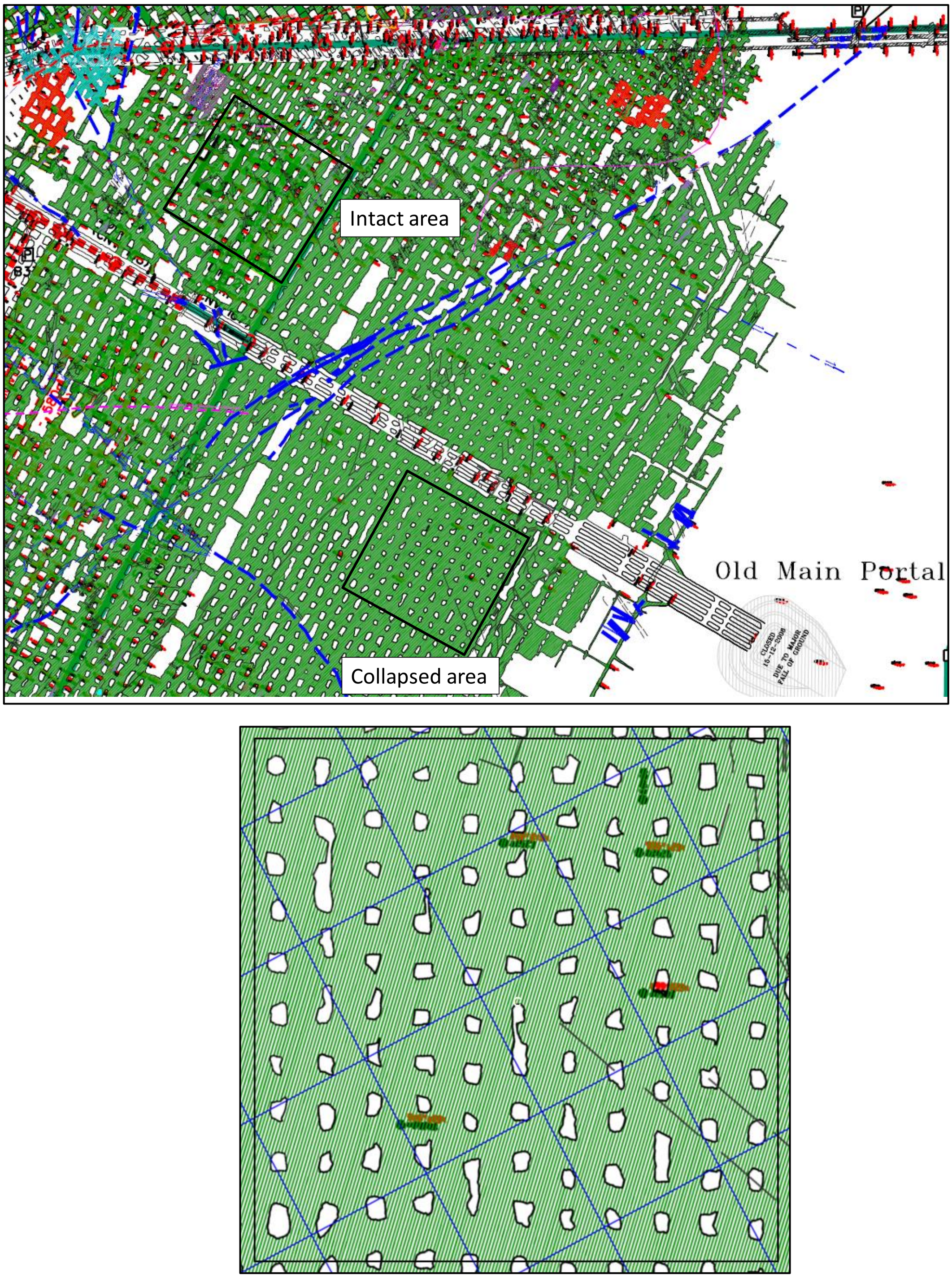


**Figure 34. Layout of the Everest Mine (top) and part of the collapsed area (bottom) that was simulated in detail (after Couto and Malan, 2023)**

The careful simulation of the collapsed area and the actual pillar shapes allowed for the back calculation of the K-value for the Hedley and Grant pillar formula. For the collapsed area, the pillars are presumed to have failed at the simulated APS values and this was therefore assumed to be the maximum strength of the pillars. The calculated K-values gave an average value of 19 MPa for the collapsed area. The value for some of the failed pillars was below

10 MPa and K = 10 MPa may therefore be a reasonable approximation to use for the Hedley and Grant formula for these pillars with the weak clay infilling. This will result in extremely conservative layouts and highlights the detrimental effect of these alteration layers on pillar strength.

### 4.2.5 Mine E - A study of the LG6/LG6A pillar strength at Wonderkop Mine

Spencer (1999) reported on the failure of the pillar system and the subsequent closure of the Wonderkop Chrome Mine in May 1998. The mine exploited the lower group chromitite seams, namely the LG6 and LG6a. It was the most easterly situated LG6 mining operation in the Rustenburg area and situated adjacent to the Spruitfontein dome (an upfold structure which separates the Rustenburg section from the Marikana section).

The Wonderkop pillars are multilayer in nature and it is expected that this will weaken its strength substantially. The clay layer was identified has having a controlling influence in the failure process and FLAC runs were conducted by Spencer to investigate the effect of the thickness of the clay layer on the peak strength of the pillar. Although it is not clear from his paper how the strain softening parameters for the FLAC model was determined, it is stated that the pillar strength decreases from 43 MPa for no clay layer to 14 MPa for a clay layer with a thickness of 20 cm. This decreased further to 7 MPa for a 30 cm clay layer. From some MINSIM runs and a comparison to the damage observed underground, it was subsequently assumed that the pillar strength at Wonderkop was only 7 MPa. This translated to a Hedley and Grant K-value as low as 4.64 MPa. The redesigned pillar layout included 24 m wide strike barrier pillars at 78 m centres on dip, 10 m wide pillars and 6 m wide panels. This only gave an extraction ratio of 38 percent, but it is not clear from the paper if this new layout was ever used in practice.

The first underground inspection of the pillars by Spencer was conducted in July 1997. During this visit it was noted that some joints were beginning to open at the corners of some pillars. Some joints were also opening at the sides of the pillars and in a few cases sliding along the clay layer was noted. Figure 35 illustrates where failure was observed on the pillars. The rating system used in Figure 35 is explained in Table 6.

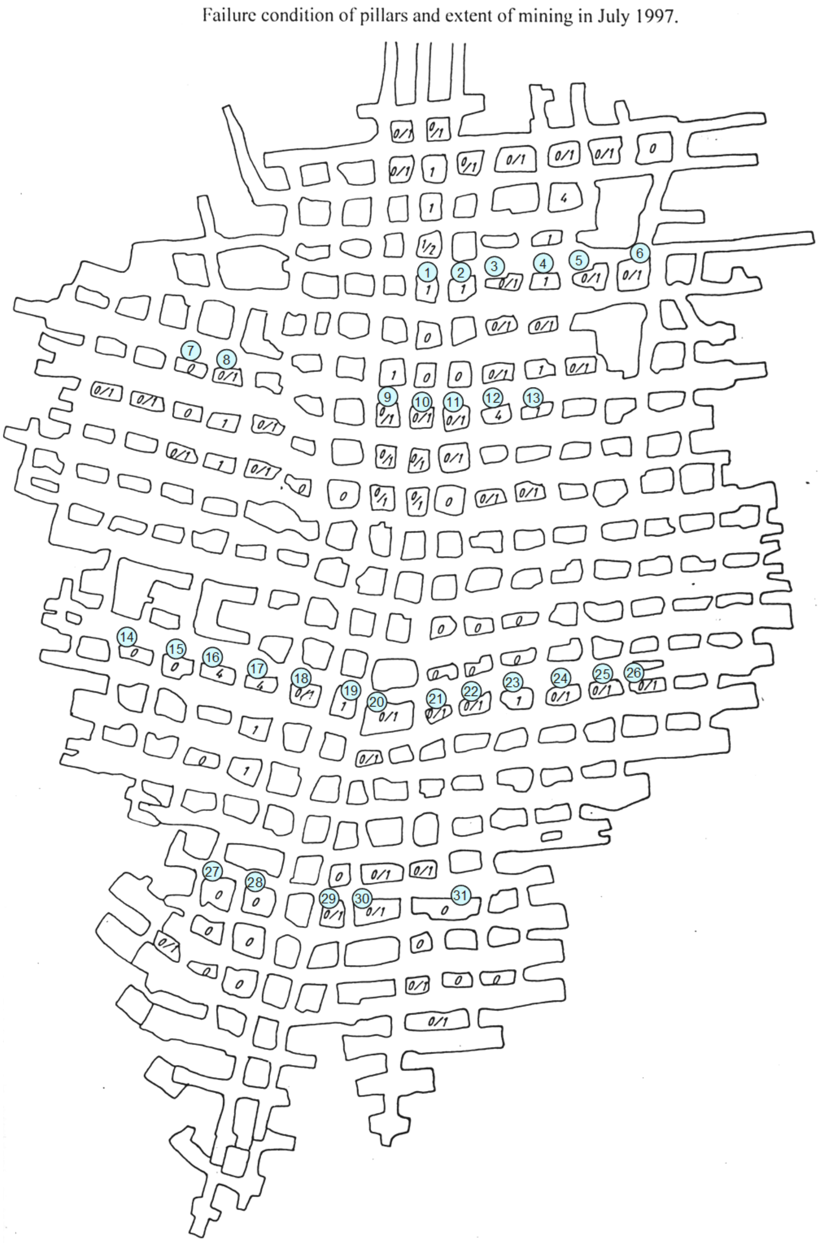


**Figure 35. Failure condition of the pillars and the extent of mining in July 1997 (after Spencer, 1999). The numbers in circles refer to the pillars for which the APS values were computed in the back-analyses conducted by the principal author of this current Samerdi report.**

**Table 6. Description of the rating system (Spencer, 1999)**

| Rating | Description |
|---|---|
| 0 | No failure |
| 1 | Opening of joints at the corners |
| 2 | Opening of joints at the corners and along the sides |
| 3 | Material slabbing off the corners and sides |
| 4 | Horizontal movement occurring along the clay layer |

Using MINSIM, Spencer plotted areas where the closure exceeded 9 mm (by varying the residual strength of pillars – see comment below) and this agreed roughly with the area where pillar failure was observed underground (Figure 36). Unfortunately, Spencer did not mention the parameters used for the MINSIM models (Young's modulus and assumed virgin stress field). Mention is also made of simulating the pillars with residual strengths. It is not clear how these residual strengths were simulated using MINSIM.

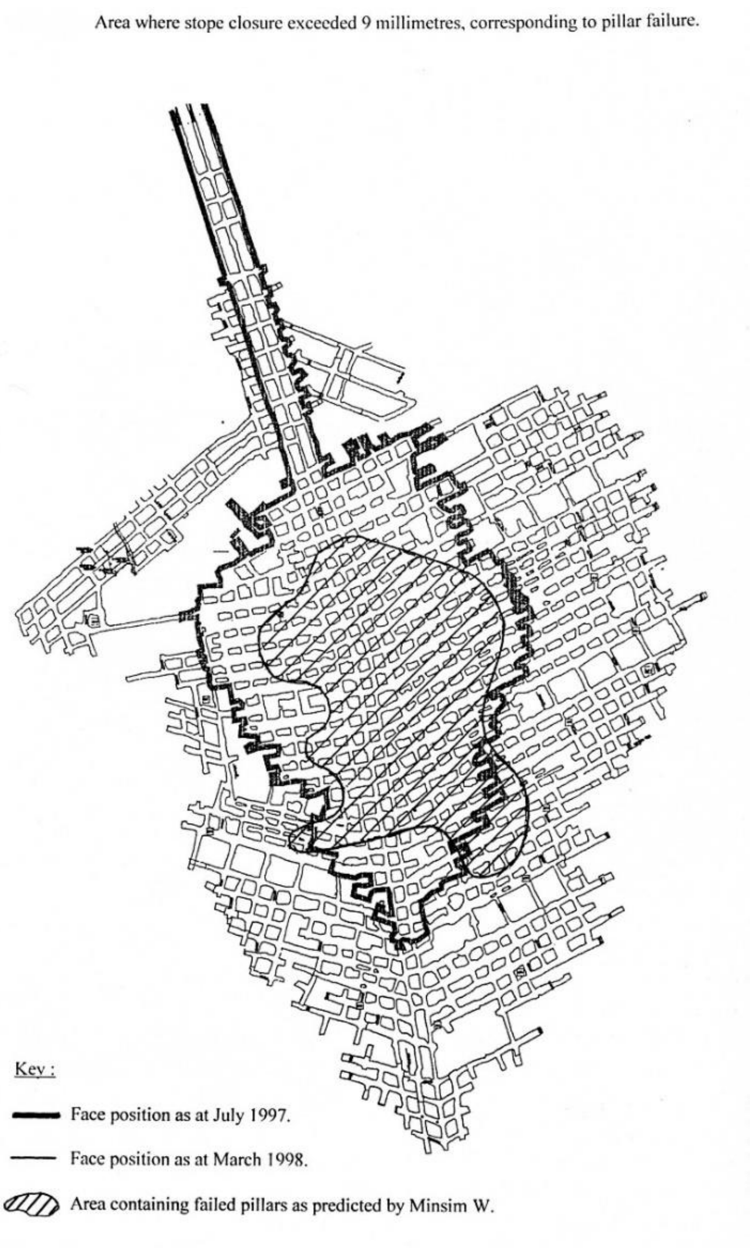


**Figure 36. Area where the simulated stope closure exceeded 9 mm (after Spencer, 1999)**

The layout of Wonderkop at the time when the mine was closed is shown in Figure 37. The entire mine was simulated using TEXAN at a later stage by the principal author of this report.

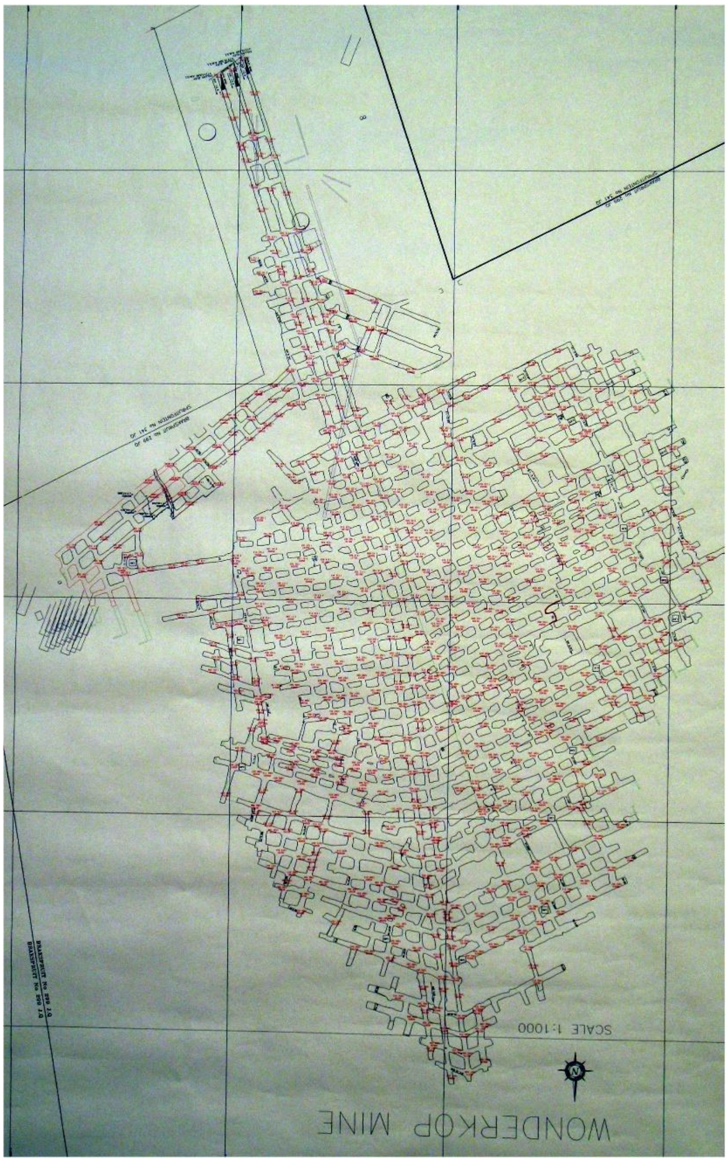


**Figure 37. Extent of the area simulated with TEXAN**

Two mining steps were simulated. The first was the extent of mining during July 1997 (Figure 35) and the second step was the final mining outline in May 1998 (Figure 37).

The mining outline and pillars were approximated by polygons to assist with the digitising process. This is shown in Figures 38 and 39. The pillar numbers used in the modelling process are indicated in the figures. The APS values of several pillars were calculated.

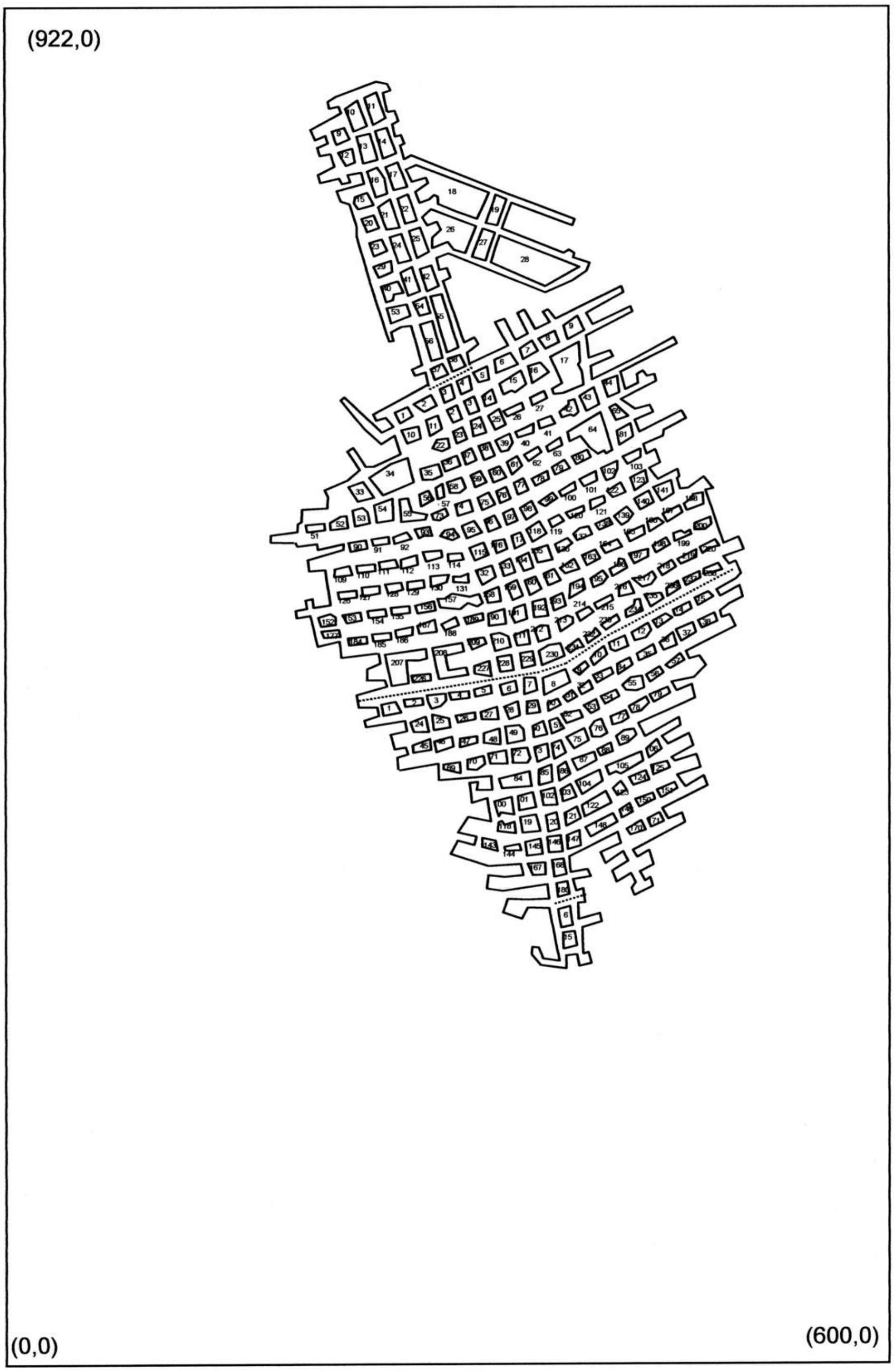


**Figure 38. Approximation of the mining outline and pillars with polygons to assist with the digitising process (extent of layout – July 1997)**

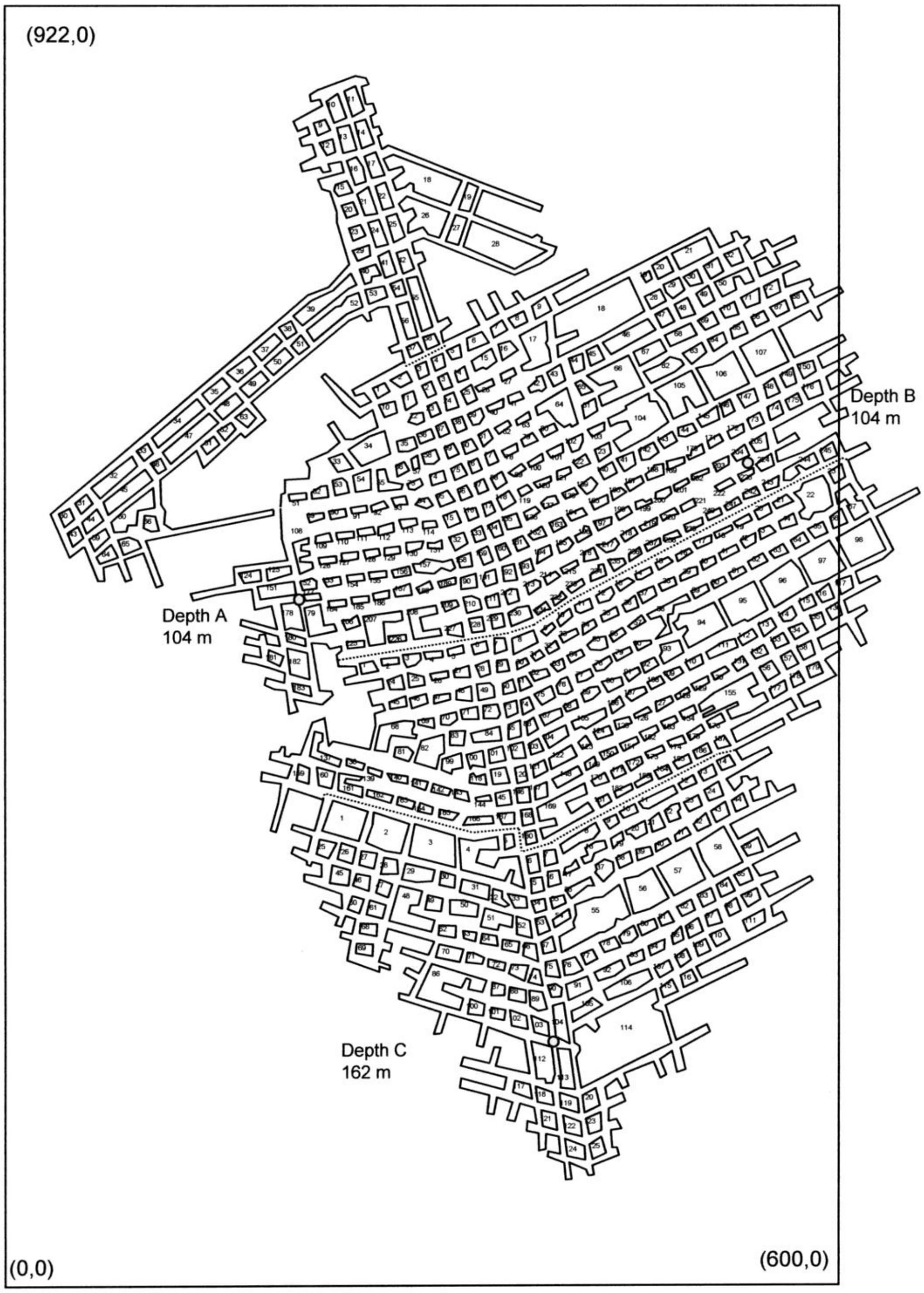


**Figure 39. Approximation of the mining outline and pillars with polygons to assist with the digitising process (extent of layout – May 1998)**

The mined regions and pillars of interest were covered with a mesh of triangular elements. The average element sizes used in the mined areas were approximately 2 m. An example of the mesh generated is shown in Figure 40.

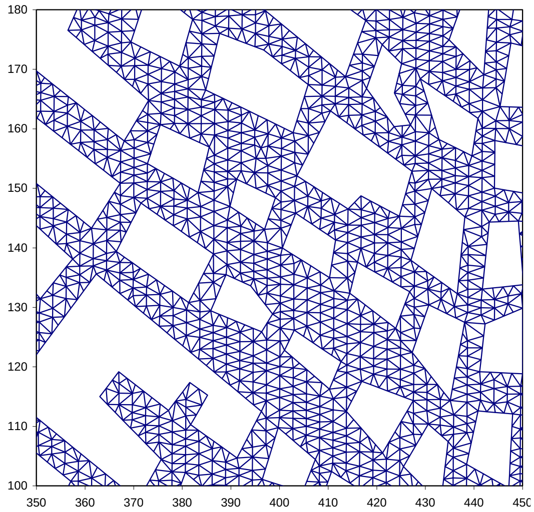


**Figure 40. Part of the element mesh generated in the area of interest**

The parameters used for the models are given below:

**Table 7. Parameters used in the numerical model**

| Parameter | Value |
|---|---|
| Young's Modulus | 70 GPa |
| Poisson's ratio | 0.25 |
| k-ratio | 1 on dip, 1 on strike |
| Average overburden density | 2900 kg/m$^3$ |

Figure 41 illustrates the APS values for pillars 1 to 31 (see Figure 35 for the pillar numbers). Note that the stresses are relatively low as the depth is shallow and the pillars are large. It should be noted that these values are first approximations only as the pillar sizes and shapes were obtained from the mine plans and were not accurately measured underground. Access to these working areas is not possible anymore.

The average simulated convergence (average of all collocation points) for the mine was 1.1 mm. Note that this is less than that simulated by Spencer (1999) as the compression of the clay layer and other inelastic movements were not simulated in TEXAN (compression of the pillars can nevertheless be simulated if required).

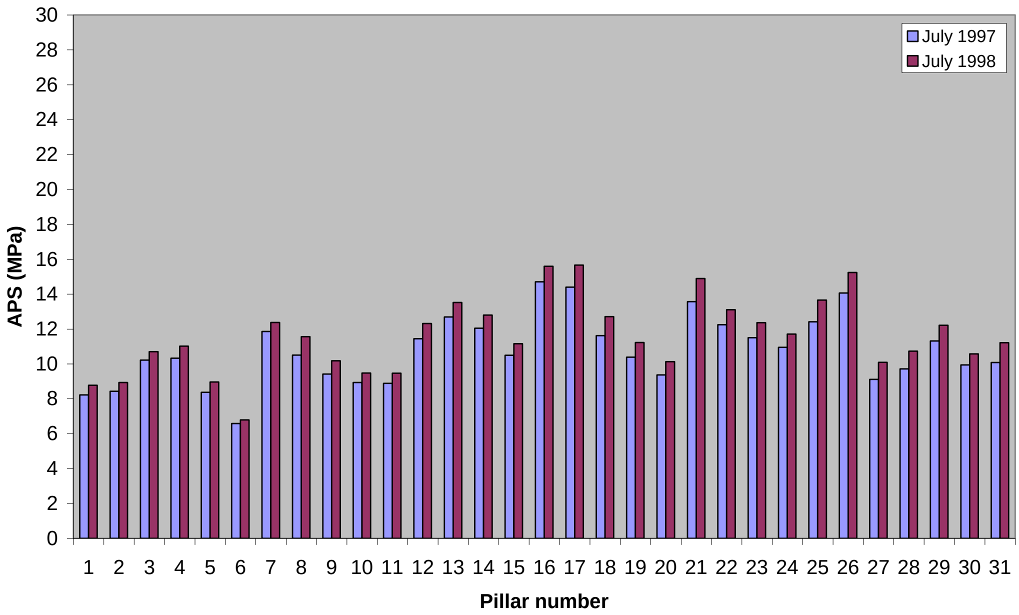


**Figure 41. Simulated pillar stresses for selected pillars in the area of interest (see Figure 35 for the positions of the pillars)**

The simulated APS values are summarised in Table 8. The pillar areas given in the table are the simulated values. Spencer (1999) mentioned that the average stoping width at Wonderkop was 2 m. Note that only a slight increase in pillar stress was experienced from July 1997 to May 1998. The state of failure of each pillar as observed by Spencer is also given in the table (see Table 6 for the codes). The Hedley and Grant formula was used to calculate the K-value for some of the pillars. This was only computed for the pillars which showed the first signs of failure as it was assumed that the factor of safety on these pillars was very close to 1.

**Table 8. Summary of simulated APS values and calculation of Hedley and Grant K-value**

| Pillar | Area | Circum-ference | Effective width | Pillar height | APS July 1997 | APS May 1998 | Increase in APS | Failure July 1998 | Calculated K - value |
|---|---|---|---|---|---|---|---|---|---|
| 1 | 75.13 | 35.24 | 8.53 | 2 | 8.22 | 8.77 | 0.55 | 1 | 4.73 |
| 2 | 80.52 | 35.07 | 9.18 | 2 | 8.43 | 8.93 | 0.5 | 1 | 4.68 |
| 3 | 62.01 | 34.34 | 7.22 | 2 | 10.22 | 10.7 | 0.48 | 0/1 | 6.40 |
| 4 | 61.11 | 31.86 | 7.67 | 2 | 10.33 | 11.02 | 0.69 | 1 | 6.27 |
| 5 | 88.98 | 43.31 | 8.22 | 2 | 8.37 | 8.96 | 0.59 | 0/1 | 4.91 |
| 6 | 118.09 | 43.81 | 10.78 | 2 | 6.58 | 6.79 | 0.21 | 0/1 | 3.37 |
| 7 | 50.41 | 30.87 | 6.53 | 2 | 11.86 | 12.37 | 0.51 | 0 | No failure |
| 8 | 60.21 | 32.96 | 7.31 | 2 | 10.5 | 11.56 | 1.06 | 0/1 | 6.53 |
| 9 | 66.96 | 32.57 | 8.22 | 2 | 9.42 | 10.18 | 0.76 | 0/1 | 5.52 |
| 10 | 69.1 | 33.18 | 8.33 | 2 | 8.93 | 9.48 | 0.55 | 0/1 | 5.20 |
| 11 | 86.54 | 37 | 9.36 | 2 | 8.88 | 9.47 | 0.59 | 0/1 | 4.88 |
| 12 | 53.47 | 31.57 | 6.77 | 2 | 11.44 | 12.31 | 0.87 | 4 | Failed |
| 13 | 49.34 | 35.24 | 5.60 | 2 | 12.69 | 13.52 | 0.83 | 1 | 9.02 |
| 14 | 56.17 | 33.23 | 6.76 | 2 | 12.05 | 12.8 | 0.75 | 0 | No failure |
| 15 | 87.55 | 36.69 | 9.54 | 2 | 10.49 | 11.16 | 0.67 | 0 | No failure |
| 16 | 48.73 | 31.31 | 6.23 | 2 | 14.7 | 15.59 | 0.89 | 4 | Failed |
| 17 | 49.59 | 31.09 | 6.38 | 2 | 14.4 | 15.66 | 1.26 | 4 | Failed |
| 18 | 69.02 | 33.64 | 8.21 | 2 | 11.62 | 12.71 | 1.09 | 0/1 | 6.82 |
| 19 | 82.38 | 36.44 | 9.04 | 2 | 10.39 | 11.23 | 0.84 | 1 | 5.81 |
| 20 | 160.3 | 53.59 | 11.96 | 2 | 9.37 | 10.13 | 0.76 | 0/1 | 4.56 |
| 21 | 46.14 | 28.97 | 6.37 | 2 | 13.57 | 14.89 | 1.32 | 0/1 | 9.04 |
| 22 | 65.78 | 35.4 | 7.43 | 2 | 12.24 | 13.1 | 0.86 | 0/1 | 7.55 |
| 23 | 79.4 | 35.76 | 8.88 | 2 | 11.5 | 12.36 | 0.86 | 1 | 6.49 |
| 24 | 86.94 | 37.43 | 9.29 | 2 | 10.95 | 11.71 | 0.76 | 0/1 | 6.04 |
| 25 | 60.42 | 33.2 | 7.28 | 2 | 12.41 | 13.66 | 1.25 | 0/1 | 7.74 |
| 26 | 52.32 | 30.84 | 6.79 | 2 | 14.06 | 15.24 | 1.18 | 0/1 | 9.08 |
| 27 | 117.43 | 43.46 | 10.81 | 2 | 9.11 | 10.09 | 0.98 | 0 | No failure |
| 28 | 100.08 | 39.87 | 10.04 | 2 | 9.71 | 10.73 | 1.02 | 0 | No failure |
| 29 | 58.59 | 30.73 | 7.63 | 2 | 11.31 | 12.21 | 0.9 | 0/1 | 6.89 |
| 30 | 135.08 | 49.65 | 10.88 | 2 | 9.94 | 10.57 | 0.63 | 0/1 | 5.07 |
| 31 | 177.59 | 64.63 | 10.99 | 2 | 10.08 | 11.22 | 1.14 | 0 | |
| | | | | | | | | Average K-value | **6.21** |

Spencer (1999) estimated a K-value of 4.64 MPa, so it agrees well with the average value of K estimated in the Table 8. The implications of this would be that a very low rate of extraction would be achieved in areas where the thick clay layer is present.

### 4.2.6 Mine F - A study of the LG6/LG6a pillar strength at a mine in the Rustenburg area

A study of LG6/LG6a pillar strength was conducted at this mine in 2009. A number of photographs were taken in the area visited and some of these are shown below. No pillar spalling was observed in the area visited, even for the very small pillars, and both the hangingwall and pillars appeared to be in a very good condition. Two pillars were of interest and these were numbered P227 and P241 for the modelling process. The position of these pillars is shown in Figure 42. The depth in this area is approximately 200 m. The dimensions of these pillars as measured underground are shown in Figure 43. The pillar edges are approximated in the drawing with straight line segments to simplify the discretisation of this pillar during the modelling exercise. The arrows and figure numbers refer to the positions and directions in which the photographs were taken.


**Figure 42. Part of the old workings at Mine F and the position of the small pillars which were examined in detail**

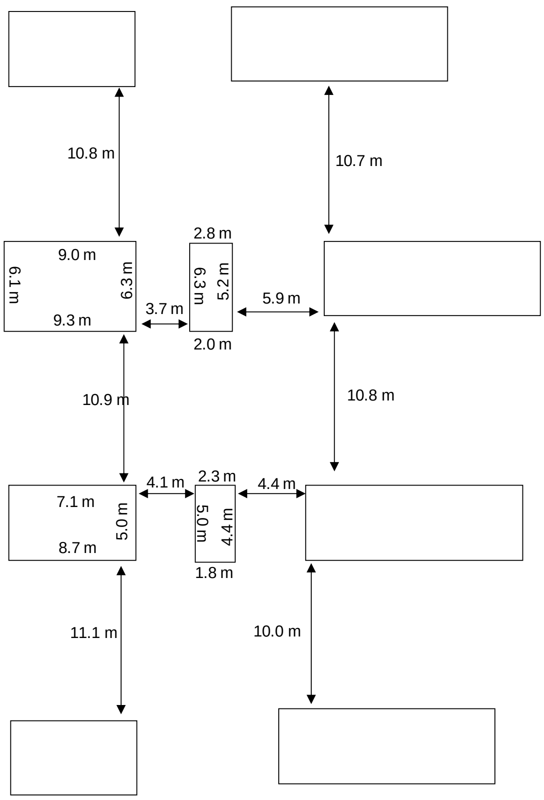


**Figure 43. Sizes of pillars P227 and P241 as measured underground. The figure numbers refer to the photographs below**

The following photographs of the two pillars were taken during the underground visit.

**Figure 44. Condition of pillar P227**

**Figure 45. Condition of pillar P227**

**Figure 46. Condition of pillar P241**

**Figure 47. Condition of pillar P241**

For the modelling, the mining outline and pillars in Figure 42 were approximated by polygons to assist with the digitising process. This is shown in Figure 48. Note the small sizes of pillars P227 and P241. A larger model than the one shown in the diagram was simulated in TEXAN by using equivalent stiffness elements to represent the far-field mining.

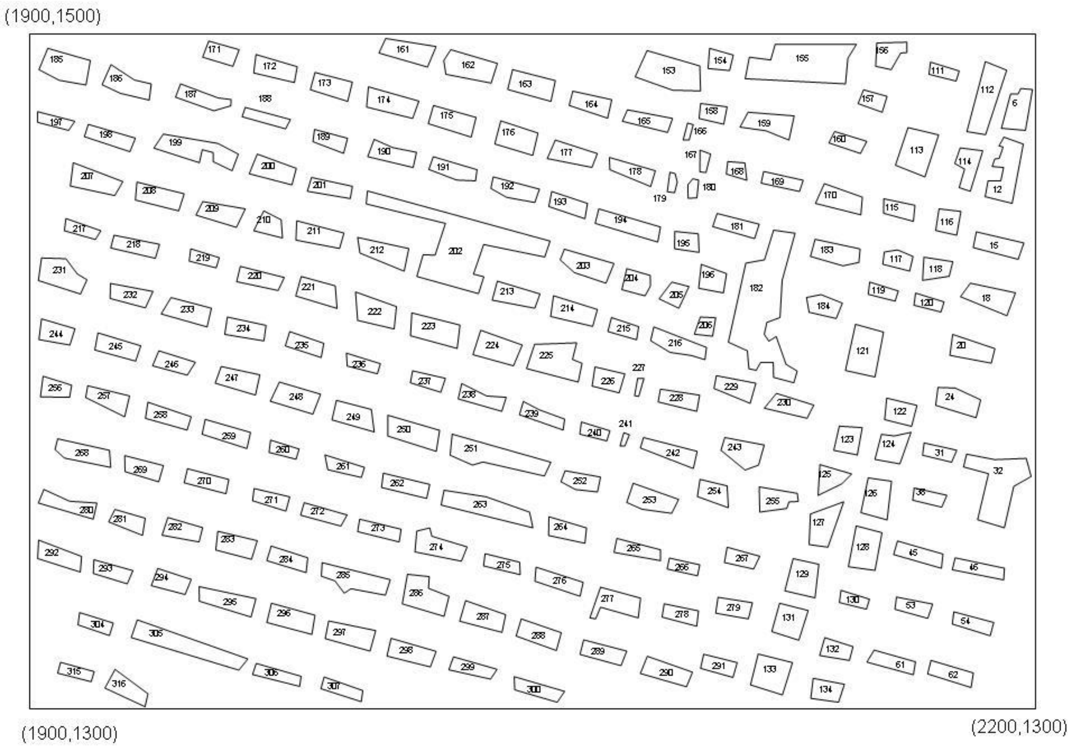


**Figure 48. Approximation of the mining outline and pillars with polygons to assist with the digitising process**

The mined regions and pillars to be investigated in detail were covered with a mesh of triangular elements. Owing to the small pillar sizes and small spans in some areas, small average element sizes (≈ 1.5 m) were used in the area that was simulated in detail. An example of the mesh generated by the mesh utility is shown in Figure 49.

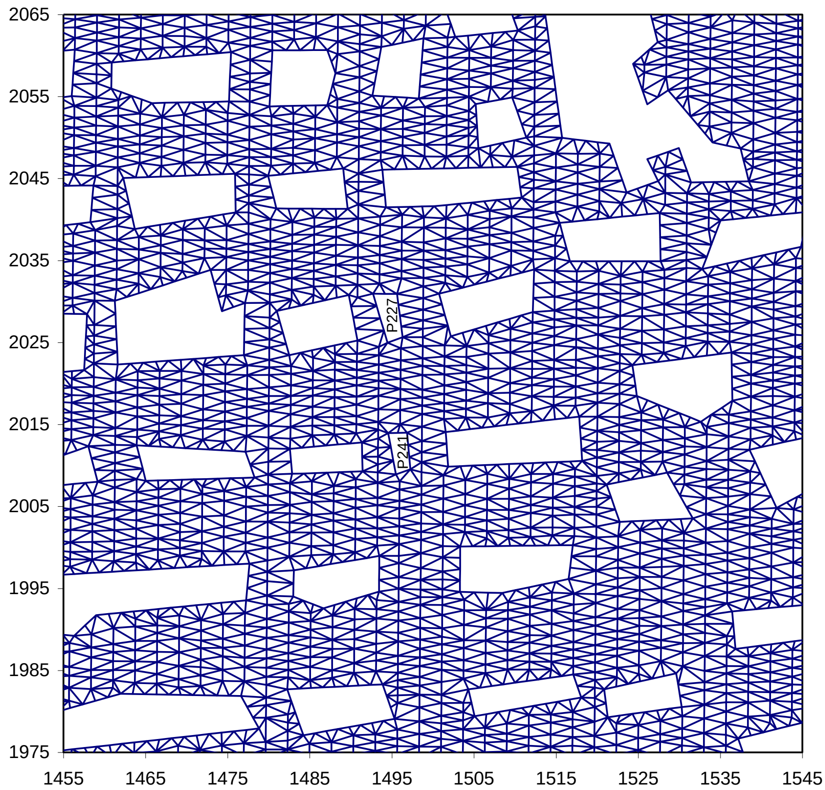


**Figure 49. Part of the element mesh used in the area of interest. The pillars P227 and P241 is visible in the middle of the diagram**

The parameters used for the model are given below:

**Table 9. Parameters used in the numerical model**

| Parameter | Value |
|---|---|
| Young's Modulus | 70 GPa |
| Poisson's ratio | 0.25 |
| k-ratio | 1 |
| Average overburden density | 2900 kg/m$^3$ |
| Equivalent stiffness | 2160 MPa/m |

The simulated APS values for pillars P227, P241 and P226 are given below in Figure 50. Two values are shown for each pillar, namely the simulated values if only the small area of interest is simulated (Figure 48) and the simulated values if the adjacent mining is included in the simulations. This leads to a slight increase in stress on the pillars. The stress on pillars P227 and P241 is relatively high. The sizes of the pillars are: P227 = 13,83 m², P241 = 9.85 m² and P226 = 49.1 m².

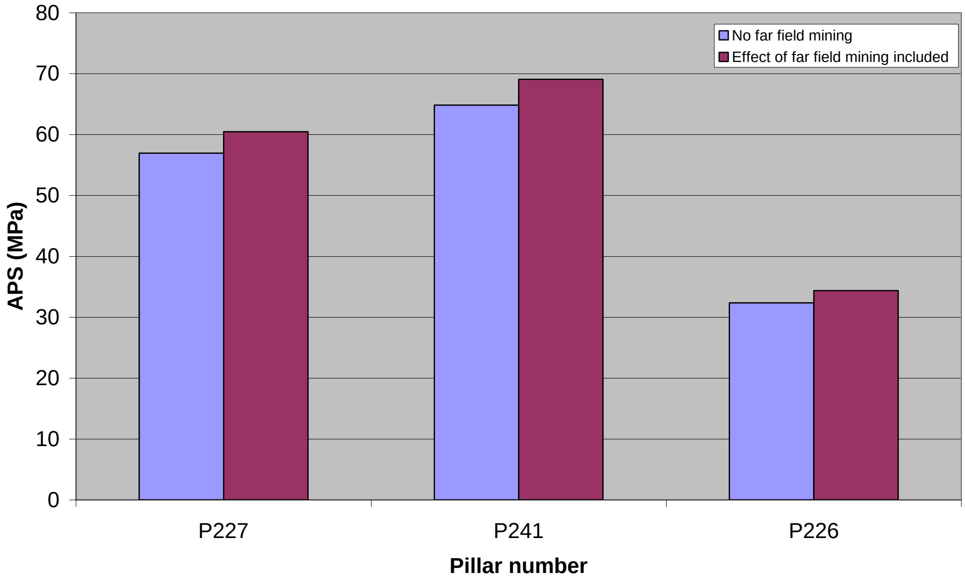


**Figure 50. Simulated APS values for three pillars of interest**

No damage could be seen on any of these three pillars, implying that the minimum strength of the pillars exceeds 69 MPa. From the formula for effective width, it follows that for pillar P241:

$$w_{eff} = \frac{4 \times Area}{Circumference} = \frac{4(9.85\ m^2)}{13.5\ m} = 2.92\ m \qquad (2)$$

The height of this pillar was measured as 1.6 m. These values can be substituted in the Hedley and Grant equation to estimate a minimum K-value:

$$69.08 = K\frac{2.92^{0.5}}{1.6^{0.75}} \qquad (3)$$

As the simulated stress of the pillar is assumed to be the minimum strength, it follows from equation (3) that a conservative estimate is **K > 57.5 MPa**.

Similar to the exercise above, another three back-analysis studies were completed at the mine. The findings are summarised below:

Study 1 - Back analysis of another small pillar at Mine F: The pillar was located at a depth of approximately 220 m and small in size (10.66 m²). Although the pillar was surrounded by a stiff environment (large pillars and small bords), the simulated APS value on the pillar was relatively high at 55 MPa. The pillar was still intact and showed no signs of fracturing. The back calculated minimum K-value from this study indicated that **K > 45.6 MPa**.

Study 2 - Back analysis of two small pillars at another mine belong to the same company: The pillars were located at a depth of approximately 265 m and the smallest pillar had a size of 13.67 $m^2$. The stiffness of the environment was very similar to that of the area reported on in Progress report 2. The APS value on the pillar was simulated to be 62 MPa. The pillar was still intact and showed no signs of fracturing. The back calculated minimum K-value from this study indicated that **K > 45.3 MPa**.

Study 3 – This is the back analysis of another small pillar at Mine F: The pillars were located at a depth of approximately 90 m and the smallest pillar had a size of 11.75 $m^2$. The pillar was in a much less stiff system compared to the pillars studied in the other areas. The APS value on the pillar was therefore high for the shallow depth with a value of 47 MPa. The pillar was still intact and showed no signs of fracturing. The back calculated minimum K-value from this study indicated that **K > 46.6 MPa**.

The mine subsequently adopted a K-value of **57.5 MPa** and the mining to date indicated a stable pillar environment.

## 4.3 *Site selection for the additional pillar back analyses*

From the historic data discussed in Section 2, the data was summarised and this is given in Table 10. It is evident from this table that the LG6/LG6A pillars have a lower calibrated K-value compared to the UG2, even though both types of pillars consist of chromite material. It was noted in the historic reports for Mine F that the back-calculated value for the LG6/LG6A material was still considered a conservative value as the test pillars had no indication of spalling. Based on this, it will add significant value if small LG6 pillars could be found to verify this value. Discussions were held with Samancor Chrome and very small LG6 pillars in the old mining areas of Millsell Mine (part of Samancor Western Chrome) was identified as a suitable area for back-analysis.

Another area identified for further back analysis was Styldrift Mine. Although a high K-value was already estimated for the Merensky Reef in one area of the mine, the excessive spalling of the pillars at this mine currently make it probably one of the best areas to study hard rock pillars in the industry. It would have been a mistake not to select a different area at this mine for further back analysis. The mine gave permission for a further study and this is described in this report. This was a good selection as an important insight was obtained from this additional analysis.

As a third case study, a recent UG2 pillar sliping project in a mine in the Eastern Bushveld is described. This provides some additional verification of UG2 pillar strength as well as some important insight when conducting pillar sliping experiments to determine K-values.

To support the new findings from the studies conducted at Styldrift Mine, some previous data collected from a manganese mine was re-analysed to investigate the effect of joint sets in the pillars, on pillar strength. This work was included as it was found from the Styldrift study that the rock mass rating of the pillars in the mines will affect pillar strength. This will have a profound effect on the layout design in mines with distinctly different geotechnical areas.

The four additional sites described in this report are:

- Merensky Reef – Styldrift Mine
- LG6/LGA Reef – Millsell Mine
- Sliping of UG2 pillars in an Eastern Bushveld mine to determine K
- Manganese pillars to describe the effect of joint spacing on pillar strength

**Table 10. Summary of back-calculated K-values from the historic reports**

| Mine | Reef type | Back calculated K - value (MPa) | Comments |
|---|---|---|---|
| Mine A - Styldrift Mine | Merensky Reef | 90 | Study conducted for a 2021 Samerdi project |
| Mine B - Rustenburg area | Merensky Reef | 90 | Bord and pillar layout at depths exceeding 1100 m |
| Mine C - Eastern Bushveld | UG2 | 75 | Work published in Oates and Malan (2023) |
| Mine D - Everest Mine | UG2 | 10 | Pillars weakened by clay layer (alteration zone) |
| Mine E - Wonderkop Mine | LG6/LG6A | 6 | Pillars weakened by clay layer (alteration zone) |
| Mine F - Rustenburg area | LG6/LG6A | 58 | This may be a minimum value and K may be higher |

## 4.4 *Further back-analysis of the Merensky Reef pillars at Styldrift Mine*

An underground visit to the mine was conducted on 16 February 2024 by Prof Francois Malan and Mr Johann Esterhuyse. The current mining outline is shown in Figure 51 and this can be compared to the outline in 2021 presented in Figure 1.


**Figure 51. Extent of mining at Styldrift Mine**

### 4.4.1 Observations of pillar behaviour

The mine used several different pillar sizes. Some of the first mining areas used a layout consisting of 8 m wide pillars with 8 m bords. This was changed to 6 m wide pillars following an industry-wide directive from the DMR that bord widths should not be greater than 6 m.

The smaller pillar sizes resulted in excessive pillar spalling at Styldrift and the pillar sizes were increased to 7 m by the time of the first back-analysis done in 2021. The recent visit on 16 February 2024 was therefore a follow-up visit to examine the behaviour of the revised pillar sizes. The key objective of the visit was nevertheless to examine the older 6 m wide pillars in a different area from that previously visited in 2021 to examine the pillar spalling and other signs of instability which may indicate that the pillars are loaded close to their peak strength. The visit was confined to the areas as indicated on the mine plan in Figure 52. The 7 m wide pillars in the face area were in a very good condition. Some of the best photographs taken are shown below. Photography is sometimes difficult due to the large open areas, poor lighting and other factors, but these photographs are nevertheless a good record of the condition of the pillars as recorded during the visit.

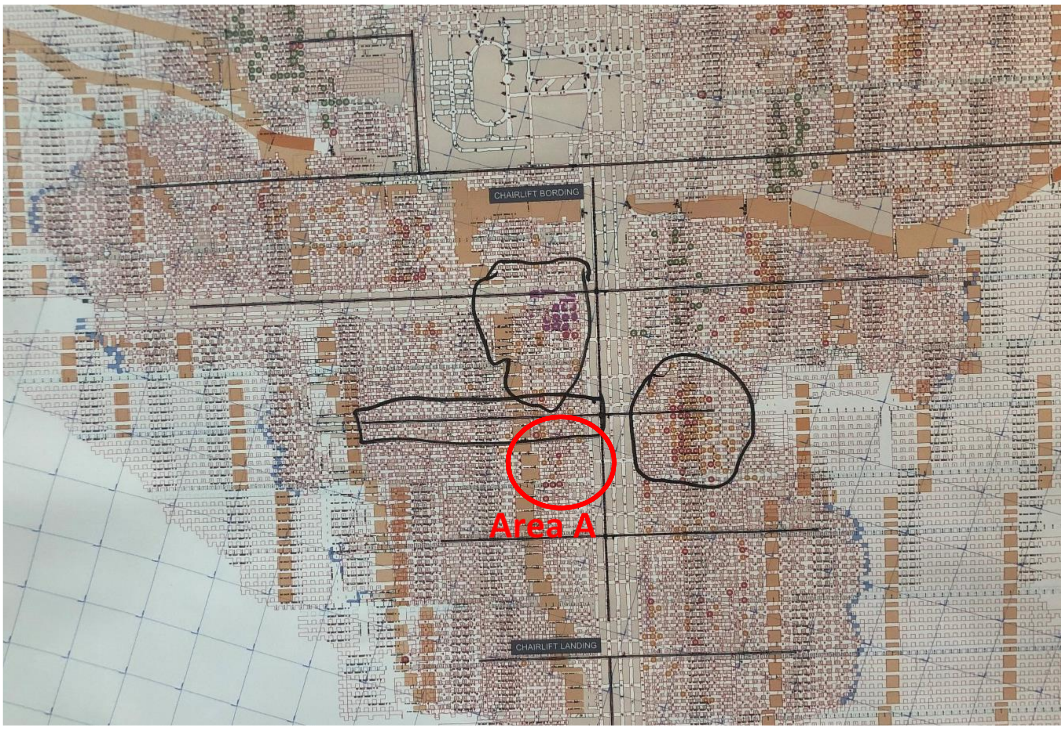


**Figure 52. Areas visited at Styldrift Mine for the back analysis of pillar strength (hand drawn outlines). The modelling was done for Area A**

The pillar classification proposed by Esterhuizen (2006) was used to record the amount of pillar damage observed. This is shown in Figure 53 and is useful to record an unbiased description of the amount of failure. Although this classification was developed for limestone pillars in the US, it was found useful in the other mines of the Bushveld Complex to make the pillar observations more objective. Esterhuizen (2006) noted that pillars with condition ratings of 1-3 can typically be made safe by regular spalling procedures and may require occasional bolting or mesh. Mine operators will typically barricade off areas that contain pillars with condition ratings of 4 and 5.

Table 1. Pillar Stress Rating

| Rating | Sketch | Description |
|---|---|---|
| 1 None | | No stress related fracturing or spalling observed. Joint or blast related damage may exist. |
| 2 Minor | | Minor slabs or spalling, fractures through intact rock at corners, pillar corners and walls may be concave, does not typically deteriorate after initial mining and scaling. |
| 3 Moderate | | Slabbing, onion-skin, fractures more than 1m long, joints opened, corner damage, pillars may need re-scaling after initial development. Original square pillar shape maintained. |
| 4 Severe | | Spalling to hourglass shape. Open cracks in pillar more than 1m long, debris around pillar, original square shape of pillar no longer visible, saw tooth slabs on ribs |
| 5 Very Severe | | Formation of large open cracks, extreme hourglass. Pillar likely lost most of its residual strength. |

Table 2. Geological Structure Rating

| Rating | Sketch | Description |
|---|---|---|
| 1 None | | Less than 0.3 m (1 ft) of joint related fallout during blasting. Blast damage may exist. |
| 2 Minor | | Pillar shape affected by 0.3- 1 m (1-3 ft). Some joint or bedding fallout during blasting, may form step at bedding planes. No or little further fallout after initial scaling. |
| 3 Moderate | | Pillar shape affected by 1-3 m (3-10 ft). Joint or bedding controlled fallout. Fallout can continue after initial mining and scaling. |
| 4 Severe | | Large block fallout >3 m (>10 ft). Pillar shape compromised by large block extrusion or block sliding on steep plane. Falls continue after initial mining and scaling. |
| 5 Very Severe | | Pillar bisected by through-going structure dipping at more than 35 degrees. Potential or actual loss of top half of pillar. Pillar strength depends on discontinuity strength. |

**Figure 53. Pillar rating system proposed for limestone mines (after Esterhuizen, 2006)**

To maximise the value of the visit, the mine plans were carefully inspected. The input from the Shaft Rock Engineer was invaluable to identify the areas where significant pillar spalling occurs. It is expected that the stresses acting on the pillars in these areas will be close to the peak strength of the pillar. The simulated APS will be a good approximation of the pillar strength and an approximate K-value can be calculated. All the area indicated by the black outlines and the red circle in Figure 52 were visited, but the main area for the back analysis is indicated as Area A. Area A was ideal for a modelling back analysis as it was between two lines of large barrier pillars and the 6 m wide pillars in this area were subjected to significant spalling. This area was in the deeper section of the mine. Several pillars were studied and the following information was recorded:

- Pillar dimensions
- Pillar classification (according to Esterhuizen, 2006)
- Comments on behaviour and geology
- Photographs of the four sides of the pillar

Not all the pillars inspected were photographed nor classifications recorded during the visit. Only a limited number of pillars are also presented in this report as these are representative of the typical conditions in the area and can be used for a representative back-calculation of the K-value in the Hedley and Grant strength formula.

Figure 54 is an image showing the typical pillar conditions observed during the visit. Some of the pillars were reinforced using shotcrete, making it difficult to identify geological structures and fracturing. It does, however, also make any time-dependent deterioration easy to identify when the shotcrete starts to crack. Only limited pillar spalling has occurred during the period from the application of the shotcrete to the date of the visit for many of the pillars, so the confinement does seem to work. In many other cases, however, the pillar dilation has destroyed the confinement as shown in Figure 55.

**Figure 54. Typical condition of the older pillars in vicinity to Area A**

**Figure 55. Examples where the pillar support failed. This is some distance away from Area A**

For Area A, the positions of the pillars of interest are indicated in Figure 56 and their associated information is shown in Table 11. The pillar numbers used are identical to those on the mine survey plans. The general conditions of the pillars in this area are poor and significant pillar sidewall deterioration was observed. Excessive spalling was observed during the visit. This is an indication that the pillars are loaded close to or even more than their peak strength. The depth of the area in Figure 56 varies as the dip is in the region of 8°. The depth at the centre of the area is 594 m and this was used for the modelling.

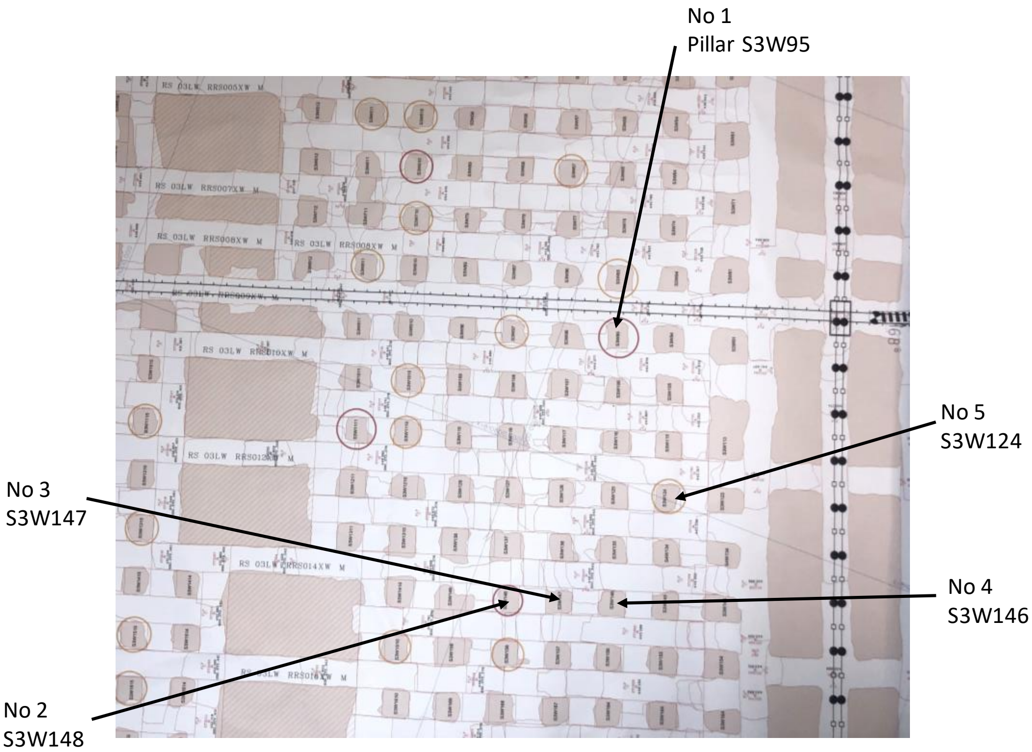


**Figure 56. Pillars of interest in Area A**

**Table 11. Pillar data for Area A.**

| No | Pillar | Pillar Area ($m^2$) | Average Height (m) | Ave. Pillar Depth (m) | Pillar Class |
|---|---|---|---|---|---|
| **1** | S3W95 | 27.94 | 2.4 | 594 | 2 - Minor |
| **2** | S3W148 | 23.78 | 2.4 | 594 | 3 - Moderate |
| **3** | S3W147 | 29.6 | 2.4 | 594 | 4 - Severe |
| **4** | S3W146 | 31.68 | 2.4 | 594 | 4 - Severe |
| **5** | S3W124 | 28.13 | 2.4 | 594 | 4 - Severe |

Some of the other photographs of the pillar conditions in Area A are shown in Figures 57 to 61. These pillars have been subjected to significant spalling.

The mining adjacent to S3W95 (Figure 57) was not conducted on a parting plane in the hangingwall and hence the top of the pillar was concave, while the bottom of the pillar had some broken ore piled against the sidewalls. The pillar showed signs of deterioration. The pillar was located along the belt drive and had been supported using mesh and strapping trusses.

**Figure 57. Photographs showing the condition of S3W95**

Figure 58 illustrates that the mining adjacent to S3W148 was also not done on a contact plane in the hangingwall and the top of the pillar has a concave contact. The pillar was the smallest pillar visited in the area, with a size of 23 m$^2$. The pillar showed indications of moderate deterioration. There was some ore laying against the bottom sidewalls of the pillar.

**Figure 58. Photographs showing the condition of S3W148**

Pillar S3W147 is shown in Figure 59. The pillar was not cut straight on all sides. The pillar showed signs of failure along the joint planes. The pillar had a sharp to concave hangingwall contact and some broken ore was laying against the bottom contact of the pillar.

**Figure 59. Photographs showing the observed conditions for S3W147**

Figure 60 illustrates the conditions observed for S3W146. The pillar was not cut on a hangingwall contact and thus had a concave contact. Some of the broken rock from the spalling were laying at the base of the pillar. The pillar seems to be in a failed condition.

**Figure 60. Photographs showing the observed conditions for S3W146**

Pillar S3W124 is shown in Figure 61. The pillar was not cut straight on all sides. The pillar had significant signs of failure. The presence of joints plays a role in the mechanism of failure. The pillar had a sharp to concave hangingwall contact and some of the failed spalling was laying against the bottom contact of the pillar.

**Figure 61. Photographs showing the conditions of S3W124**

#### 4.4.2 Numerical modelling of pillar stress

Like the previous back analysis of Styldrift Mine described in Section 4.2.1, the TEXAN code was also used for this second study. It is a displacement discontinuity boundary element (DD) code and it was developed specifically to simulate many small pillars in tabular layouts (Napier and Malan, 2007; Esterhuyse and Malan, 2018). The code allows the use of triangular boundary elements and these elements and the modelling approach circumvent the problem of "partially mined" elements.

For a database of pillar behaviour, such as for the data collected in this study, it is necessary to know the stress acting on each pillar to enable pillar strength calculations to be done. For the earlier study on pillar strength, such as Salamon and Munro (1967) and Hedley and Grant (1972), the pillar stress was estimated using tributary area theory (TAT). TAT is a conservative approach as it assumes a regular layout, with all pillars of equal size, with the layout continuing to infinity in all directions. The effect of large pillars and abutments are not considered (see Napier and Malan, 2011). A more accurate approach was used for this study by simulating the average pillar stress (APS) using numerical modelling techniques.

To simplify the digitising of the outlines and the meshing procedure, the pillar outlines were approximated using straight line segments, Figure 62 represents the model of Area A meshed with triangular elements. The triangular elements are too small to see in the diagram. It should be emphasised that the simulation done for this study is state of the art as it is practically impossible to build this model, with the irregular pillar shapes, using finite difference of finite element codes. An enlarged of part of the model is shown in Figure 63. Some of the pillar numbers used in the study are also shown in the figures.

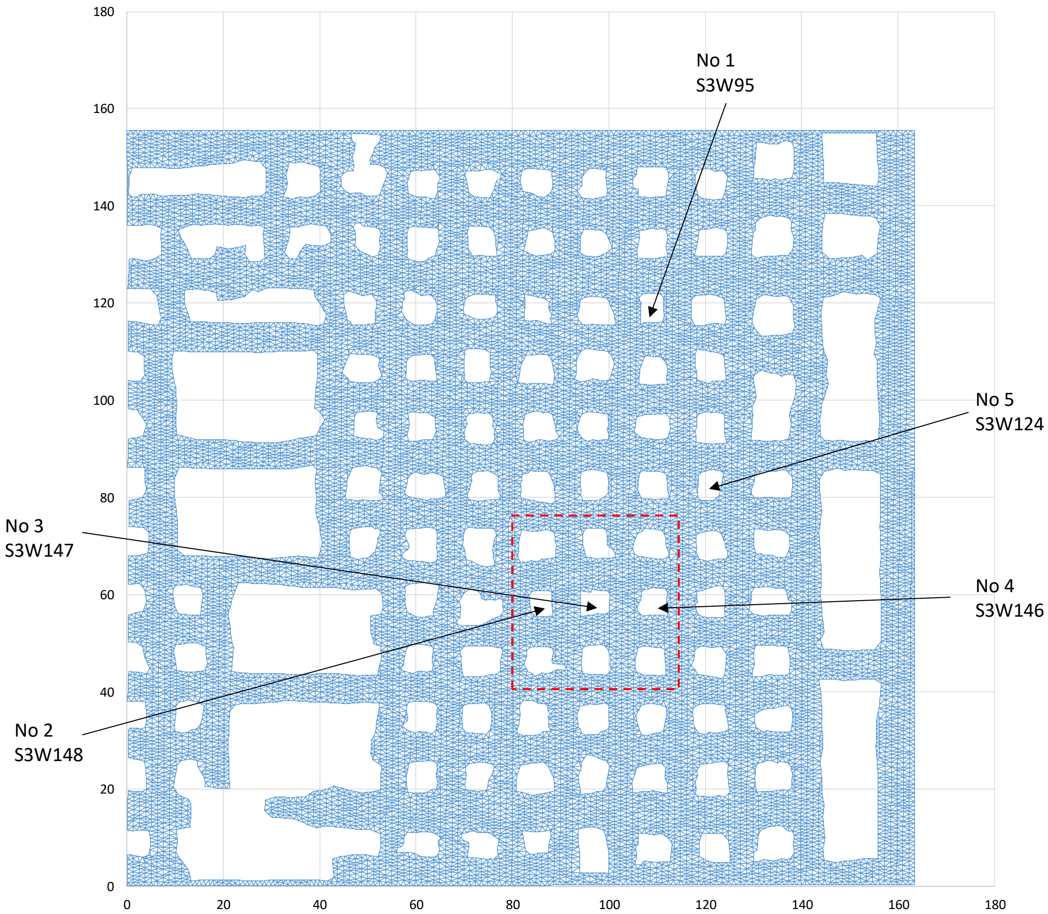


**Figure 62. Diagram illustrating a portion of the digitised layout. Note the irregular pillar shapes and triangular elements that forms the mesh. The pillar numbers are according to the numbering on the mine plans. A zoomed plot of the area enclosed by the red dashed line is given in Figure 63**

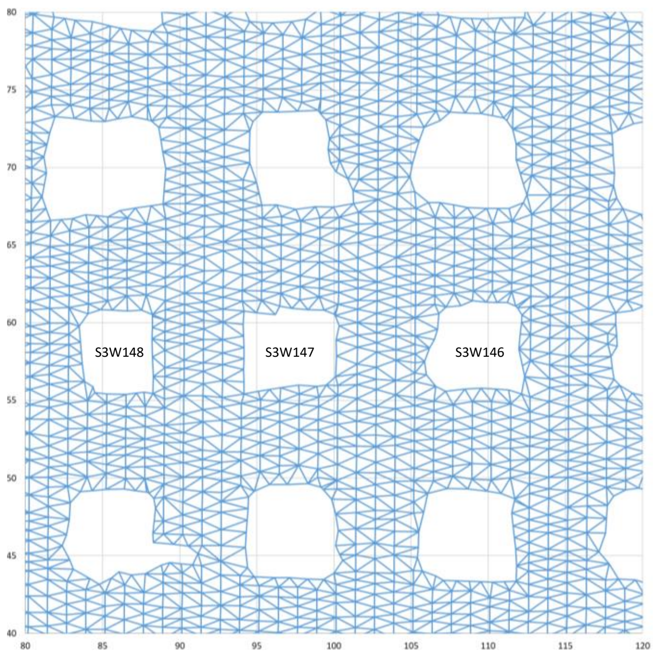


**Figure 63. Diagram illustrating the digitised and meshed model of Area A of the layout at Styldrift Mine. The pillar numbers are according to the numbering on the mine plans**

As part of the analysis, the pillars also had to be covered with a triangular mesh to enable the calculation of the average pillar stress (APS). Figure 64 illustrates the mesh for pillar S3W146 as an example. Regarding element size, it is known that when using displacement discontinuity boundary element modelling, the simulated average pillar stress (APS) is affected by element size. This was explored by Napier and Malan (2011). For known analytical solutions of APS, it was found that the simulated APS approximates the analytical values closely if the element size tends to zero. Small element sizes are therefore needed for these simulations. For the purposes of this study, the element sizes shown were considered adequate and it should be noted that these sizes are significantly smaller than the typical 5 m - 10 m square element sizes used for many years in industry for the MINSIM-type simulations.

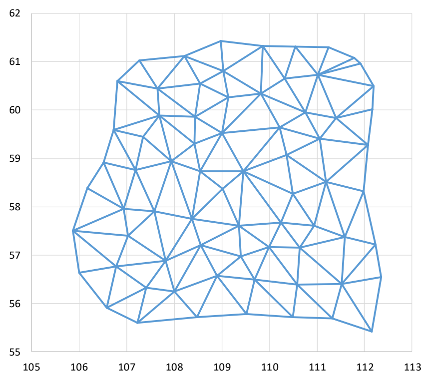


**Figure 64. Example of the mesh generated for S3W146**

The input parameters of the numerical model were selected to match the information supplied by the client as far as possible. For the unknown values, reasonable figures had to be assumed. The density of the overburden rock was assumed to be 3000 kg/m$^3$. The stress k-ratio was assumed to be unity in both horizontal directions.

For the mining excavations, a constant depth below surface of 594 m was used for the simulation of Area A. Although there are variations in depth as indicated on the plan, the excavation was simulated with no dip to simplify the model, while the depth was selected as an average of the simulated area.

From the underground visits and discussions, it was noted that the mining height varied throughout the operation, although an average of 2.4 m was estimated for the pillars of interest. This value was used to back-calculate the K-value.

### 4.4.3 Numerical modelling results

A simple elastic model with "rigid" pillars was used to simulate the average pillar stresses. The pillars were not allowed to fail or to deform. This is like the MINSIM-type models used in the gold mining industry for many decades. Figure 65 illustrates the simulated APS values for the selected pillars. This graph is included to illustrate the variation in pillar stress. This is caused by the size and position of each pillar. It will be difficult to identify individual pillars on this graph and Table 12 is included to search for individual pillars. This illustrates the advantage of simulating the actual pillar shapes as the pillar stress is not uniform throughout the layout. In general, the pillar stress is reduced if the pillar size is increased or if the pillar is close to other large pillars or the solid abutments.

The virgin vertical stress at a depth of 594 m for the assumed overburden density is 17.8 MPa. The simulated pillar APS values are significantly higher than the virgin stress.

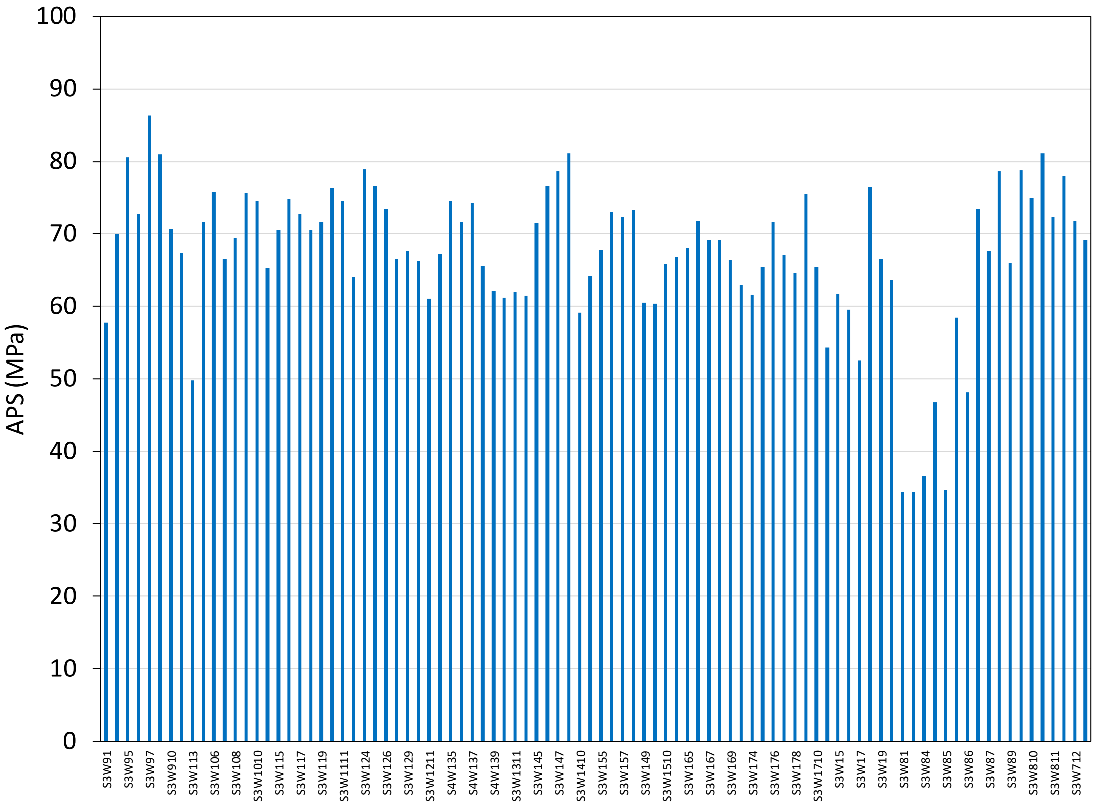


**Figure 65. Simulated pillar APS**

**Table 12. Simulated pillar stress in Area A. The pillars for which the photographs are given above is highlighted in bold**

| Report No | Pillar No | Area ($m^2$) | Circumference (m) | APS (MPa) |
|---|---|---|---|---|
| | S3W91 | 63.96 | 29.54 | 57.8 |
| | S3W94 | 41.43 | 24.42 | 69.99 |
| **1** | **S3W95** | **27.94** | **20.35** | **80.52** |
| | S3W96 | 39.27 | 24.25 | 72.75 |
| | S3W97 | 26.51 | 21.11 | 86.27 |
| | S3W98 | 31.49 | 21.01 | 80.93 |
| | S3W910 | 41.13 | 23.69 | 70.63 |
| | S3W911 | 39.65 | 23.98 | 67.42 |
| | S3W113 | 113 | 43.98 | 49.73 |
| | S3W105 | 37.11 | 23.35 | 71.63 |
| | S3W106 | 30.84 | 21 | 75.69 |
| | S3W107 | 45.03 | 25.63 | 66.49 |
| | S3W108 | 39.6 | 24.15 | 69.45 |
| | S3W109 | 36.58 | 23.13 | 75.65 |
| | S3W1010 | 31.5 | 21.34 | 74.48 |
| | S3W1011 | 39.51 | 23.71 | 65.33 |
| | S3W115 | 37.08 | 23.37 | 70.53 |
| | S3W116 | 34.21 | 21.96 | 74.84 |
| | S3W117 | 33.39 | 21.7 | 72.74 |
| | S3W118 | 38.36 | 23.78 | 70.57 |
| | S3W119 | 36.69 | 22.69 | 71.65 |
| | S3W1110 | 31.45 | 21.49 | 76.37 |
| | S3W1111 | 28.65 | 21.54 | 74.49 |
| | S3W123 | 43.93 | 25.19 | 64.02 |
| **5** | **S3W124** | **28.13** | **19.72** | **78.94** |
| | S3W125 | 33.28 | 21.85 | 76.62 |
| | S3W126 | 33.22 | 21.5 | 73.4 |
| | S3W127 | 40.13 | 23.89 | 66.59 |
| | S3W129 | 34.37 | 22.42 | 67.58 |
| | S3W1210 | 40.07 | 24.6 | 66.28 |
| | S3W1211 | 46.99 | 26.47 | 61.03 |
| | S4W134 | 37.56 | 23.61 | 67.2 |
| | S4W135 | 33.73 | 21.63 | 74.48 |
| | S4W136 | 37.54 | 22.77 | 71.68 |
| | S4W137 | 32.69 | 22.64 | 74.21 |
| | S4W138 | 45.63 | 26.05 | 65.64 |
| | S4W139 | 46.38 | 27.47 | 62.09 |
| | S3W1310 | 44.29 | 26.55 | 61.24 |
| | S3W1311 | 35.5 | 22.55 | 61.99 |
| | S3W144 | 45.05 | 26.1 | 61.41 |
| | S3W145 | 34.57 | 22.62 | 71.45 |
| **4** | **S3W146** | **31.68** | **21.73** | **76.51** |
| **3** | **S3W147** | **29.6** | **21.78** | **78.62** |
| **2** | **S3W148** | **23.78** | **18.63** | **81.14** |

### 4.4.4 Calibration of the pillar strength formula

As stated above, based on the previous project, the power-law equation and exponents of the Hedley and Grant formula appears to be a reasonable approximation to account for variations in pillar width and height. This formula was therefore also used for this study. The typical general form of this formula is given below for completeness:

$$\sigma_s = K\frac{w^\alpha}{h^\beta} \tag{4}$$

where $K$ reflects the fitted 'strength' of the in-situ rock, $w$ is the width of the pillar and $h$ is the mining height.

Based on the poor conditions of the Styldrift pillars illustrated in Figures 57 to 61, a reasonable minimum estimation of the K-value can be obtained by using the simulated APS value in the previous section as the pillar strength. To calculate the estimated K-value ($K_{min}$), equation (4) can be rewritten as:

$$K = \frac{\sigma_s h^\beta}{w^\alpha} \tag{5}$$

If it is assumed that $\sigma_s = APS$, then $K = K_{min}$ and it follows

$$K_{min} = \frac{(APS)h^\beta}{w^\alpha} = \frac{(APS)h^{0.75}}{w^{0.5}} \tag{6}$$

Equation (6) was used to calculate $K_{min}$ for the APS values given above in Table 12 for the five pillars of interest. This is given in Table 13 below. The nature of the power-law equation is such that the calculated value for $K_{min}$ is sensitive to the mining height. For example, $2.2^{0.75} = 1.8061$ whereas $2.5^{0.75} = 1.98818$. A 300 mm difference in pillar height therefore results in a 10% difference in back-calculated $K_{min}$. Also, important to understand is the following: As this is a back-calculation of the K-value, a larger mining height gives a larger value for $K_{min}$. A first estimate for this area was done by assuming the average mining height for the area is 2.4 m.

**Table 13. Back calculated K-values ($K_{min}$) for a selected number of pillars in Area A**

| Report No | Pillar No | Area ($m^2$) | Circumference (m) | APS (MPa) | $W_{eff}$ (m) | h (m) | $K_{min}$ (MPa) |
|---|---|---|---|---|---|---|---|
| **1** | **S3W95** | 27.94 | 20.35 | 80.52 | 5.49 | 2.40 | 66.25 |
| **5** | **S3W124** | 28.13 | 19.72 | 78.94 | 5.71 | 2.40 | 63.72 |
| **4** | **S3W146** | 31.68 | 21.73 | 76.51 | 5.83 | 2.40 | 61.09 |
| **3** | **S3W147** | 29.60 | 21.78 | 78.62 | 5.44 | 2.40 | 65.02 |
| **2** | **S3W148** | 23.78 | 18.63 | 81.14 | 5.11 | 2.40 | 69.24 |

These back-calculated values for K (65 MPa - 70 MPa) appears to be less than for the other area simulated at Styldrift Mine in 2021. A likely reason for this difference is the nature of the rock mass in this second area visited. It appears different owing to the presence of prominent, high density joint sets. This can be seen by comparing Figures 66 and 67 (2024 visit) to Figure 68 and 69 (2021 visit). A different pillar strength calibration will probably have to be used for the different areas in the mine. This is further explored in Section 5.2.

**Figure 66. Typical high density of jointing in the recent area visit in the S3E and S3W areas**

**Figure 67. Another photograph of the high density of jointing in the recent area visit in the S3E and S3W areas. Note the continuation of the joints into the hangingwall**

**Figure 68. Typical condition of the pillars in the N1E and N2E areas of Styldrift Mine simulated in 2021. The joints appear to be less prominent than shown in Figures 66 and 67**

**Figure 69. Another photograph of the typical condition of the pillars in the N1E and N2E areas of Styldrift Mine simulated in 2021. The joints appear to be less prominent than shown in Figures 66 and 67**

## 4.5 *Back-analysis of the pillar strength at Millsell Mine*

The site at Millsell is an interesting case study as very small pillars were left in a section of the mine that was exploited in the 1970s. Figure 70 illustrates part of the larger layout and the area of interest is shown in Figure 71. Note the different layouts, pillar sizes and extraction ratios used at the mine. The LG6/LG6A reef is exploited in this area.

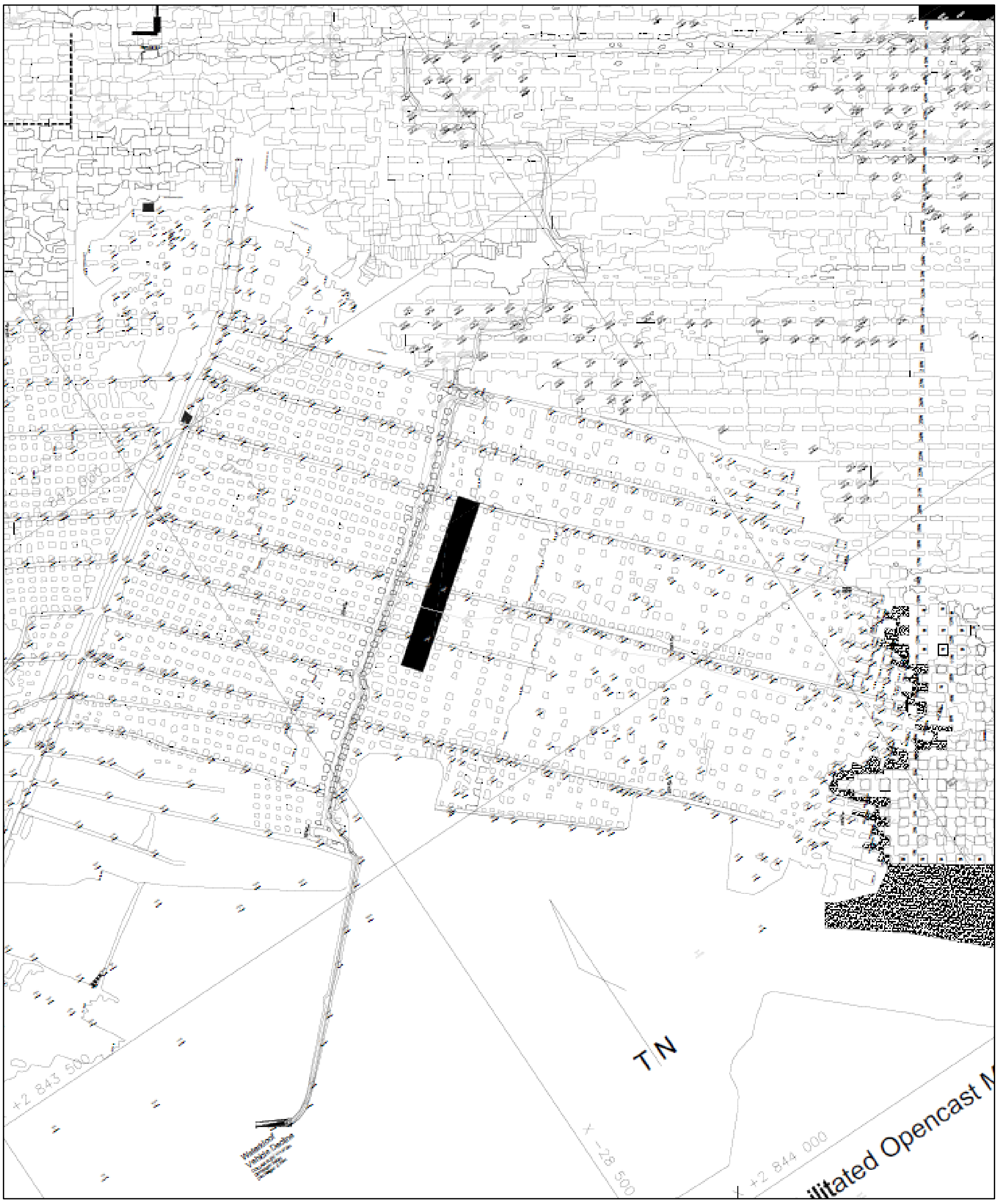


**Figure 70. An older section of the Millsell Mine**

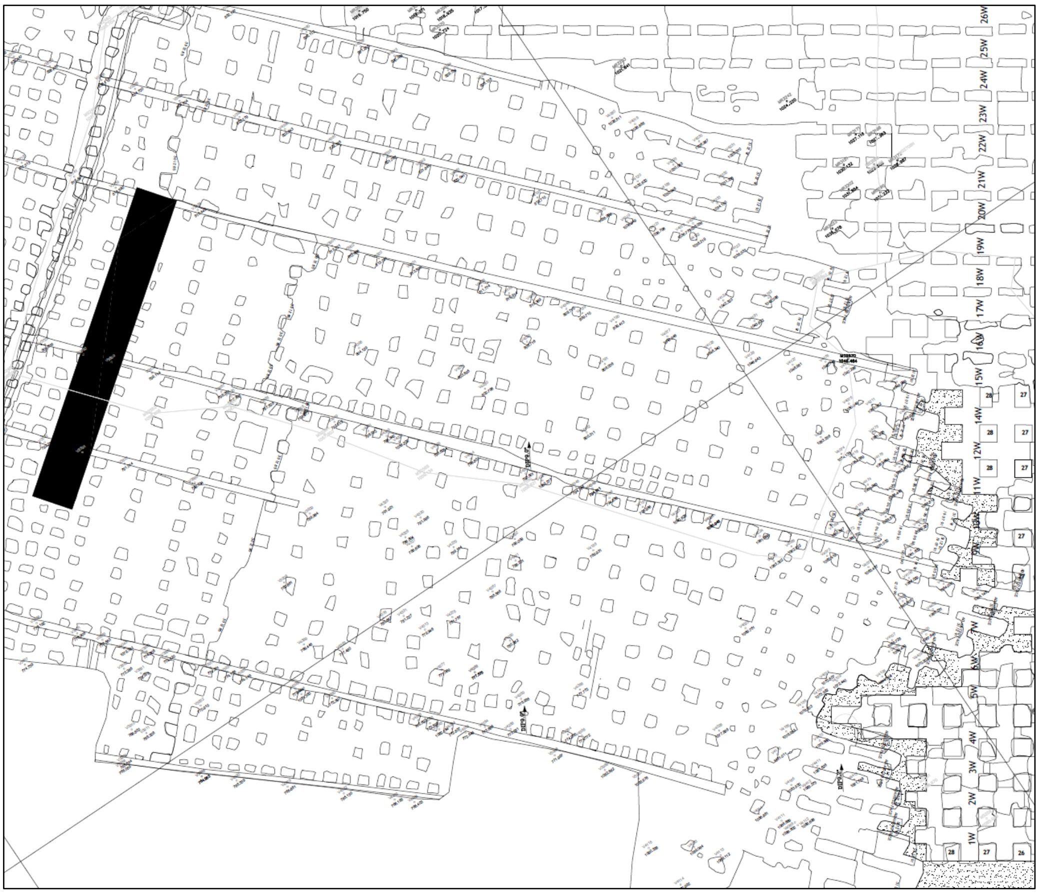

**Figure 71. A zoomed portion of Figure 70 illustrating the small pillars and large spans in some areas**

### 4.5.1 Observations of pillar behaviour

The pillar observations focussed on the area shown in Figure 72 and the photographs were taken on 23 February 2023. The pillar numbers are those used for the numerical modelling described in the next section. Of interest was that pillar 92 had a small area (5.38 $m^2$) with large spans mined adjacent to it. The condition of this pillar was still surprisingly good. These are important observations as the back analysis indicated that the pillars have a higher peak strength than that predicted by the original Hedley and Grant assumptions of $K=\frac{1}{3}UCS$. Only the best images are shown in Figures 73 to 26 as photography was very difficult with the dark chrome pillars and the large open spaces. Standalone light systems with enough brightness will be required to improve the quality of these photographs.

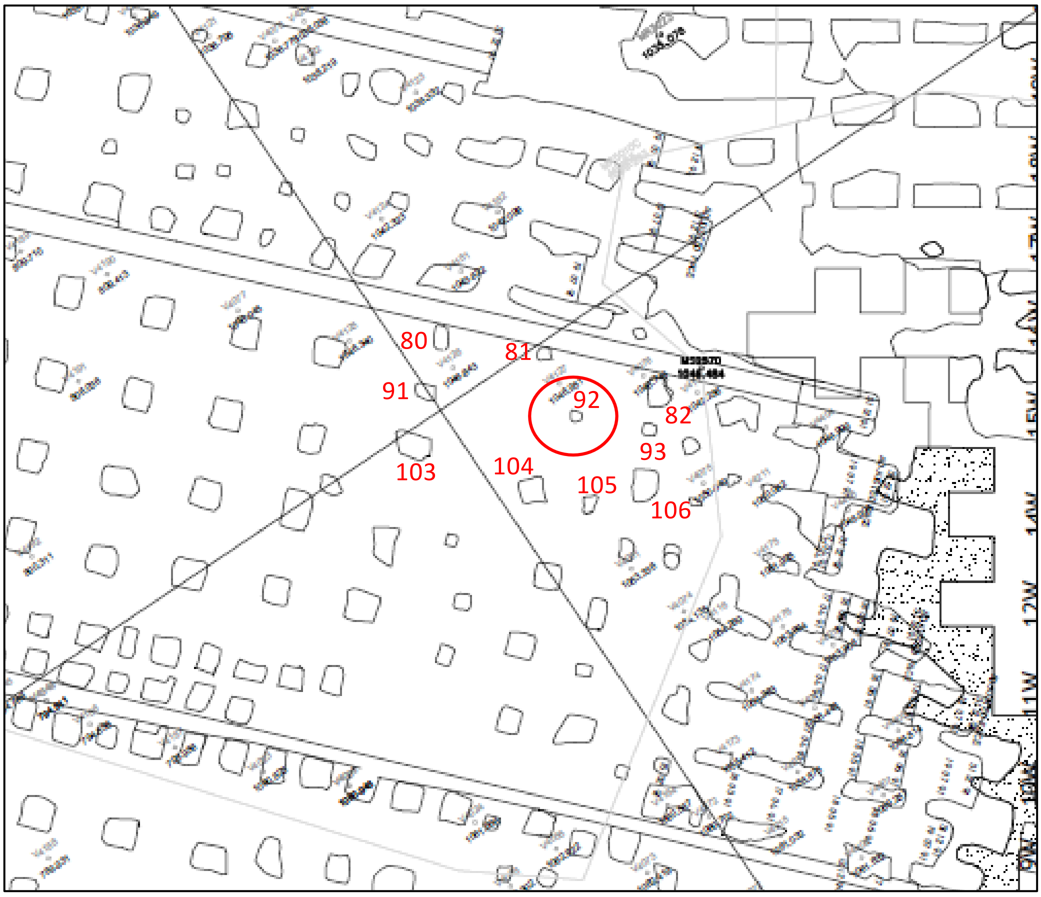


**Figure 72. The pillars of interest are numbered in this figure. Note the small pillars in this area**


**Figure 73. A photograph of pillar 92. This pillar was still in a very good condition and it is deemed to be intact**


**Figure 74. A photograph of pillar 93. This pillar was still in a very good condition**


**Figure 75. View of pillar 105. This pillar was still in a very good condition**


**Figure 76. View of pillar 82. This pillar was still in a very good condition**

### 4.5.2 Numerical modelling of pillar stress

Similar to the methodology described in Section 3.2.2, the TEXAN code was used for the modelling analysis. The reader is referred to that section for general background. The key aspect for the modelling in this section is that pillar 92 is only 101 m below surface and it is therefore shallow. The traditional "infinite" depth DD solvers do not account for this shallow depth and it underestimates the pillar stress, unless a "mined" stope of sufficiently large extent is included at the surface position.

A valuable attribute of the TEXAN code is the inclusion of a finite depth solver. Compared to the historical DD codes used in the industry, a more accurate method to represent the free surface is to make use of special boundary element influence functions that automatically meet the prescribed boundary conditions along the surface. The need for the physical inclusion of a plane of elements along the surface is therefore not required. The derivation of these special boundary element solutions can be accomplished by the application of the classical "method of images" described by Landau and Lifschitz (1986). Many of the published results relate either to two-dimensional cases (Crouch, 1973) or to restricted three-dimensional problems such as the case of a surface-parallel excavation or an excavation with square elements having one axis parallel to the free surface. Napier and Malan (2007) derived the influence function expressions in a general form to allow these to be incorporated in polygonal shaped elements and to allow for the employment of higher order discontinuity variation shape functions in each element.

Like the analysis described above, the pillar outlines were approximated using straight line segments, Figure 77 represents the simplified model.

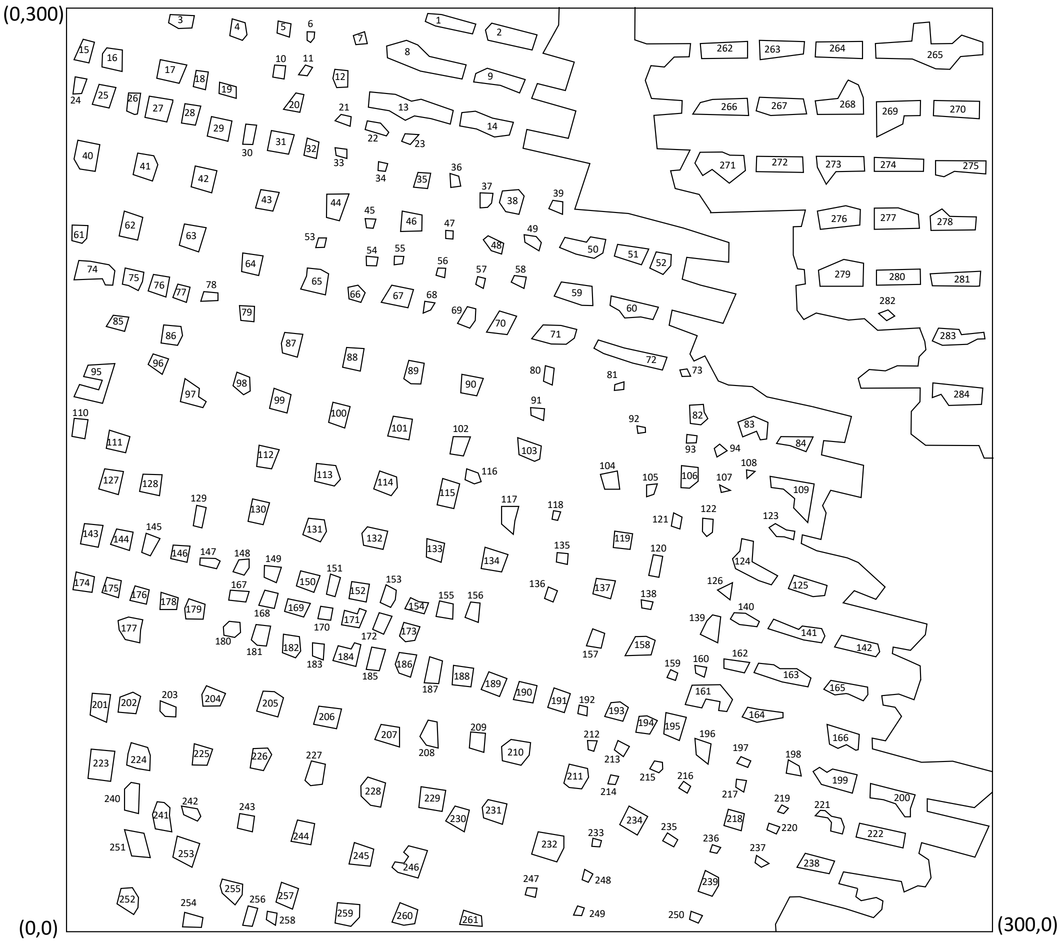


**Figure 77. A simplified outline of the geometry using straight-line polygons. This simplified the digitising and meshing process**

Different mesh sizes were used to simulate the geometry. An example of the fine mesh for pillar P92 is shown in Figure 78. The entire mined geometry was covered with a similar mesh.

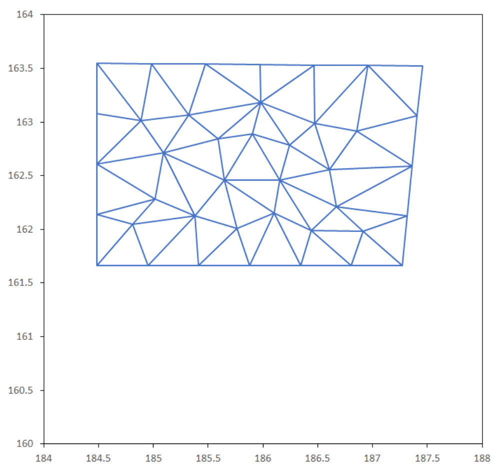


**Figure 78. Mesh used for pillar 92**

Again, the model input parameters of the numerical model were selected to match the information supplied by the client as far as possible. The density of the overburden rock was assumed to be 3100 kg/m$^3$. This is slightly higher than that used for Styldrift as the density of the overlying pyroxenite is 3400 kg/m$^3$. When considering the weathering close to surface, an average density of 3100 kg/m$^3$ is estimated by the mine. This will have to be verified in future as it greatly affects the simulated APS values. The stress k-ratio was assumed to be unity in both horizontal directions, but this is irrelevant if the workings is simulated with a dip of zero degrees.

For the mining excavations, a constant depth below surface of 101 m was used for the simulation. Although there are variations in depth as indicated on the plan, the excavation was simulated with no dip to simplify the model, while the depth was selected as an average of the simulated area. The average mining height in the area of interest was 1.8 m.

### 4.5.3 Numerical modelling results

As the excavation is shallow, a number of simulations were run using different element sizes and both the “finite” depth and “infinite depth solves in TEXAN. The summary of the results is shown in Figure 79. This plots the APS of pillar 92 for the different modelling parameters.

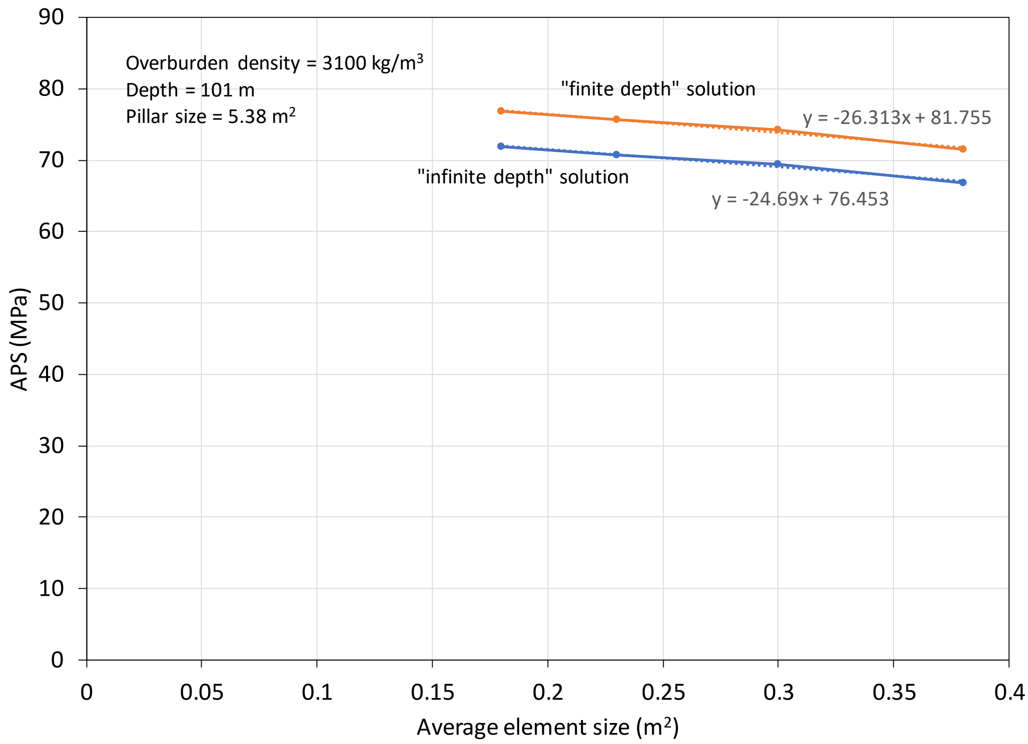


**Figure 79. Effect of element size on simulated APS for pillar 92**

The results shown in Figure 79 has been noted earlier by Napier and Malan (2011) and the simulated APS will approach the analytical APS as the element sizes tends to zero. This dependency on element size is an artefact of the displacement discontinuity modelling technique and will be encountered by codes such as MINSIM, MAP3D and TEXAN using this numerical modelling methodology. To obtain a more accurate answer for the pillar APS, Napier and Malan (2011) proposed a two-step modelling procedure where the geometry is simulated with two different element sizes. The straight line between the two simulated values can be extrapolated to get the y-intercept. In practice the authors always used as small as possible element size and this was deemed acceptable as the slightly lower simulated APS value is a conservative value giving a conservative K-value. This is deemed acceptable as other assumptions, such as the overburden density, may not be correct. The element size used in Section 3.2.2 is therefore considered acceptable.

The linear trend shown in Figure 79 imply that if two APS values of $APS_1$ and $APS_2$ are found, corresponding to grid size values of $g_1$ and $g_2$ respectively, then the extrapolated value (for the APS limit as the grid size tends to zero) can be estimated from the equation (also see Napier and Malan, 2011):

$$APS = \frac{(APS_2 \times g_1) - (APS_1 \times g_2)}{g_1 - g_2} \tag{7}$$

A further important aspect from the graph shown in Figure 79 is that the "finite depth" solution is important when the excavations are close to surface. This predicts a APS of 81.76 MPa (on the y-intercept) versus 76.45 MPa for the infinite depth solution. Table 14 illustrates the calculated APS for several pillars highlighted in Figure 72. The APS values were calculated from the two simulated values with different grid sizes using equation (7) and the $K_{min}$ was calculated using equation (6).

**Table 14. Calculated $K_{min}$ for the simulation and observations done at Millsell Mine**

| Pillar | Area ($m^2$) | Circum-ference (m) | $W_{eff}$ (m) | h (m) | APS (MPa) Infinite depth El size ≈ 0.38 $m^2$ | APS (MPa) Infinite depth El size ≈ 0.18 $m^3$ | APS (MPa) Infinite depth Calculated | $K_{min}$ (MPa) Infinite depth Calculated | APS (MPa) Finite depth El size ≈ 0.38 $m^2$ | APS (MPa) Finite depth El size ≈ 0.18 $m^3$ | APS (MPa) Finite depth Calculated | $K_{min}$ (MPa) Finite depth Calculated |
|---|---|---|---|---|---|---|---|---|---|---|---|---|
| 80 | 16.12 | 16.97 | 3.80 | 1.80 | 40.53 | 43.78 | 46.71 | 37.23 | 43.60 | 47.06 | 50.17 | 40.00 |
| 81 | 6.77 | 10.79 | 2.51 | 1.80 | 52.88 | 59.60 | 65.65 | 64.40 | 56.56 | 63.70 | 70.13 | 68.79 |
| 82 | 29.00 | 21.45 | 5.41 | 1.80 | 24.85 | 26.03 | 27.09 | 18.10 | 26.35 | 27.58 | 28.69 | 19.17 |
| 91 | 14.10 | 15.42 | 3.66 | 1.80 | 45.20 | 50.64 | 55.54 | 45.13 | 48.78 | 54.61 | 59.86 | 48.64 |
| 92 | 5.38 | 9.50 | 2.27 | 1.80 | 66.84 | 71.89 | 76.44 | 78.92 | 71.51 | 76.85 | 81.66 | 84.31 |
| 93 | 7.70 | 11.28 | 2.73 | 1.80 | 40.95 | 45.22 | 49.06 | 46.14 | 43.54 | 48.04 | 52.09 | 48.99 |
| 103 | 40.64 | 25.45 | 6.39 | 1.80 | 31.04 | 32.92 | 34.61 | 21.28 | 33.59 | 35.60 | 37.41 | 23.00 |
| 104 | 27.11 | 20.99 | 5.17 | 1.80 | 37.42 | 38.92 | 40.27 | 27.53 | 40.28 | 41.86 | 43.28 | 29.59 |
| 105 | 10.34 | 13.65 | 3.03 | 1.80 | 48.45 | 52.87 | 56.85 | 50.75 | 51.92 | 56.62 | 60.85 | 54.32 |
| 106 | 31.49 | 22.24 | 5.66 | 1.80 | 28.45 | 30.34 | 32.04 | 20.92 | 30.31 | 32.30 | 34.09 | 22.26 |

The K-value for pillar 92 is high at 84 MPa. A value of K = 69 MPa is calculated for pillar 81 and 54 MPa for pillar 105. A good estimate of the K-value of the LG6/LG6A pillars may be between 70 MPa – 80 MPa. This agrees approximately with the current back-calculated values for the UG2 pillars. Note that the modelling correctly predicts that pillar 93 will have a much lower APS than 91 as it is in close proximity of the two larger pillars 82 and 106.

In summary, this case study is valuable as it illustrated that the LG6/LG6A pillars may be stronger than the historical case study where K = 58 MPa was determined. This, however, needs to be verified in other areas as well.

## 4.6 *Sliping of UG2 pillars to determine the K-value*

The authors did a numerical modelling back-analysis on an experimental pillar sliping area in a mine in the Eastern Bushveld. The mine reduced the sizes of the pillars to determine improved estimates of the UG2 pillar strength and it was therefore a very good case-study to analyse. The layout is shown in Figure 80 and an enlarged view of the pillars is given in Figure 81.


**Figure 80. Layout in the experimental area where sliping of the UG2 pillars were done**

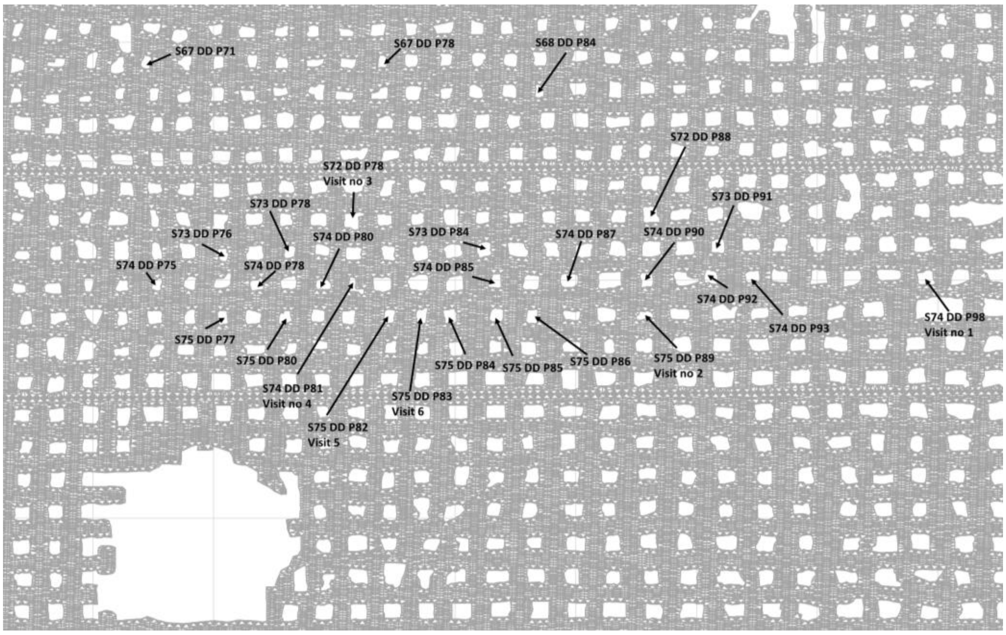


**Figure 81. Pillars studied in the experimental area**

### 4.6.1 Observations of pillar behaviour

Photography was difficult owing to no cameras from visitors being allowed on the premises by the mine. A camera supplied by the mine had to be used. Some of the best photographs are nevertheless illustrated below. The important observation is that no pillar spalling was observed for any of the pillars studied. The pillars are therefore not loaded close to their peak strength yet and the back-calculated K-value will be a low estimate. Figure 82 is an image showing the typical pillar conditions as observed during the visit. Some of the pillars were "white-washed", making it difficult to identify geological structures and fracturing. It does, however, also make any ongoing deterioration easy to identify. Almost no pillar spalling has occurred during the period from the application of the "white-wash" to the date of the visit.

**Figure 82. General condition of the pillars in the area visited. This is for pillar S74 DD P81**

Some of the other photographs of the pillar conditions are shown in Figures 83 to 86. It is clear these pillars are still in a very good condition. The mining adjacent to S74 DD P98 (Figure 83) was not done on a parting plane in the hangingwall and hence the top of the pillar was concave, while the bottom of the pillar had some broken ore piled against the sidewalls. The pillar showed no signs of deterioration.


**Figure 83. Photographs showing the condition of pillar S74 DD P98**

Figure 84 illustrates that the mining adjacent to S75 DD P89 occurred on a parting plane and the top of the pillar has a sharp contact with the hangingwall. The pillar was the smallest pillar visited in the area, with a size of 20 m². The pillar showed no signs of deterioration.


**Figure 84. Photographs showing the condition of pillar S75 DD P89**

Pillars S75 DD P82 and S75 DD P83 are shown in Figures 85 and 86 respectively. No spalling was observed for these pillars.


**Figure 85. Photographs illustrating the condition of pillar S75 DD P82**


**Figure 86. Photographs illustrating the condition of S75 DD P83**

### 4.6.2 Numerical modelling results

The numerical modelling methodology is similar to that described above and the information will not be repeated here. The input parameters were selected based on the information supplied by the mine. The density of the overburden rock was assumed to be 2900 kg/m$^3$. The stress k-ratio was assumed to be unity in both horizontal directions.

For the mining excavations, a constant depth below surface of 245 m was used. Although there are slight variations in depth as indicated on the plan, the excavation was simulated with no dip to simplify the model. The depth was selected as an average of the area simulated. The average mining height in the areas visited was 2.2 m. The simulated APS and the calculated $K_{min}$ is given in Table 15 below.

**Table 15. Calculated $K_{min}$ for the simulation of the UG2 pillar sliping area**

| Pillar number | Area (m$^2$) | Circumference (m) | APS (MPa) | $W_{eff}$ (m) | Height (m) | $K_{min}$ (MPa) |
|---|---|---|---|---|---|---|
| **S75 DD P77** | 23.8 | 18.0 | 54.7 | 5.3 | 2.2 | 42.9 |
| **S74 DD P75** | 18.2 | 16.2 | 69.4 | 4.5 | 2.2 | **59.0** |
| **S74 DD P78** | 24.0 | 18.2 | 56.3 | 5.3 | 2.2 | 44.3 |
| **S73 DD P79** | 24.3 | 18.9 | 58.7 | 5.1 | 2.2 | 46.8 |
| **S74 DD P80** | 25.5 | 17.8 | 54.8 | 5.7 | 2.2 | 41.3 |
| **S73 DD P78** | 22.9 | 16.8 | 54.6 | 5.5 | 2.2 | 42.2 |
| **S73 DD P76** | 20.1 | 16.5 | 60.5 | 4.8 | 2.2 | 49.6 |
| **S72 DD P78** | 44.4 | 28.4 | 42.5 | 6.3 | 2.2 | 30.7 |
| **S74 DD P81** | 23.2 | 23.7 | 58.8 | 3.9 | 2.2 | **53.7** |
| **S75 DD P82** | 25.0 | 17.9 | 57.4 | 5.6 | 2.2 | 43.9 |
| **S75 DD P83** | 26.9 | 20.0 | 56.0 | 5.4 | 2.2 | 43.7 |
| **S73 DD P84** | 33.9 | 21.6 | 46.2 | 6.3 | 2.2 | 33.4 |
| **S74 DD P85** | 25.9 | 19.6 | 56.8 | 5.3 | 2.2 | 44.5 |
| **S75 DD P84** | 29.3 | 20.6 | 53.5 | 5.7 | 2.2 | 40.4 |
| **S75 DD P85** | 29.7 | 18.9 | 55.6 | 6.3 | 2.2 | 40.1 |
| **S75 DD P86** | 27.1 | 18.4 | 57.4 | 5.9 | 2.2 | 42.8 |
| **S74 DD P87** | 26.5 | 20.5 | 55.2 | 5.2 | 2.2 | 43.8 |
| **S67 DD P71** | 19.9 | 15.9 | 53.7 | 5.0 | 2.2 | 43.3 |
| **S67 DD P78** | 18.0 | 14.8 | 60.6 | 4.9 | 2.2 | 49.5 |
| **S68 DD P84** | 17.6 | 15.7 | 64.5 | 4.5 | 2.2 | **55.0** |
| **S72 DD P88** | 39.0 | 24.5 | 39.0 | 6.4 | 2.2 | 27.9 |
| **S73 DD P91** | 31.5 | 20.0 | 45.6 | 6.3 | 2.2 | 32.9 |
| **S75 DD P89** | 20.5 | 17.7 | 58.5 | 4.6 | 2.2 | 49.1 |
| **S74 DD P90** | 29.6 | 20.6 | 49.3 | 5.7 | 2.2 | 37.2 |
| **S74 DD P92** | 29.4 | 19.6 | 46.5 | 6.0 | 2.2 | 34.3 |
| **S74 DD P93** | 27.8 | 19.2 | 49.4 | 5.8 | 2.2 | 37.0 |
| **S74 DD P98** | 37.5 | 22.3 | 36.7 | 6.7 | 2.2 | 25.6 |

The calculated $K_{min}$ for the pillars with a smaller size resulted values as high as 54 MPa, 55 MPa and 59 MPa. These pillars are not showing any signs of failure and these values are therefore considered very conservative. It is therefore indirect evidence that the K-value of 75 MPa given Oates and Malan (2023) is indeed plausible, but additional sliping and smaller pillars will be required to test for this larger value.

## 4.7 *Manganese pillar strength and the effect of joint spacing*

Although manganese pillars are not directly part of the scope of this project, some historic data was included in his study to illustrate the effect of joint spacing and rock mass rating on pillar strength. This provided additional insight as a possible reason for the variable pillar strength at Styldrift Mine in different sections and some new interpretations are given below. Wessels and Malan (2023) conducted a study of the manganese pillars and noted that the pillar spalling behaviour is strongly affected by the spacing of the joint sets. This is illustrated in Figure 87. Although significant spalling was observed for some pillars with a low rock mass rating, all the pillars still appeared to have an intact core and no pillar appeared to be completely failed.

**Figure 87. Differences in the behaviour of manganese pillars caused by the number of joint sets and the spacing of the joints (after Wessels and Malan, 2023)**

Wessels (2022) conducted many back-analyses of manganese pillars in different areas. The modelling was done using a similar methodology as described in the sections above. An example of one of the layouts simulated is given in Figure 88 and the back-calculated $K_{min}$ is given in Table 16.

The pillar rating given in Figure 53 was also used to classify the pillars and the relationship between rock mass rating (RMR) and pillar condition is shown in Figure 89. This is an important result for this study as it indicates that if prominent joints sets are present, significant pillar spalling may occur and the visual appearance of the pillar and the classification will be poor. Interestingly, the $K_{min}$ values given on the graph next to the dots shows no correlation with the pillar condition.

In summary, the back-calculated $K_{min}$ determined from an area with a high rock mass rating should be used with caution in areas with a low rock mass rating. This is particularly important if there are different geotechnical areas with different rock mass rating on a mine.

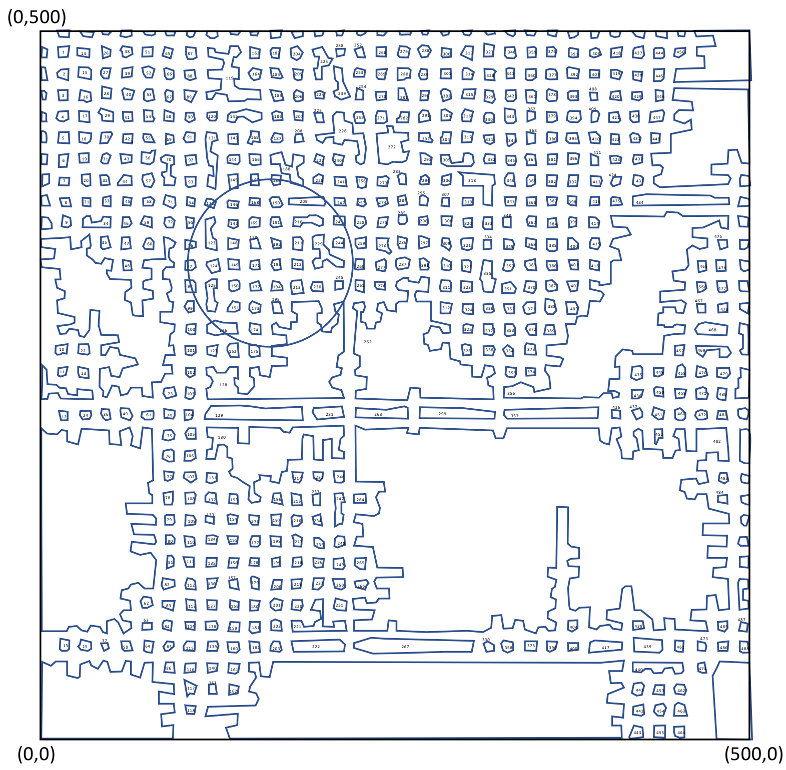


**Figure 88. Typical layout of a manganese bord and pillar mine used to calculate the $K_{min}$ for these pillars (after Wessels, 2022)**

**Table 16. Calculated $K_{min}$ for the simulation of the manganese pillars (after Wessels, 2022)**

| Pillar number | Simulated APS (MPa) | Area ($m^2$) | Circum-ference (m) | $W_{eff}$ (m) | Height (m) | $K_{min}$ (MPa) |
|---|---|---|---|---|---|---|
| **P96** | 75.6 | 42.5 | 26.7 | 6.4 | 4.8 | 97.1 |
| **P97** | 68.9 | 48.2 | 26.8 | 7.2 | 4.8 | 83.3 |
| **P98** | 60.9 | 64.9 | 31.8 | 8.2 | 4.8 | 69.2 |
| **P99** | 67.7 | 41.2 | 25.8 | 6.4 | 4.8 | 86.9 |
| **P125** | 55.7 | 144.4 | 61.6 | 9.4 | 4.8 | 59.0 |
| **P126** | 46.7 | 173.2 | 54.0 | 12.8 | 4.8 | 42.3 |
| **P149** | 69.4 | 60.6 | 31.4 | 7.7 | 4.8 | 81.0 |
| **P150** | 73.4 | 49.1 | 27.1 | 7.2 | 4.8 | 88.4 |
| **P151 (N3_2)** | 71.0 | 46.4 | 27.8 | 6.7 | 5.0 | 91.9 |
| **P171** | 75.4 | 51.8 | 28.9 | 7.2 | 4.8 | 91.3 |
| **P172** | 84.4 | 33.9 | 24.0 | 5.6 | 4.8 | 115.2 |
| **P173 (N3_1)** | 67.7 | 56.5 | 28.5 | 7.9 | 4.8 | 77.9 |
| **P174** | 69.6 | 47.7 | 27.0 | 7.1 | 4.8 | 84.9 |
| **P192** | 85.5 | 37.8 | 25.6 | 5.9 | 4.8 | 114.2 |
| **P193 (N3_9)** | 76.1 | 47.2 | 26.9 | 7.0 | 4.5 | 88.8 |
| **P194** | 72.9 | 43.0 | 25.7 | 6.7 | 4.8 | 91.5 |
| **P195** | 64.6 | 47.9 | 28.2 | 6.8 | 4.8 | 80.4 |
| **P212** | 70.9 | 42.7 | 26.4 | 6.5 | 4.8 | 90.4 |
| **P213** | 53.2 | 81.3 | 35.1 | 9.3 | 4.8 | 56.7 |

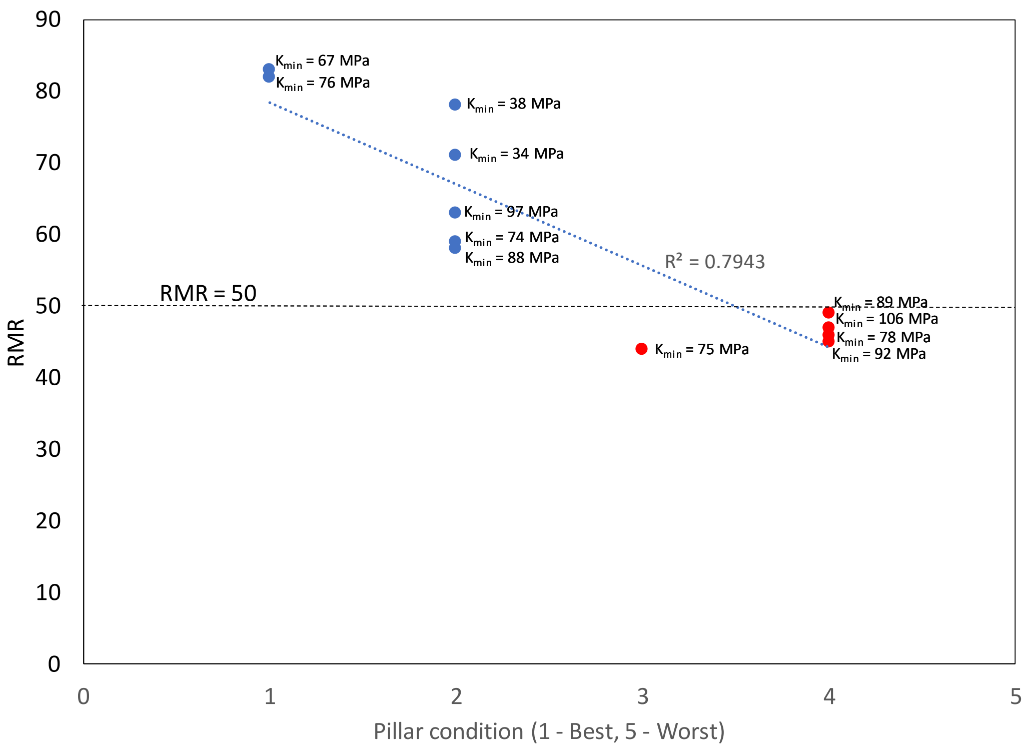


**Figure 89**. Empirical relationship between pillar condition and rock mass rating at BRMO. The red dots indicate the unstable pillars or the pillars with severe spalling. The pillar conditions correspond to the rating given in Figure 53 above (after Wessels, 2022).

# 5 DISCUSSION

## 5.1 *Results Summary*

Based on the information collected, the information in Table 17 was compiled.

**Table 17. Summary of back-calculated K-values**

| Mine | Reef type | Back calculated K - value (MPa) | Comments |
|---|---|---|---|
| *Historic data set* | | | |
| Styldrift Mine | Merensky Reef | 90 | Study conducted for a 2021 Samerdi project |
| Mine in Rustenburg area | Merensky Reef | 90 | Bord and pillar layout at depths exceeding 1100 m |
| Mine in Eastern Bushveld | UG2 | 75 | Work published in Oates and Malan (2023) |
| Everest Mine | UG2 | 10 | Pillars weakened by clay layer (alteration zone) |
| Wonderkop Mine | LG6/LG6A | 6 | Pillars weakened by clay layer (alteration zone) |
| Mine in Rustenburg area | LG6/LG6A | 58 | This is a conservative value and K may be higher |
| *Data set - CSIR* | | | |
| Manganese operations, Hotazel | Manganese | 133 | Evaluated statistical stress and strength distributions and indicated that since no pillar failures have been observed, pillar stress and strength distributions (normal distributions) should not intersect. Tested this assumption for several different K-values and concluded that the applied value appears appropriate. |
| Manganese operations, Hotazel | Manganese | 133 | Several methods were applied and concluded that the indicated K-value is appropriate, based on correlation with local observations. |
| | Massive Sulphide Zone (MSZ) | 34-36 (Poor rock) 56-59 (Good rock) | Substantial work executed including non-linear modelling. DRMS results were applied to derive a K-value. Concluded that the K-value on an operation should be variable and a single value should not be allocated. The applied value is thus rock mass quality related. |
| Managanse operations, Hotazel | Manganese | 131 | Based on previous back analyses, pillar behaviours were confirmed using observations and found the previously back analysed K-value is acceptable. |
| | Chrome (LG6) | 39 | Applied several methods to derive appropriate k-values, including DMRS and back analyses. By looking at failed and stable pillar FOS distributions, it was concluded that the reported K-value is valid if exponents to Hedley and Grant formulation is also increased to α=β=1.0 |
| Styldrift Mine | Platinum (Merensky) | 90 | The noted K-value is concluded to be appropriate for areas with a rock mass quality better than RMR=78.3 only. FOS distributions were analysed using numerical modelling to determine the average pillar stresses. Adding some variability to the K-value, the risk of experiencing pillar failures (defined at FOS<1), was determined. Variability in the K-value increases the risk of pillar failures when a single K-value is utilised, thus various values, |
| *Data set - New analyses* | | ($K_{min}$) | |
| Millsell Mine | LG6/LG6A | 70 - 80 | Pillars intact in spite of small areas and large spans |
| Styldrif - 2nd geotechnical area | Merensky Reef | 61-69 | Area with lower rock mass rating than 2021 study |
| Mine in Eastern Bushveld | UG2 | 59 | Pillars in very good conditions - a conservative value |
| Manganese operations | Manganese | > 100 | Pillar conditions highly dependent on rock mass rating |

Based on the data collected the following conclusions are drawn:

- The hard rock pillars are typically substantially stronger compared to the historic $\boldsymbol{K = \frac{1}{3}UCS}$ assumption in the Hedley and Grant pillar strength formulation. This historic assumption should not be used anymore and the pillar strength should be determined using back analysis, numerical modelling and trial sections. The information below is useful guidelines for this process.
- The following maximum pillar strengths were obtained from the historic and new back analyses (these values are only applicable to rock with a high rock mass rating):
    - Merensky Reef: K = 90 MPa
    - UG2 Reef: K = 75 MPa
    - LG6 Reef: K = 70 MPa
    - Manganese ore: K = 133 MPa
- If there is a weak alteration zone (clay layer) in the pillars, this substantially reduces the pillars strength and a realistic value for the strength, when using the Hedley and Grant formula, will be obtained by using a value of K = 6-10 MPa.

- The rock mass rating and the nature of the joint sets may significantly affect the pillar strength. An important new finding from this study is that a K-value determined from the back-calculated for one area of the mine should be used with caution in other areas with distinctly different rock mass ratings. The design rock-mass strength (DRMS) to estimate a reduced value of K, will be valuable for cases with a low rock mass rating.

## 5.2 *Discussion on the use of DMRS as an estimate for K*

Based on the results above, the following new interpretation should be considered in terms of pillar strength. To account for the effect of rock mass rating on pillar strength, some workers suggested that $K = DRMS$ will be a good approximation (e.g. Stacey and Swart, 2001). The Hedley and Grant equation can then be written as:

$$\sigma_s = DRMS \frac{w^{0.5}}{h^{0.75}} \tag{8}$$

Laubscher (1990) originally proposed that the DRMS can be determined from the empirical rock mass strength (RMR), which is adjusted to consider weathering, mining induced stresses, joint orientation and blasting effects. His full proposed equation for DRMS is (a different notation is used here):

$$DRMS = IRS \times 0.8 \times \frac{RMR - IRS_{rating}}{80} \times Weathering_{adj} \times Orientation_{adj} \times Stress_{adj} \times Blasting_{adj} \tag{9}$$

where

$IRS$ = intact rock strength

$Weathering_{adj}$ = a possible adjustment for weathering of the rock (30% – 100%)

$Orientation_{adj}$= a possible adjustment for the joint orientation (63% - 100%)

$Stress_{adj}$ = a possible adjustment for the difference between maximum and minimum stress (60% - 120%)

$Blasting_{adj}$= an adjustment based on the quality of blasting (80% - 100%)

Note that Laubscher's intention with his original equation was to downrate the UCS to a default value of 80% (the 0.8 factor in the equation – based on work in two Zimbabwean mines) and then apply a further downrating based on the remainder of the ratings in the RMR scheme. To get the remainder as a new fraction, the rating for the UCS is subtracted and the remainder is divided by 80 as the maximum score in RMR for UCS is 20. The 80% downrating of the UCS is "hard-wired" into equation (9). The equation effectively applies a "double downrating" and this may lead to a too conservative value for K.

Furthermore, equation (9) is complex and is difficult to use as many parameters need to be estimated. Probably for this reason, it is rarely used in practical designs in the South African hard rock bord and pillar mines. Many mines use a simplified version by assuming $Weathering_{adj}$ = 100%, $Orientation_{adj}$ = 100%, $Stress_{adj}$ = 100% and $Blasting_{adj}$ = 100%. When these assumptions are inserted into equation (9), it can be simplified as:

$$DRMS = IRS \times \frac{80}{100} \times \frac{RMR - IRS_{rating}}{80} \times 1 \times 1 \times 1 \times 1 = IRS \times \frac{RMR - IRS_{rating}}{100} \qquad (10)$$

As an alternative, if the 80% downrating of the IRS is not adopted and it is assumed that the full rock mass rating value will provide enough “downrating”, equation (9) can be written as:

$$DRMS_{mod} = IRS \times \frac{RMR}{100} \times Weathering_{adj} \times Orientation_{adj} \times Stress_{adj} \times Blasting_{adj} \qquad (11)$$

With the same assumptions of 100% for the last four factors, this can be simplified as

$$DRMS_{mod} = IRS \times \frac{RMR}{100} \qquad (12)$$

This equation should be tested for possible application at Styldrift to calibrate the pillar K-value for different geotechnical areas. If it is assumed that $K = DRMS_{mod}$, then the K-value will be a linear function of the RMR. As a crude example, if the IRS = 120 MPa, a RMR value of 75% will imply K = 90 MPa whereas a RMR of 50% will give a K = 60 MPa.

## 5.3 *Some aspects regarding trial pillar sections*

The recommendation above is to test pillar strength using trial mining sections. The position of a trial site needs to be carefully selected. Ideally, it should be in an isolated area or between regional pillars, that can arrest a potential collapse.

One method to test the estimated pillar strength is to mine a new experimental section. The pillar sizes should be cut according to the dimensions dictated by the new estimate of the pillar strength. A sufficiently large area with enough pillars needs to be mined to ensure the pillars are loaded close to the tributary area stress. As an indication of the size of the experimental area required, Figure 90 illustrates different models simulated with the TEXAN code. Pillar sizes of 7 m x 7 m and an 8 m bord width were used. This is an expanding rectangular mining area and it should preferably be mined between two rows of barrier pillars. The square mining area with a span of 158 m (100 pillars) was used as a base model. For the rectangular models, lengths (L) of W, 2W, 3W, 4W and 5W were simulated (Figure 90). The models were simulated at a depth of 600 m.

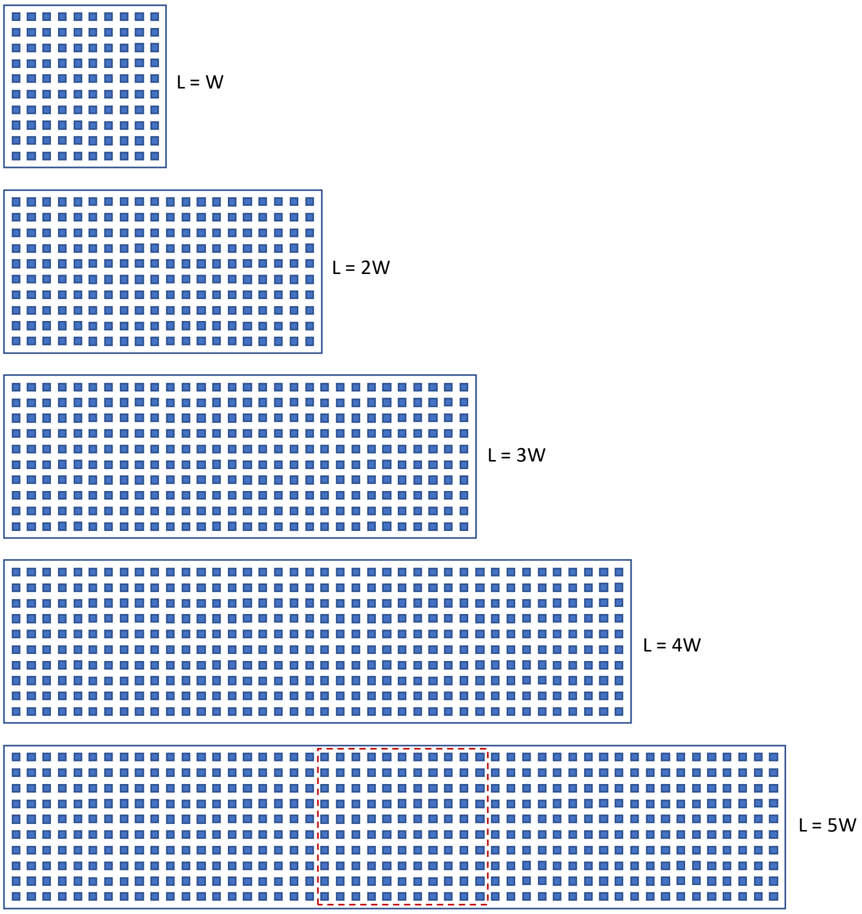


**Figure 90. The rectangular geometries simulated**

The average pillar stress (APS) in each case was calculated for the 100 pillars in the centre of the layout as indicated by the yellow block with a red-dotted borderline for the L = 5W geometry (Figure 90).

The modelling results are shown in Figure 91. The average data was calculated for the centre of each model containing 100 pillars (10 pillars x 10 pillars) as indicated for L = 5W block in Figure 90. An important finding is that for the geometry containing 100 pillars, the peak stress for the pillar in the centre is only 79.6 MPa whereas the tributary area theory (TAT) value is 85.4 MPa. The peak stress is only 93% of the TAT value. This increases to 81.4 MPa for a geometry of L = 5W. This is 95% of the TAT value. Interestingly, this is only slightly more than the square geometry (L = W). The experimental trial section can therefore be of a size 160 m x 160 m, containing approximately 100 pillars, and no significant benefit is derived by increasing the dimension along the strike.

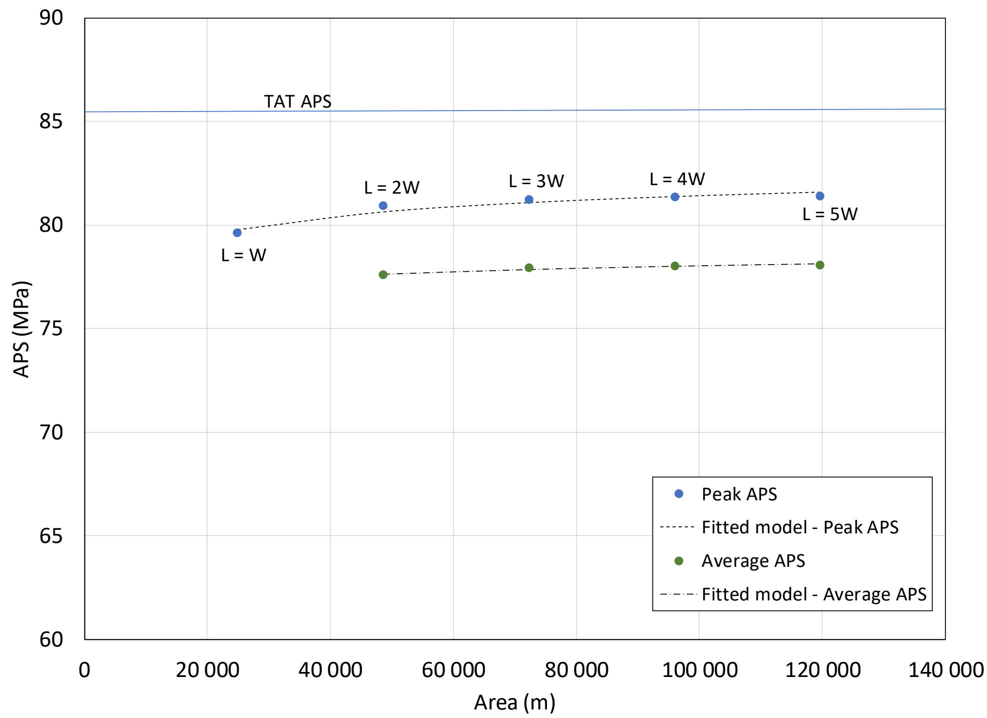


**Figure 91. Simulated peak and average APS values for L=5W block**

Simulated peak and average APS values for the rectangular layouts of increasing length (L) at a depth of 600 m**.**

The second option for a trial section is to do pillar sliping in an old bord and pillar section. A key question to address is what reduction in pillar size is required in this experimental section to test for a K-value when doing a back analysis. Ideally, the pillars need to be reduced in size until the point is reached where the factor of safety ($FOS$) reaches unity. The back-analysis will then confirm the K-value at the point of failure and the actual pillar strength.

This is a difficult problem as the reduction in pillar size decreases the pillar strength, but it also increases the APS values on the pillars. An iterative solution scheme is therefore required to find the correct pillar width for a $FOS = 1$. Consider the partial pillar reclamation in the section shown in Figure 92. The pillar centres, $P_c$, remain constant, while the bords increase from $b_1$ to $b_2$ and the pillar width decreases from $w_1$ to $w_2$. As the pillar centres remain constant, the following requirement must be met:

$$P_c = w_1 + b_1 = w_2 + b_2 \tag{13}$$

After the pillar reclamation, the extraction ratio increases from $e_1$ to $e_2$. The extraction ratio after reclamation is given by:

$$e_2 = \frac{(w_2+b_2)^2-(w_2)^2}{(w_2+b_2)^2} \quad (14)$$

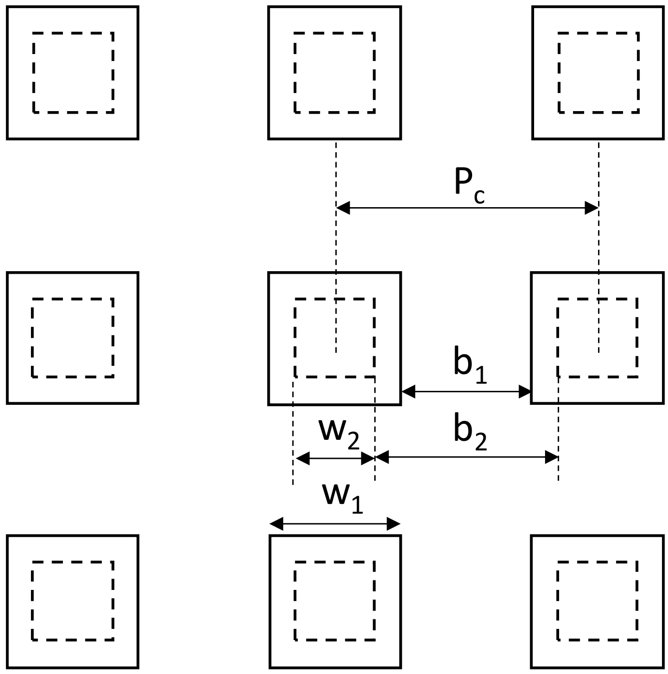


**Figure 92. Notation used for bord and pillar dimensions during partial pillar reclamation.**

By inserting equation (13), equation (14) can be written as:

$$e_2 = \frac{P_c^2-w_2^2}{P_c^2} \quad (15)$$

This can be written as:

$$w_2 = P_c\sqrt{1-e_2} \quad (16)$$

When assuming tributary area theory (TAT), the *APS* after pillar reclamation is given by:

$$APS_2 = \frac{\rho g H}{1-e_2} \quad (17)$$

This can be rewritten as:

$$e_2 = 1 - \frac{\rho g H}{APS_2} \tag{18}$$

Equation (18) can be inserted in equation (16):

$$w_2 = P_c \sqrt{\frac{\rho g H}{APS_2}} \tag{19}$$

For a $FOS = 1$, the APS on the pillars will be equal to the pillar strength or $APS_2 = \sigma_s$ where $\sigma_s$ is given by the general power-law strength equation:

$$\sigma_s = K \frac{w^\alpha}{h^\beta} \tag{20}$$

For this condition, equation (20) can be inserted in equation (19):

$$w_2 = P_c \sqrt{\frac{\rho g H h^\beta}{K w_2^\alpha}} \tag{21}$$

This can be simplified as:

$$\left(\frac{w_2}{P_c}\right)^2 = \frac{\rho g H h^\beta}{K w_2^\alpha} \tag{22}$$

If the exponents of Hedley and Grant are assumed, it becomes:

$$\frac{w_2^{2.5}}{P_c^2} = \frac{\rho g H h^{0.75}}{K} \tag{23}$$

Equation (23) illustrates the complexity of finding the correct pillar width as $w_2$ needs to be solved for the value of K that is required to be tested in the trial pillar reclamation area. Note that the TAT assumption is built into equation (11) and as any trial section will always be smaller than an “infinitely large bord and pillar layout” (see Figure 1), the $w_2$ calculated from this equation will be larger than that for the width at the point of peak pillar strength. There is therefore an automatic increase in the factor of safety, built into equation (23) when applying it in actual layouts of a finite size.

Furthermore, the ensure a stable bord span, a maximum bord width, $b_{max}$, may be specified. From equation (13):

$$b_2 = P_c - w_2 \;\; where \;\; b_2 < b_{max} \tag{24}$$

An interactive process is required to solve for w in equation (23) and a simple method to do is to use the function "Goal Seek" in Excel. The calculated required pillar widths to test for a specific K-value (to load the pillar to the point of failure) for an increase in depth is given in Figure 93. The parameters used were $P_c$ = 14 m, $\rho$ = 2900 kg/m³, $g$ = 9.81 m/s² and $h$ = 2.2 m. It is clear from this solution that it is important to have the experimental trial section at the greatest possible depth as at these greater depths, the K-values can be tested for larger pillars. At shallow depths, very small pillar sizes will be required for large K-values. This may not be feasible. Furthermore, as the restriction of equation (24) also applies, if the maximum bord is restricted to for example $b_{max}$ = 10 m, this will restrict the pillar sizes and K-values that can be tested at shallow depth. This is illustrated in Figure 94 where the bord width is plotted as a function of the K-value to be tested.

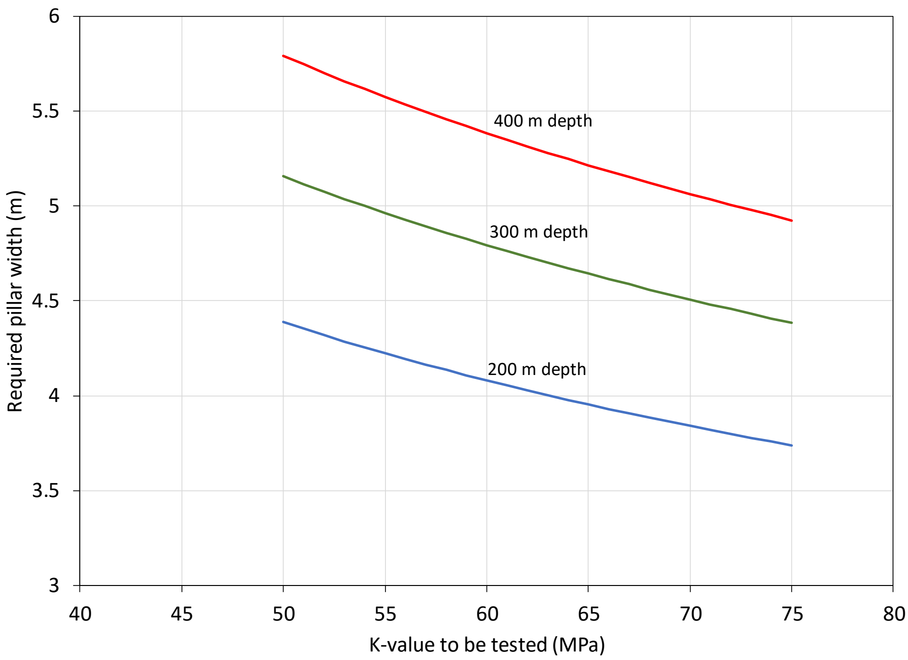


**Figure 93. Pillar width required to test peak pillar strength**

Figure 4 show the required pillar width in a trial pillar reclamation section to test the peak pillar strength in a subsequent back analysis study. Note that this is only applicable to the parameters specified in the text.

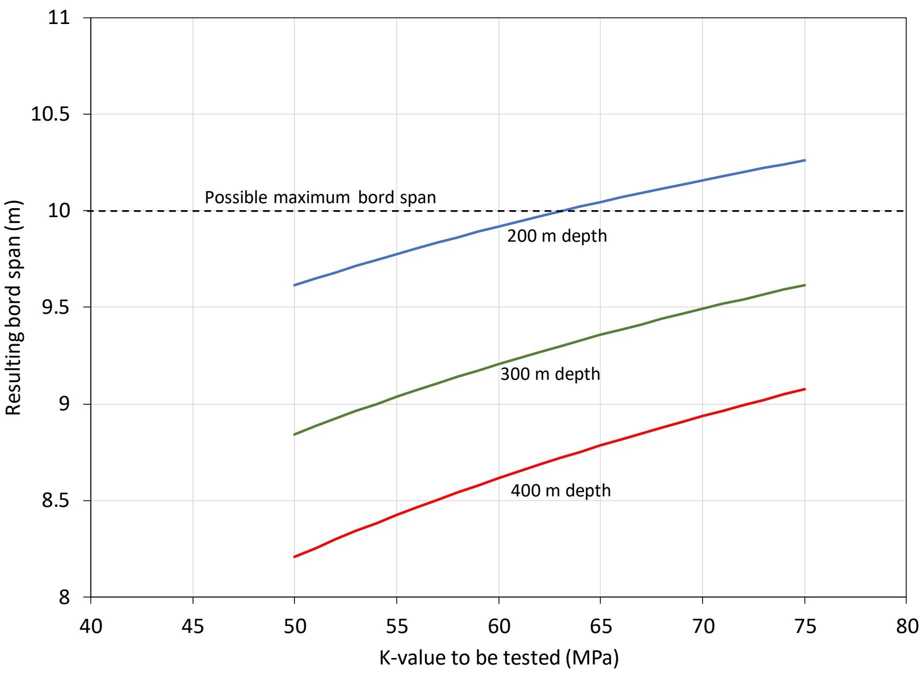


**Figure 94. Resulting bord span for reduced pillar sizes**

Figure 94 show the resulting bord span in a trial pillar reclamation section if the pillar sizes are reduced as shown in Figure 4. This is for a pillar centre distance of 14 m. Note that this is only applicable to the other parameters specified in the text.

# 6 CONCLUSIONS

The objective of this project was to use several new and historic back analyses of bord and pillar layouts to obtain the best estimates of hard rock pillar strength. From the data collected, most of the hard rock pillars are substantially stronger than the historic assumption of using $K = \frac{1}{3}UCS$ in the Hedley and Grant pillar strength formulation. Based on the database compiled, the following peak K-values were obtained:

- Merensky Reef: K = 90 MPa
- UG2 Reef: K = 75 MPa
- LG6 Reef: K = 70 MPa
- Manganese ore: K = 133 MPa

The rock mass rating and the nature of the joint sets may significantly affect the pillar strength, however, and for poor rock masses these values will be lower. An important finding from this study is that a K-value determined from the back-calculated for one area of the mine should be used with caution in other areas of the same mine with distinctly different rock mass ratings. The modified design rock-mass strength (DRMS), to estimate a reduced value of K, will be valuable for cases with a low rock mass rating.

# 7 RECOMMENDATIONS

The K-values given in this report can be used as a first order estimate of pillar strength for the different commodities in areas with a good rock mass rating. Very important is that the rock mass rating can significantly affect pillar strength. Mines with different geotechnical areas should consider the use of different pillar designs in different geotechnical areas. **Furthermore, as a cautionary note, any new pillar strength calibration should be tested in trial sections with suitable instrumentation and monitoring before it is adopted at any mine.** Rock mass strength and the geological features present are highly variable from area to area and this may affect pillar strength.

Currently, a topical area that requires additional research is the reclamation of pillars in hard rock mines. Some of the mature mines need to implement this method to extend the life of mine. Guidelines on when this secondary mining is possible in South African mines need to be developed. Stiffness concepts are very important in this regard. It is proposed to use the TEXAN code to do simulations of pillar extraction and to calculate the local system stiffness. Practical aspects that should studied will include the changes in the system stiffness as pillar reclamation, in different sequences, is implemented. A proposed project will therefore typically include:

- Conduct a literature study on the use of stiffness calculations in pillar layouts using numerical codes.
- Explore the use of stiffness calculations in TEXAN and the ability of the code to simulate this behaviour
- Conduct numerical modelling experiments on different pillar extraction methodologies and the value of the stiffness calculations. The limit equilibrium model in TEXAN will be used in these simulations to simulate the pillar failure of the remaining pillars.

# 8 REFERENCES

Bieniawski, Z.T. 1968a. The effect of specimen size on compressive strength of coal, Int J Rock Mech Min Sci & Geomech Abstr, 5(4):325-335.

Bieniawski, Z.T. 1968b. The compressive strength of hard rock. Tydskrif vir Natuurwetenskappe, 8(3-4).

Couto, P.M. and Malan, D.F. (2023) A Limit Equilibrium Model to Simulate the Large-Scale Pillar Collapse at the Everest Platinum Mine. Rock Mech Rock Eng 56, 183–197.

Crouch, S.L. (1973) Two-dimensional analysis of near-surface, single-seam extraction. Int. J. Rock Mech. Min. Sci. & Geomech. Abstr., Vol. 10, pp. 85-96.

Esterhuyse JC, Malan DF (2018) Some rock engineering aspects of multi-reef pillar extraction on the Ventersdorp Contact Reef. J. S. Afr. Inst. Min. Metall. 118(12):1285-1296.

Esterhuizen GS (2006) An evaluation of the strength of slender pillars. SME Annual Meeting, St. Louis, Missouri.

Esterhuizen, G., Iannacchione, A., Ellenberger, J. and Dolinar, D. (2006) Pillar stability issues based on a survey of pillar performance in underground limestone mines. pp. 354-361.

Hedley, D.G.F. and Grant, F. 1972. Stope-and-pillar design for the Elliot Lake Uranium Mines. Bull Can Inst Min Metall 65:37-44.

Landau, L.D. and Lifshitz, E.M. (1986) Theory of Elasticity, Third Edition, Pergamon Press.

Laubscher DH (1990) A geomechanics classification system for the rating of rock mass in mine design. J S Afr Inst Min Metall 90(10): 257-273.

Le Bron, K. and Malan, D.F. (2011) Laboratory test results and a comparison with the assumed numerical modelling parameters, Royal Bafokeng Platinum, Groundwork Consultancy, Report.

Malan, D.F. (2021) SAMERDI MMS21WP3 - Milestone 3 & 4 – Numerical simulation of pillar stability at the Styldrift Mine, 1 November 2021.

Martin, C.D. and Maybee, W.G. 2000. The strength of hard-rock pillars. Int. J. Rock. Mech. Min. Sci. 37:1239-1246.

Napier JAL, Malan DF (2007) The computational analysis of shallow depth tabular mining problems. J. S. Afr. Inst. Min. Metall. 107:725-742.

Napier JAL, Malan DF (2011) Numerical computation of average pillar stress and implications for pillar design. J S Afr Inst Min Metall 837-846

Napier, J.A.L. and Malan, D.F. (2021) A Limit Equilibrium Model of Tabular Mine Pillar Failure. Rock Mechanics and Rock Engineering, 54, pp. 71-89.

Oates, T. and Malan, D.F. (2023) A study of UG2 pillar strength using a new pillar database. J. S. Afr. Inst. Min. Metall, vol. 123, no. 5. pp. 265–274.

Salamon, M.D.G. and Munro, A.H. 1967. A study of the strength of coal pillars. J. S. Afr. Inst. Min. Metall. 68:55–67.

Stacey TR, Swart AH (2001) Booklet – Practical rock engineering practice for shallow and opencast mines. SIMRAC, October 2001.

Watson, B.P., Theron, W., Fernandes, N. Kekana, W.O., Mahlangu, M.P., Betz, G. and Carpede, A. (2021) UG2 pillar strength: Verification of the PlatMine formula. Journal of the Southern African Institute of Mining and Metallurgy, pp. 449-456.

Wessels, D.G. (2022) A review of the pillar design methodology for manganese mining operations in South Africa, M Eng dissertation, University of Pretoria.

Wessels, D.G. and Malan, D.F. (2023) A limit equilibrium model to simulate time-dependent pillar spalling, Rock Mechanics and Rock Engineering, 56:3773–3786.

# 9 APPENDIX A

## 9.1 *Contribution to the project by the CSIR*

(*The work pesented in this appendix is the report submitted by Mr Johan Hanekom*)

Historical case studies conducted on pillar behaviours, as recorded by various mines and authors, were summarised from reports generated between 1985 and 2017. The reports sourced were limited to studies conducted at South African Manganese, Platinum and Chrome Mines, but for interest and completion, also include work executed on Zimbabwean Platinum mines.

Since some sources requested data anonymity, mine names have been excluded from this report. However, enough detail is provided to ensure that the data can be utilised as intended in this project.

A summary of the rock mass strengths (K-values), as applied by the different authors during the individual back analyses, is provided below in Table A1,

The methodologies applied during pillar behaviour back-analyses varied substantially between the authors and environments. However, the following agreements seems possible:

- The general Hedley and Grant power law for determining pillar strength is broadly accepted and only one source suggested that other exponents would be more suitable.
- Statistical analyses of the back-analyses data appear to address the impact of many variables that affect pillar behaviour. ‘
- More than one K-value would probably be appropriate is suggested by some reports, to cater for substantial rock mass variabilities and that accurate knowledge of the variabilities in material strength and rock mass quality is essential.

**Table A1. Summary of K-values**

| Mine | Reef type | Back calculated / applied K-value (MPA) | Comments |
|---|---|---|---|
| A | Manganese | 133 | Evaluated statistical stress and strength distributions and indicated that since no pillar failures have been observed, pillar stress and strength distributions (normal distributions) should not intersect. Tested this assumption for several different K-values and concluded that the applied value appears appropriate. |
| B | Manganese | 133 | Several methods were applied and concluded that the indicated k-value is appropriate, based on corelation with local observations. |
| C | Massive Sulphide Zone (MSZ) | 34-36 (Poor rock)<br>56-59<br>(Good rock) | Substantial work executed including non-linear modelling. DRMS results were applied to derive a k-value. Concluded that the K-value on an operation should be variable and a single value should not be allocated. The applied value is thus rock mass quality related. |
| D | Manganese | 131 | Based on previous back analyses, pillar behaviours were confirmed using observations and found the previously back analysed K-value is acceptable. |
| E | Chrome (LG6) | 39 | Applied several methods to derive appropriate k-values, including DMRS and back analyses. By looking at failed and stable pillar FOS distributions, it was concluded that the reported K-value is valid if exponents to Hedley and Grant formulation is also increased to $\alpha=\beta=1.0$ |
| F | Platinum (Merensky) | 90 | The noted k-value is concluded to be appropriate for areas with a rock mass quality better than RMR=78.3 only. FOS distributions were analysed using numerical modelling to determine the average pillar stresses. Adding some variability to the k-value, the risk of experiencing pillar failures (defined at FOS<1), was determined. Variability in the K-value increases the risk of pillar failures when a single K-value is utilised, thus various values, depending on rock mass quality is thus promoted. |

## 9.2 *Mine A – Manganese mine*

The mine is a mechanised operation, using a bord and pillar layout to exploit the Manganese Lower and Upper Seams at a depth of 240-390 mbs. Square pillar widths vary from 6m to 8m depending on the depth and geotechnical area and are between 4 and 5m high. In areas where pillar stability was evaluated, some pillars had contact areas (width x length) of 3.5m$^2$ compared to the standard 36-64m$^2$, suggesting a +90% extraction in these small pillar areas, resulting in Factors of Safety < 0.5.

Even in these small pillar areas, pillars have traditionally been very stable with limited spalling noted, and where spalling was mentioned, appeared to have been geological structure driven. However, limited reports of hourglass shaped pillars exist, even though historically, no pillar failures had occurred in this environment. This absence of spalling / pillar failures limits the use of the results from the case study, as it is possible that the actual pillar strengths still exceed the final estimated strengths.

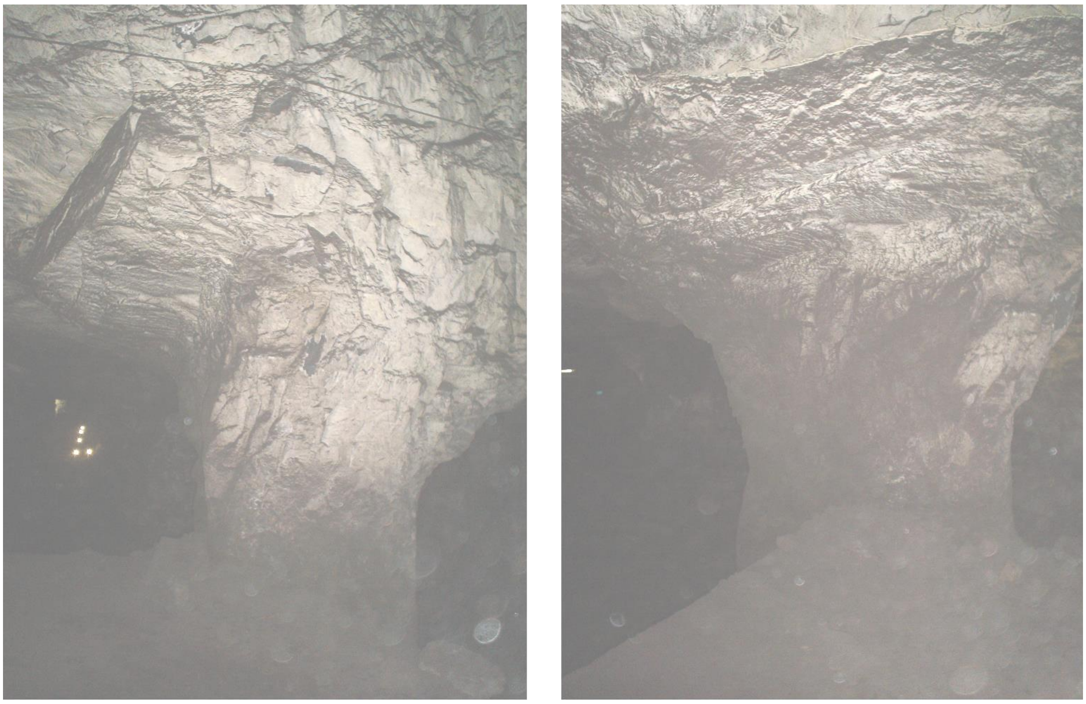

**Figure A1. Small pillars with limited hourglass shapes**

No laboratory testing of the rock strengths were conducted for this study, but use was made of previous tests to determine the DRMS. The empirical formula to estimate the strength for hard rock pillars was defined by Hedley and Grant. The K-value is substituted for Laubscher's design rock mass strength (DRMS) which is approximately 30% of the UCS of the rock or 131 MPa. Therefore:

$$P_{strength} = DRMS.\frac{w_{Eff}^{0.5}}{h^{0.75}}(MPa) \qquad \text{(A1)}$$

Where h is the pillar height and w is the pillar width.

For the various pillar widths reported, the standard pillar strengths are suggested to range between 95 MPa and 131 MPa, depending on the actual dimensions.

To determine the vertical stress or load acting on these pillars, the tributary area theory was applied where $P_{stress} = \frac{\sigma_v}{1-e}$, and $\sigma_v$ is the virgin stress, *e* is the extraction ratio.

A few mining areas were investigated and showed the following wrt pillar sizes:

- Area 1:
  - 66.6% of the pillars in this area are the correct size and larger.
  - 33.4% are undersized pillars of which 13% are less than 50% of their design size.
  - The average pillar area is 34.2m$^2$ in size, compared against the design area of 36m$^2$.
  - Fair pillar cutting discipline is reported.
- Area 2:
  - 59.4% of the pillars in this area are the correct size and larger.
  - 40.6% are undersized pillars of which.
    - 25% are less than 50% of their design size.
    - But area isolated in one area, and clustered in another area.
  - The average pillar area is 34.6m$^2$ in size compared against the design area of 36m$^2$.

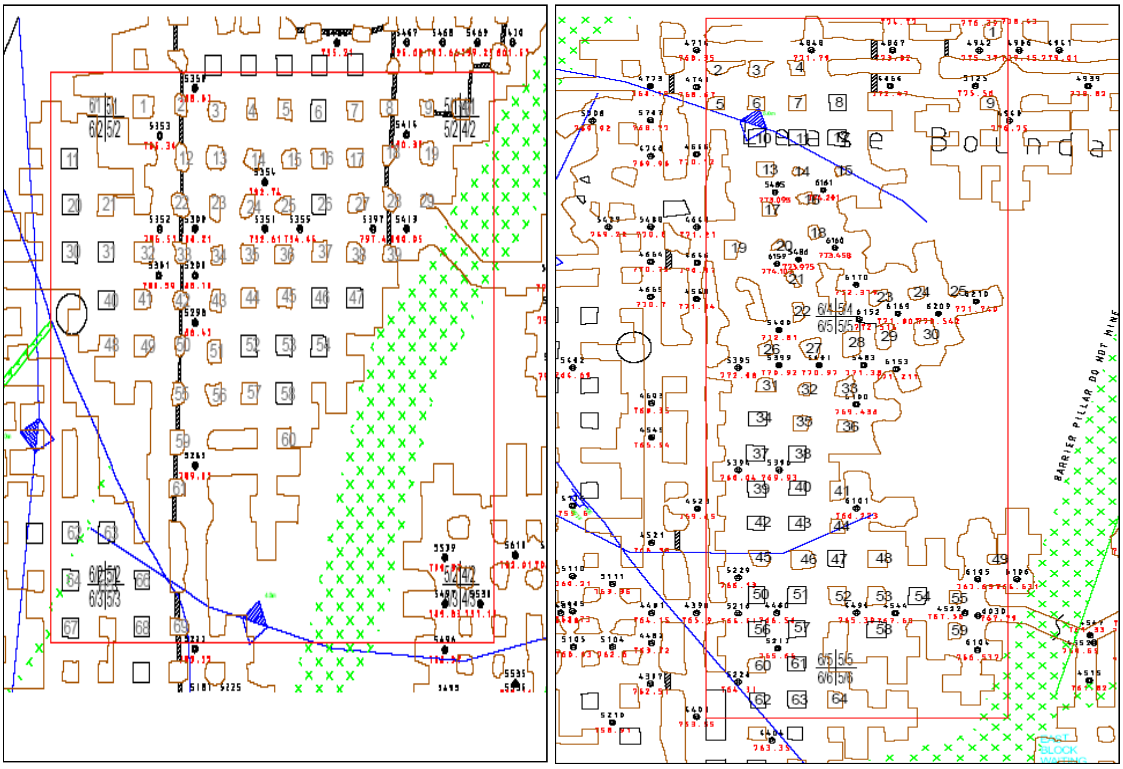

**Figure A2. Mining areas considered**

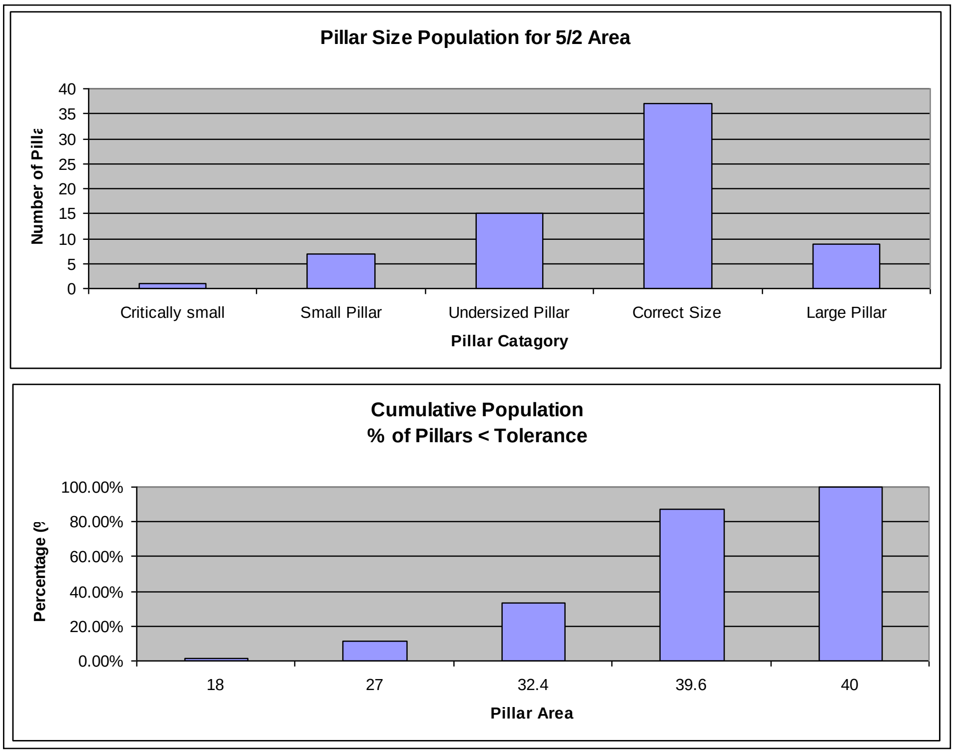


**Figure A3. Area 1: Pillar size distributions**

Horizontal fractures in two of the newly formed pillars have been observed and seem to correspond to two parting planes contained within the pillar, approximately 1.95m and

2.1m above the footwall. No shear fractures or abnormal spalling was noticed that could have been an indicator that the pillar was possibly being overloaded and therefore torn apart.

TAT as well as Modelled Map3D average pillar stress values were used to compare strength and average pillar stress distributions across all the pillars in the database (Figure A4). Accepting the application of the standard Hedley and Grant pillar strength formula, the strength distributions several possible K-values were determined and displayed. Distributions for all areas showed that the 133 MPa K-value (back analysed by previous authors for this environment), is probably the lowest K-value that would apply. This is based on the absence of pillar strength and stress distribution intersection, suggesting that no pillar failures are possible, as correlated with observations.

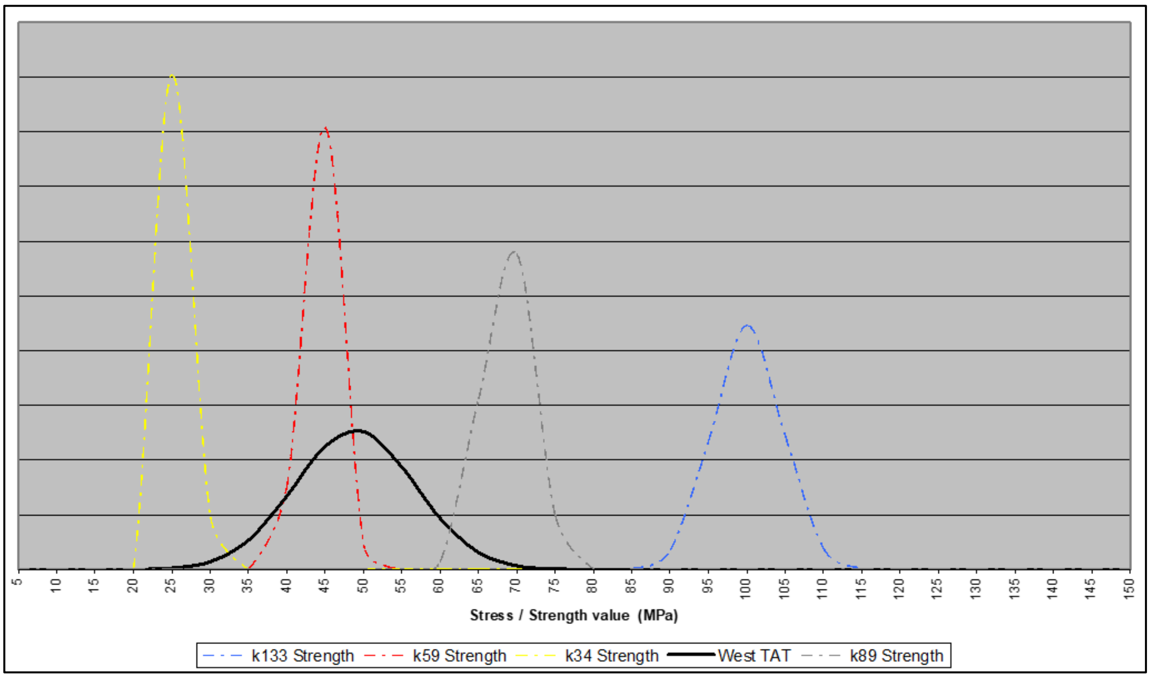


**Figure A4. Pillar loading vs Pillar strength distributions for various K-values**

## 9.3 *Mine B – Manganese mine*

The actual behaviour of pillars and bord hanging wall stability was studied in areas with sub-standard pillar and bord layouts. Pillars in the areas investigated measured 5.2-7.3m in width and 3.1-3.5m in height, with 7.2m-98.3m bord widths.

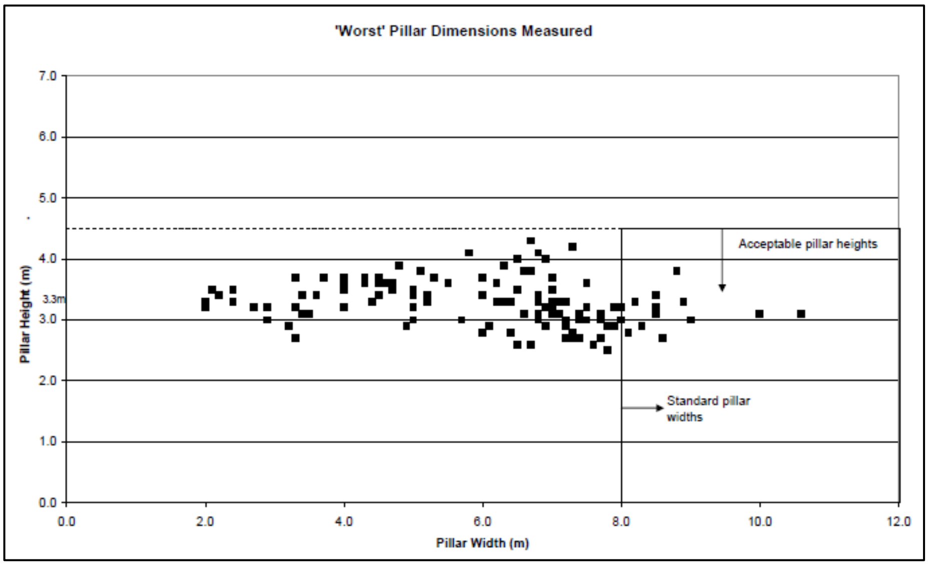


**Figure A5. Pillar dimensions measured**

In the study, the rock mass quality, varying pillar heights and mining depths were considered. The study described the following phases of investigation: Overview of existing workings, Determination of potential pillar mining options, Design of bords, pillars and support for new and secondary extraction areas, Involvement of other parties in the design process, Implementation of the designs and Monitoring of the rock mass behaviour. The study comprised several reports of the first phases, but no reports describing the implementation and monitoring phases have been sourced.

Pillar behaviours were noted to include limited spalling of wall skins on geological structures only, with no clear stress fracturing or pillar failures.

Numerical models provided average stress levels in pillars as well stress distributions within the middling between the seams to estimate middling impacts between the two manganese seams being mined. The codes applied during these back analyses include Map3D (BE), Phase 2 (FE) and UDEC (Discrete element). The models considered varying middlings, depths, pillar dimensions and bord widths as well as degrees of pillar misalignment between the two seams.

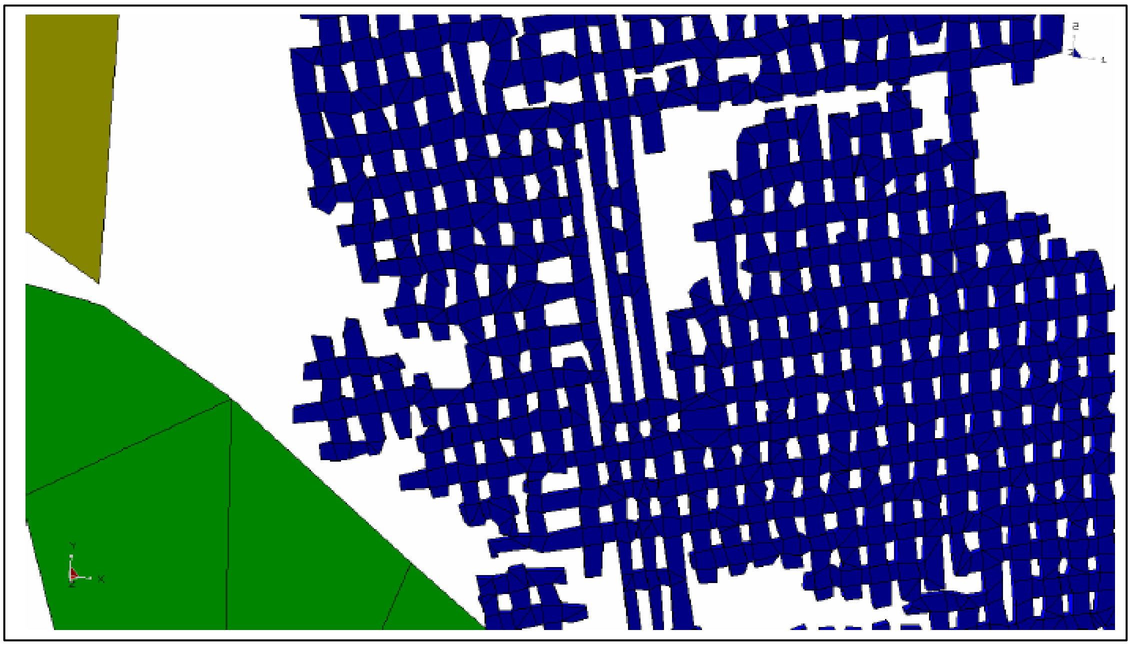

**Figure A6. Mine layout (Map3D)**

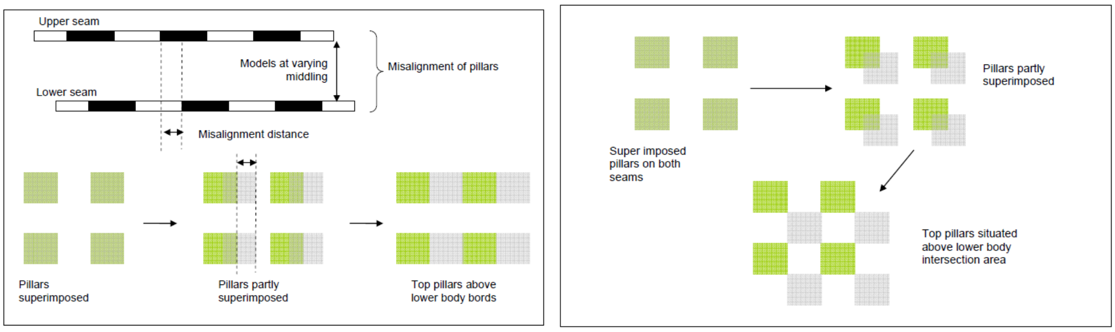


**Figure A7. Pillar misalignment considered for pillar interaction on seams**

Confirmation of middling and pillar stability at various depths and middlings used actual rock mass quality and strength data as well as stress measurements conducted within selected lower and upper seam pillars.

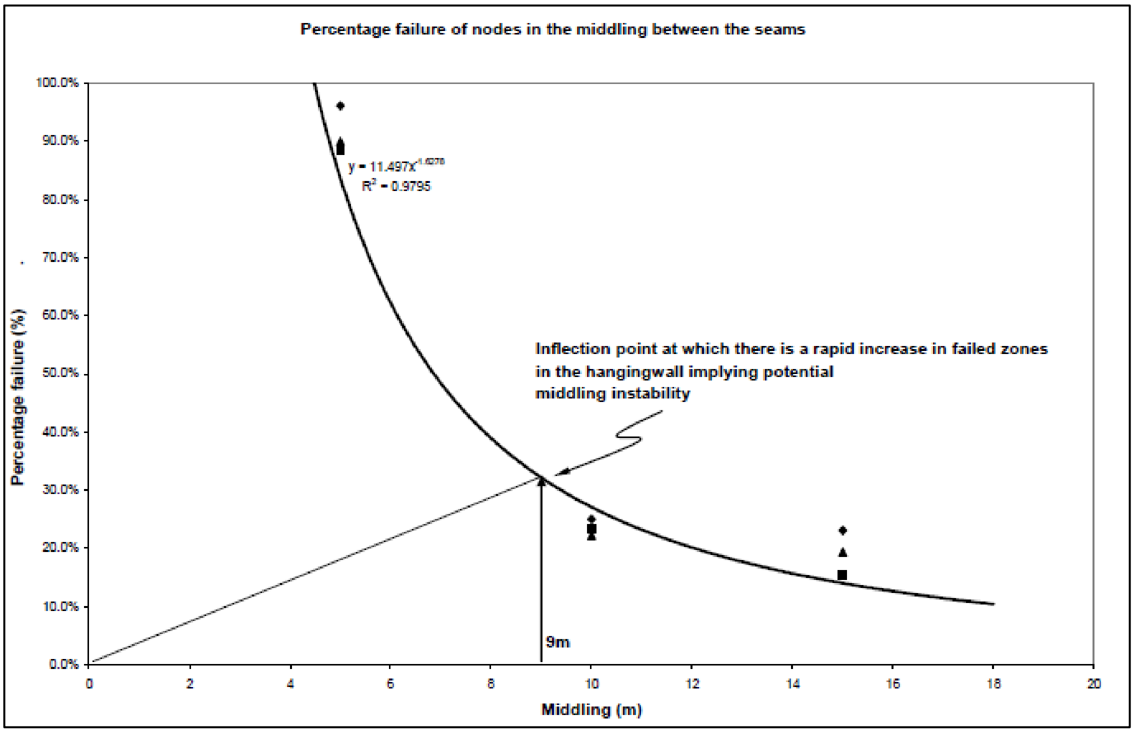


**Figure A8. Minimum stable middling between seams**

Map3D average pillar stress levels, after correlation with stress measurements conducted, were used to calculate an 'appropriate' overburden density and was applied in the TAT loading calculations. This calculated overburden density was defined as the 'loaded density'.

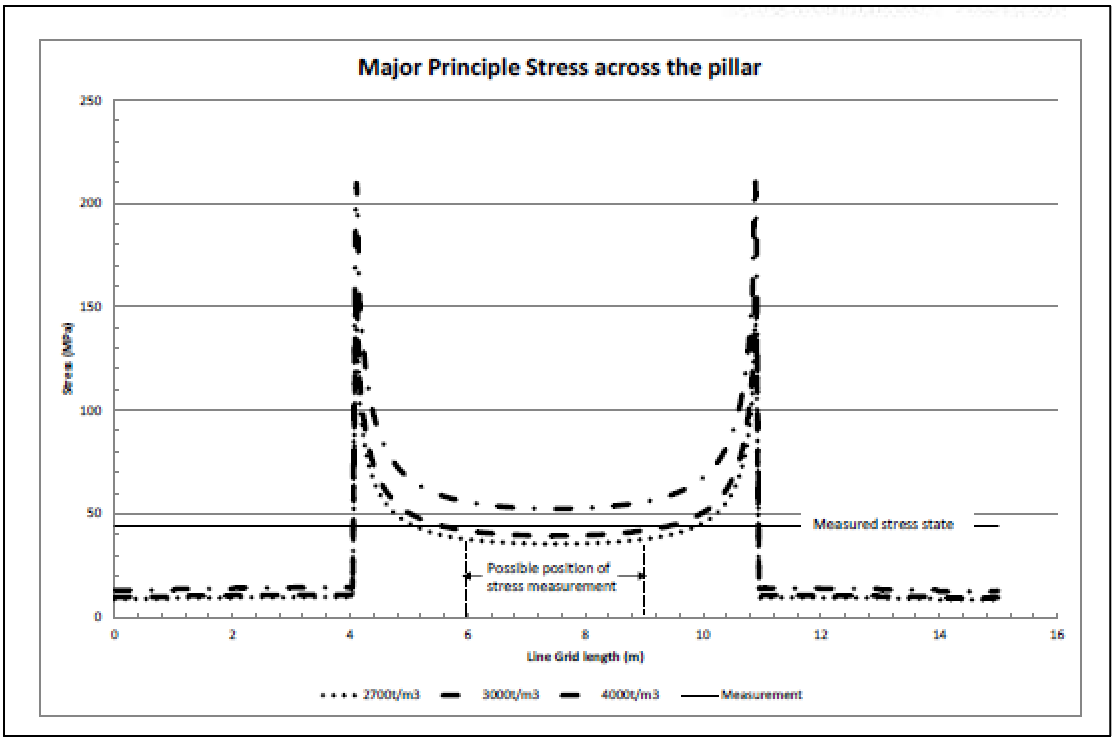


**Figure A9. Modelled pillar stress distribution (Map3D) correlated with pillar stress measurements**

Historical rock strength test results were reported but were not provided in detail. The report noted a 140-421 MPa range for the Manganese UCS from samples taken during the stress measurements exercise, with the following Manganese results:

- UCS = 172 ± 51 MPa,
- E = 91 ± 12 GPa,
- v = 0.32 ± 0.03,
- density = 4.47 t/$m^3$

For pillar strength determination, the following relationships were evaluated to determine the appropriate K-value:

- RMR and UCS: Using a UCS of 280 MPa (from quoted historical data) for Manganese:
  - 66% of UCS is a k = 184 MPa,
  - Actual RMR gives k = 201 MPa.
- Using Rocscience software to estimate the rock mass strength for the reported UCS and jointing data, indicated a k = 34-43 MPa, for a UCS range of 140 MPa to 421 MPa (minimum and maximum from stress measurements tests) was used.
  - This was deemed to be very low after calculated FOS of existing pillars audited underground ranged between 0.8 and 1.3.
- Back analysed from small pillar areas (total of 63 pillars), assuming a FOS=1 for all small pillars, back calculated that k = 85 MPa, but the area within which small pillars was limited in span, suggesting that full pillar loading could not be estimated, which affected the calculated K-value.
  - The approach for the selection of the 85 MPa as the minimum K-value at which all pillars evaluated will be stable (as observed) is extremely conservative, suggesting that the K-value should be higher than 85 MPa.
- Neighbouring mine back analyses by different authors were quoted to have been determined from much larger small-pillar mining spans (w:h = 0.9 provided k = 131-133 MPa.
- It was assumed 133 MPa appropriate based on observations and neighbouring mine's back analyses and applied to design new pillar dimensions.

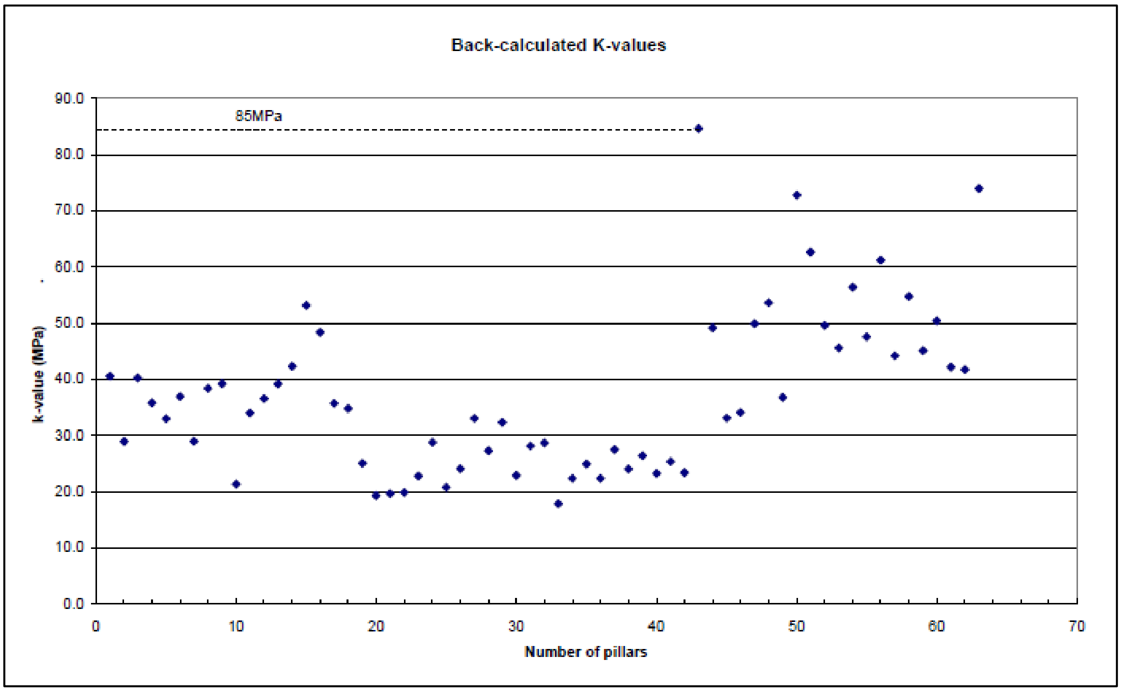


**Figure A10. Back calculated K-value**

The Hedley and Grant power formula for pillar strength was applied in all relevant evaluations, using 0.5 and 0.75 for the α and β exponents respectively.

## 9.4 *Mine C – Platinum mine (MSZ, Zimbabwe)*

A relook at pillar design (minimum 5m pillar widths in good and 6.5m in poor conditions) was required following pillar failures, attributed to a shear zone that undulated in and out of the MSZ. The back analysis evaluated geotechnical data, utilised numerical modelling and actual observations of footwall heave, pillar spalling and FOG to determine the way forward.

- Extensive re-logging of previously logged core was included to isolate the shear zone position and extent.
- Rock strengths were confirmed through rock sample testing yielding a UCS of between 200 and 295 MPa with a high Elastic Modulus of 150Gpa.
- Rock mass behaviour was evaluated using the location of the shear in and around the orebody, its thickness and infill type.

The back analysis aimed to understand the origin of the weakness and the stress transfer that occurs following onset of failure. A modelled APS was related to w:h ratio and underground observations to indicate areas of 'failed' and 'stable' pillars. Applying the maximum likelihood function the K-value and the exponents α and β (Hedley and Grant pillar strength formulation) was determined, but discarded due to the substantial scatter in the data and the uncertainty in the selection of 'failed' pillars.

It was assumed, despite weaknesses, that of the Hedley and Grant pillar strength formulation remains valid and that the K-value is a function of the UCS, which is typically 0.33xUCS.

However, DRMS was applied using logged orebody core and the distribution of the data indicated the possible existence of more than one distinct ground classes, to which different K-values should be applied. K-values were then defined for two classes: (1). 34-36 MPa for class D ground which correlates well with a 20th percentile value of all data indicating 35 MPa. (2). 56-59 MPa for class C ground, aligning well with the mean DRMS value of 61 MPa.

The report concludes that it seems insufficient to allocate a single K-value when the geotechnical conditions are variable.

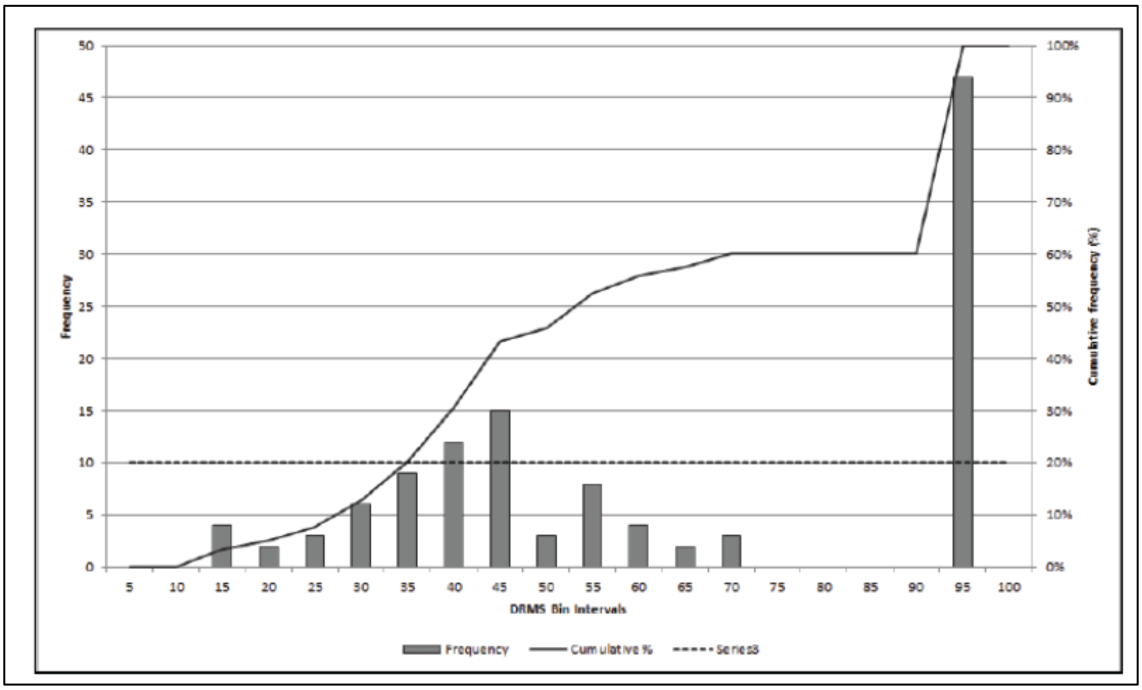


**Figure A11. DRMS distribution**

Numerical modelling then applied an iterative pillar failure transfer process, where the model iterates through several stages using a progressive failure model in Map3D and mXrap (allow a statistical approach to address spatial variability). The model excluded 'failed pillars' with FOS < 1 from the model and then re-ran the layout to emulate the ‘pillar failures’, varying the K-value between 55 MPa and 45 MPa. A 4 m wide pillar, at a 2.5m stopting width was used as reference, but 2 m and 6 m wide pillars were also examined to assess the effect of pillar size on stability.

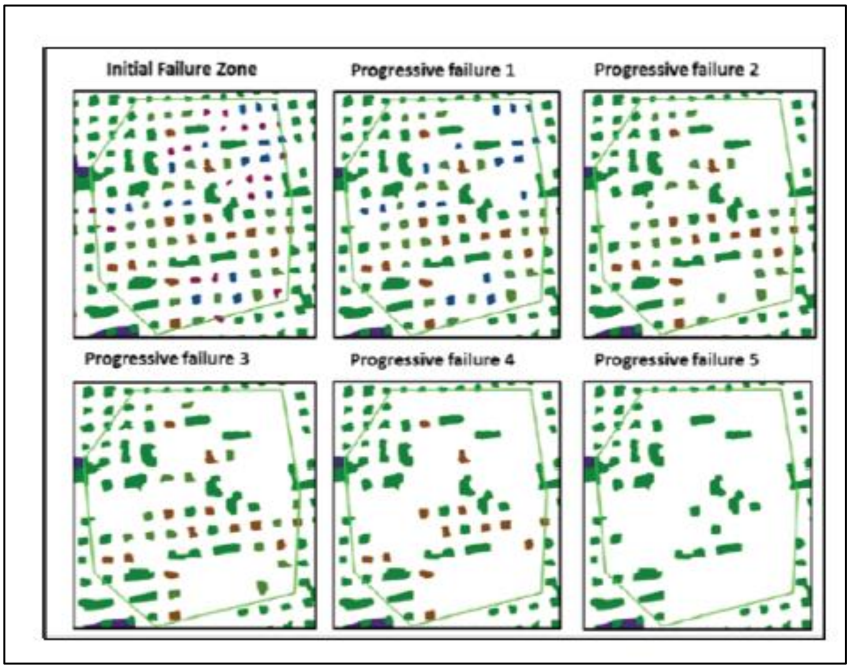


**Figure A12. Progressive failure of pillars**

## 9.5 *Mine D – Manganese mine*

This work was recorded in 1982, but substantial work appeared to have already been executed in especially the Manganese orebody mining area. The document refers to back analyses conducted at a neighbouring mine where the K-value was back-calculated to be approximately 131 MPa. This report simply established that the rock mass is very similar to the neighbouring mine and that the back analyses conducted is thus also applicable to this mine's orebody and overburden. Since mining spans on this operation was still too small to ensure full pillar loading had occurred and allow a local back analysis, the results obtained elsewhere was applied.

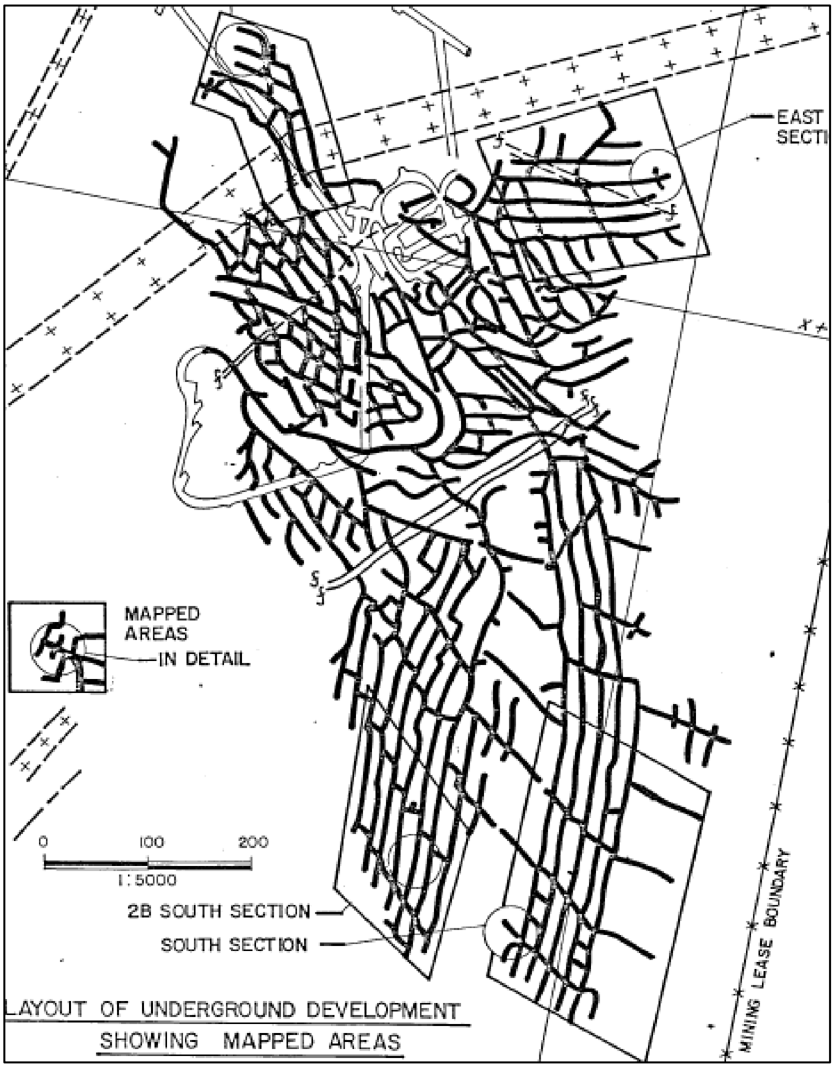


**Figure A13. Limited mining spans at operation**

## 9.6 *Mine E – Chrome (LG6) mine*

The back analysis applied several different approaches to quantify the exponents applied in the Hedley and Grant power law pillar strength formulation.

At first, a probabilistic approach of the normal design methodology and standard Hedley and Grant formulation was taken. It was noted that the value of k within this formulation is historically lower than intact strength of rock (UCS) and suggested that extrapolation from rock sample tests to in-situ behaviour is not appropriate. It is suggested that DRMS is used to derive the appropriate K-value.

The approach then evaluated pillars using the FoS achieved for 203 pillars, of which 90 had failed and the remaining 113 pillars were reported to be stable. The average pillar stress was determined using BESOLMS whilst a DRMS (K-value) of 21 MPa for the chrome strength was based on underground mapping. The standard Hedley and Grant formula to derive pillar strengths was applied. The results were displayed as FOS distributions and analysed to provide

- a Mean and Standard Deviation of 0.59 and 0.19 for stable and 0.43 and 0.06 for the failed pillars.

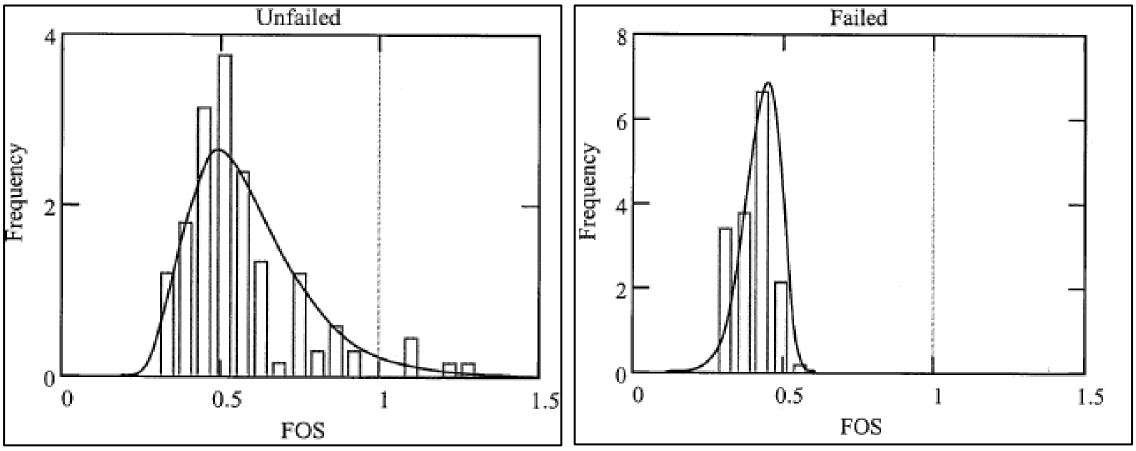


**Figure A14. FOS distributions for stable and failed pillars**

- The appropriate distribution of FOS for stable pillars was argued to be around a FOS = 1, with that for failed pillars at some smaller FOS, whilst overlap is possible. The results indicated stable pillars to have FOS well below 1.
- The conventional design formulation for pillar strength was not deemed appropriate.

A back analysis process, consisting of two different approaches then followed:

- Using failed pillars only.
    - The Hedley and Grant formula was used with standard α and β exponents and the K-value was back-calculated for each of the failed pillars, providing a Mean K-value of 50.6 ± 7.67 MPa
    - Then, fixing the β exponent and the K-value, the α exponent was determined using the least squares method.

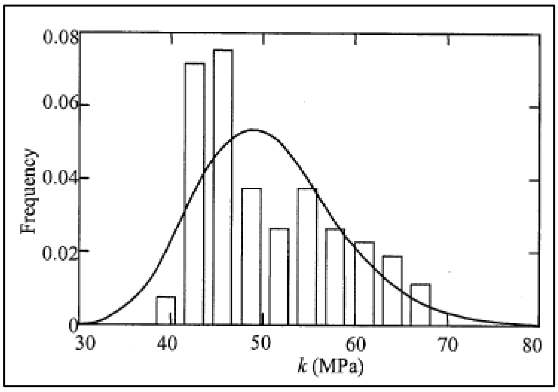


| | β | | | | | |
|---|---|---|---|---|---|---|
| **k** | **0.5** | **0.6** | **0.7** | **0.8** | **0.9** | **1** |
| **35** | 0,88 | 0,91 | 0,94 | 0,97 | 0,99 | 1,02 |
| **40** | 0,68 | 0,70 | 0,73 | 0,76 | 0,79 | 0,82 |
| **45** | 0,50 | 0,52 | 0,54 | 0,58 | 0,60 | 0,63 |
| **46** | 0,44 | 0,47 | 0,50 | 0,53 | 0,56 | 0,59 |

**Figure A15. K-value distribution and calculated α values for various constant β and K-values.**

- Using these results and applying α and β exponents as in the standard Hedley and Gant formulation, the Mean K-value would be 50.5 MPa, which far exceeds the DMRS value.

- Using both failed and stable pillars.
  - The selection of a critical FOS ($FOS_{cr}$), where
    - if the real FOS > $FOS_{cr}$, pillars will be stable, and
    - if the real FOS < $FOS_{cr}$, pillars would fail, but
    - where $FOS_{cr}$ is not known, forms the basis of this approach.
  - It was assumed that:
    - the Mean FOS for the pillars should be 1.0, with clustering of the failed pillar data around FOS=1.0,
    - the probability of having stable pillars at FOS < 1 should be minimal, and
    - FOS results follows a log-normal distribution.
    - Using these assumptions, the α and β exponents that would best provide these distributions were determined.

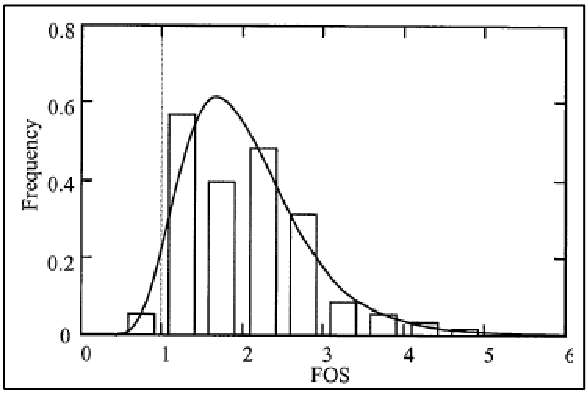


**Figure A16. Approach 2 distribution of FOS**

  - These assumed distribution results were best achieved using α and β exponents of 1.0 and a K-value of 39 MPa. A Monte Carlo analysis showed a
    - 10% PoF for α = β = 1 and k = 39 MPa and
    - 35% PoF for DRMS (k) value of 21 MPa.
  - Since underground observations on pillar behaviour support low PoF for pillars, it was concluded that the exponents should be high (even though β changes have low impact due to low pillar heights) whilst the K-value should be closer to 39 MPa.

## 9.7 *Mine F – Platinum (Merensky)*

The study analysed 99 pillars to evaluate the suitability of the K-value applied during pillar design and form part of a 2-phase project in which phase 1 provided data on observed pillar instabilities.

In the analysed layout, two distinct pillar widths were reported. In 6m ($34m^2 \pm 5.7m^2$) pillar width areas, bords are on average 6.1m wide at a stoping width of 2.46 ± 0.26m and in 8m ($66m^2 \pm 12.7m^2$) wide pillar areas, bords are 7.9m wide at stoping widths of 2.5 ± 0.4m.

All original pillar designs were executed using the Hedley and Grant power law formulation for pillar strength and a K-value of 90 MPa (approximately 65% of the material UCS), which was the result of a back analysis study conducted by other authors on the same operation.

Geotechnical data in the form of rock mass classification data was provided, but is the result of the implementation of an in-house rock mass quality classification system. Using the Rock Mass Strength concept, the RMR (Bienawski) was back calculated (RMR = 78.3), applying a K-value of 90 MPa and a UCS of 140 MPa. This means that this K-value is only appropriate to areas where the RMR > 78.3.

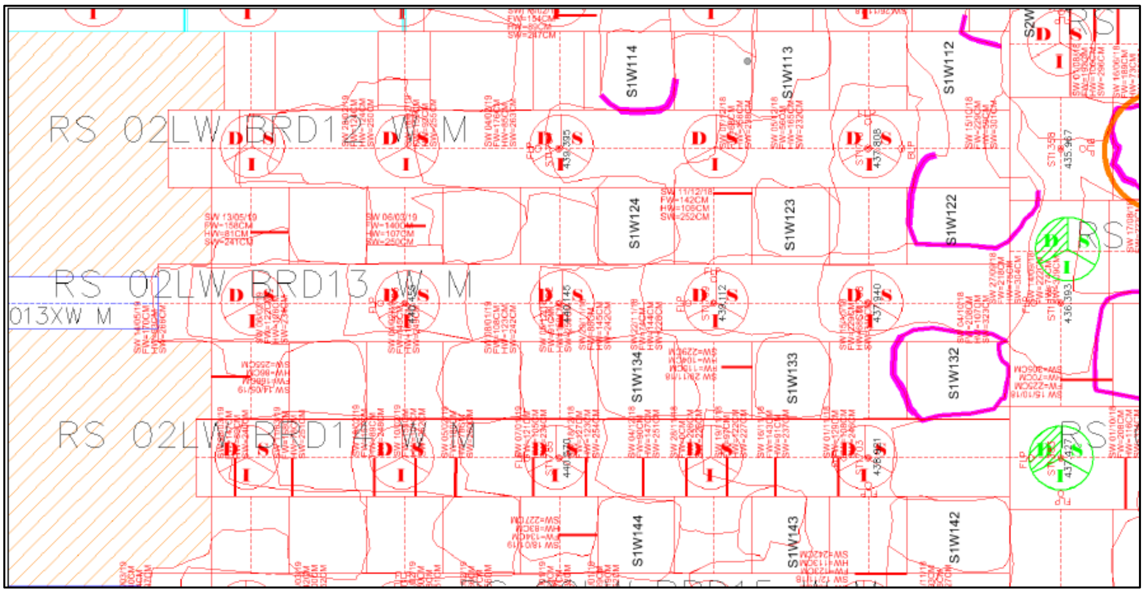


**Figure A17. Example mine plan data gathered**

Underground mapping and detail pillar behaviour / condition of the 99 pillars included in the study formed part of this back analyses. Correlation of observed pillar conditions and individual pillar width:height ratios resulted in the following conclusions:

- All pillars with w:h < 2 had high, underground stress ratings (conditions).
- 40% Of pillars with 2 < w:h < 2.2, had high stress ratings
- 16% of pillars with 2.2 < w:h < 3 had high stress ratings and
- Only 1 pillar (out of 8) with a w:h > 3 had high stress ratings.

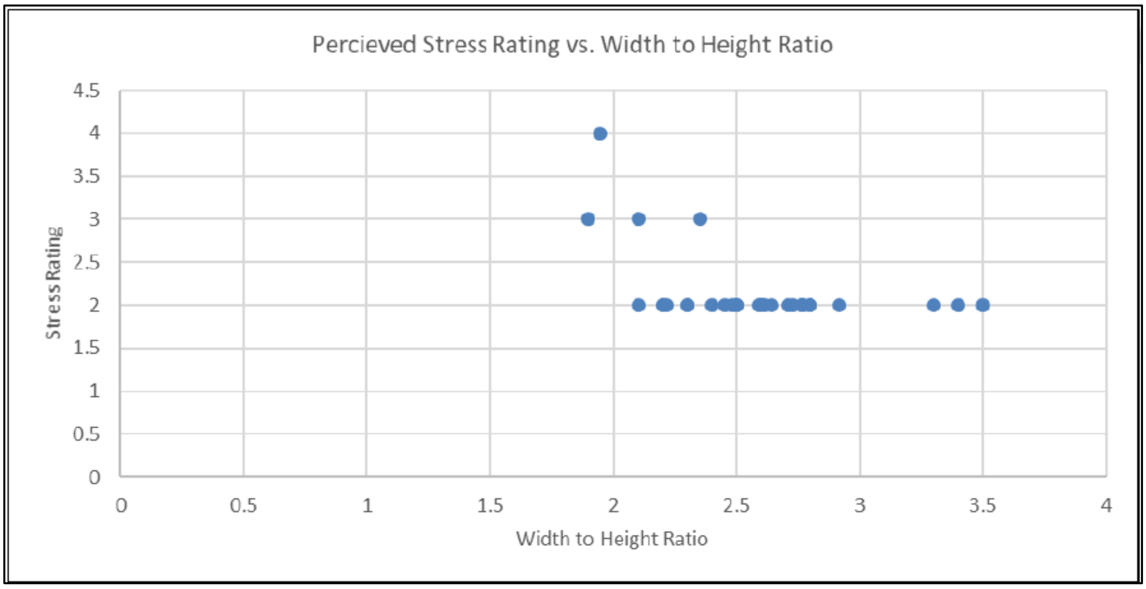


**Figure A18. Width to height ratio and observed conditions**

Using numerical modelling (Map3D) to derive average pillar stress levels, calibration with actual stress measurements yielded the code's input parameters. When using the Normal stress component results to determine average pillar stresses, the pillar stress levels were under-estimated in comparison to that provided by the analytical method. Applying Sigma 1 results slightly overestimated, but correlated well, with the analytical method's average pillar stress levels.

The standard Hedley and Grant power law pillar strength formulation was applied with a K-value of 90 MPa, and the FOS results, using the modelled pillar stresses, statistically analysed the FOS distributions:

- Pillar width 6m:
  - Mean FOS is 1.45 with a 4% probability to have FOS < 1.
- Pillar width 8m:
  - Mean FOS is 1.8.

To back calculate an appropriate K-value, changes in k was measured in terms of the increase in probability that the pillar FOS < 1. Introducing a standard deviation of 11 MPa to the K-value, it was shown that the risk of having pillar FOS < 1 (and thus suggest some level of pillar failure) will increase by 4-5% in the 6m pillar area and 1-2% in the 8m pillar area.

Variations in rock mass quality across an operation thus has the potential to increase the risk of pillar failure. The larger this variation, and thus the larger the standard deviation of the single K-value eventually applied, increases this risk of potential pillar failure.

# 10 APPENDIX B

## 10.1 *Contribution to the project by the University of the Witwatersrand*

(*The work pesented in this appendix is the report submitted by Prof Bryan Watson*)

This work is an extension of the project *MMS22WP1 Developing an effective pillar design methodology for mechanised mining*. It was concluded from the previous study that significant uncertainty still exists in terms of the best equation to describe the pillar strength behaviour and this can only be resolved using further laboratory testing and underground observations of pillar behaviour. Both the power-law and linear formulae, and variations of these, are widely used. It appears that the problem of finding a "universal" strength equation is because strength parameters are lumped together to provide a simple equation. Some of the effects of variable parameters can be mitigated by providing a dedicated formula for a particular reef, to be used where there is little variation in the geotechnical and geomechanical conditions. The need for dedicated formulae was recognised by the platinum industry in South Africa in the early 2000s, and projects were initiated to collect data from the Merensky and UG2 reefs. The work was done in collaboration between the three largest groups of platinum producers at the time and the government. The research group that was formed was named "PlatMine". A maximum likelihood regression analysis was used to evaluate the data and a linear and power formula was assumed. The analysis provided values for the unknown constants for each of the two databases. In the case of the UG2 reef, the rock mass strength result (k) in the linear formula was considered to be too high. The power formula provides a curved relationship of strength as a function of the w/h ratio, which agrees with laboratory strength tests that have been done recently. In addition, a single pillar that was instrumented at Booysendal showed similar strength to what was predicted by the power formula. This new UG2 formula (PlatMine formula) predicts a much greater strength than the traditional formula used for pillar design on the UG2 mines, meaning that smaller pillars can be left in a bord and pillar operation with an associated increase in extraction and profit. The PlatMine formula was criticised because it predicts an increase in strength with volume. This effect may be a function of the small variation of height in the database, and laboratory tests are planned to determine the volume effect soon.

The implication of the maximum likelihood regression analysis suggests that the PlatMine formula applies to UG2 pillars that have the same properties and w/h ratios as the pillars in the database. Bearing the volumetric criticism in mind, the original database was re-evaluated as part of this project and the formula with the lowest standard deviation coefficient was considered to be the most appropriate. The following evaluations were done:

- a form of the linear formula (Formula 1);
- power formula on the database consisting of pillars with a height of about 2 m (Formula 2);
- power formula on the database where all slender pillars were removed (Formula 3);
- power formula with one fixed unknown to ensure a single exponent for w/h-ratio (Formula 4); and
- The existing formula exponents were fixed according to the Hedley & Grant formula (1972) and the regression analysis was used to calculate the K'-value (Formula 5).

The formula with the lowest standard deviation coefficient was considered to be the best evaluation of the data in the database. It was found to be Formula 4. The finding suggests that the effect of volume on strength as predicted by the original PlatMine formula, may not be true. Importantly, there was very little variation in the predicted pillar strength for the range of w/h ratio in the database whether the original or Formula 4 was used.

In addition, the performance of the power formulae was evaluated based on established metrics for the classification of models, i.e. accuracy, precision, and recall. The analyses considered the overall correctness of the predictions, the ratio of true positive predictions to the total number of positive predictions (true positives + false positives), and the proportion of actual "Stable" pillars that were identified correctly. All the evaluations were compared to visual observations made underground. This analysis suggested the original formula and Formula 4 to be equally well-rated and better than the other formulae.

## 10.2 *Introduction*

In the realm of mechanized mining, various empirical formulae have been widely employed to delineate pillar strength behaviour in both coal mines and hard rock mines. These formulae usually use the power-law and linear functions and their derivatives. Notable contributions in this field have been made by esteemed authors such as Salamon and Munro (1976), Hedley and Grant (1972), Von Kimmermann (1984), Lunder and Pakalnis (1997), and more recently, Van der Merwe and Mathey (2013) along with Watson et al. (2021) who proposed the new UG2 formula, to mention a few. Despite the wealth of research, many of these formulae are hindered by limitations such as reliance on a restricted number of observed pillars (Oates and Malan, 2023), considerable uncertainty, or applicability only to specific reef formations characterized by specific geological and geomechanical conditions. While the PlatMine formula has demonstrated a notable increase in predicted pillar strength compared to traditional formulae, it has faced criticism for its tendency to forecast strength augmentation with volume. The pursuit of a "universal" strength equation remains elusive, primarily due to the formidable challenge of reconciling a multitude of diverse strength parameters into a single, simplistic equation.

## 10.3 *Aim of this particular component*

Based on many considerations of past research, a different approach in terms of future research was proposed. In the short term, back analyses of carefully selected bord and pillar layouts were suggested as a means to estimate pillar strength. This project re-analysed an existing database of failed and unfailed pillars to determine a more reliable pillar strength formula for the UG2 Reef. The research described in this report will focus on an existing database of failed and unfailed UG2 pillars, commonly known as the PlatMine database (Watson et al., 2021). The database consists of a total of 177 pillars, of which 33 were failed. Elastic numerical modelling was used to determine the stresses on the pillars that were observed. Since the date that the pillars failed was not known, the strengths of many of these pillars were overestimated by the models. It was therefore necessary to use a similar analysis approach to Salamon & Munro (1967). A maximum likelihood regression analysis was used to find the best fit to the available data by assuming a power formula and varying the values of the unknown exponents and "k". This milestone will aim to reassess the PlatMine database to find a new improved set of constants for the power formula or a linear formula that better describes the observed data.

## 10.4 *Methodology used*

Very little research has been conducted to develop reef-type specific pillar strength formulae for the hard rock mines in South Africa. Considering the importance of this, the existing PlatMine database was re-evaluated to determine a more robust formula that can be used to design UG2 pillars confidently. The published PlatMine formula suggests a power formula to determine pillar strength. A maximum likelihood regression analysis was used to determine the combinations of unknown parameters in the formula, that would provide the lowest standard deviation coefficient without any manipulation. The original formula suggested increased strength with volume, which requires further investigation. The current analysis included a re-evaluation of the data using various forms of the power formula and a linear formula. The chosen linear formula was originally suggested by Bieniawski & van Heerden (1975) and confirmed by York & Canbulat (1998), with a modification for pillar length, as described in Watson et al. (2008).

$$\text{Strength} = K_i \left[ \frac{1+a}{1+{}^{aw}\!/_{L}} \right] \left[ b + (1-b)\frac{w}{h_e} \right] \tag{B1}$$

where: '$K_i$' is the in-situ cube strength; 'a' is the pillar length parameter and 'b' is the linear $w/h_e$ parameter.

Further analyses were performed on the database by assuming a power formula and fixing the β-value so that the α and β-values were equal. Further analyses were run using the exponents suggested by Hedley & Grant (1972) and solving for 'k'.

Esterhuizen (2006) found a significant increase in strength variability below a w/h ratio of about 1.5. Later, Oke & Esterhuizen (2017) showed that the influence of structure has a major influence on the stability of slender pillars. Zipf (2001) also noted that slender pillars have little load-bearing capacity. Bearing these findings in mind, it was decided that further analyses should be made on the database excluding all pillars with a w/h ratio of less than 1.5.

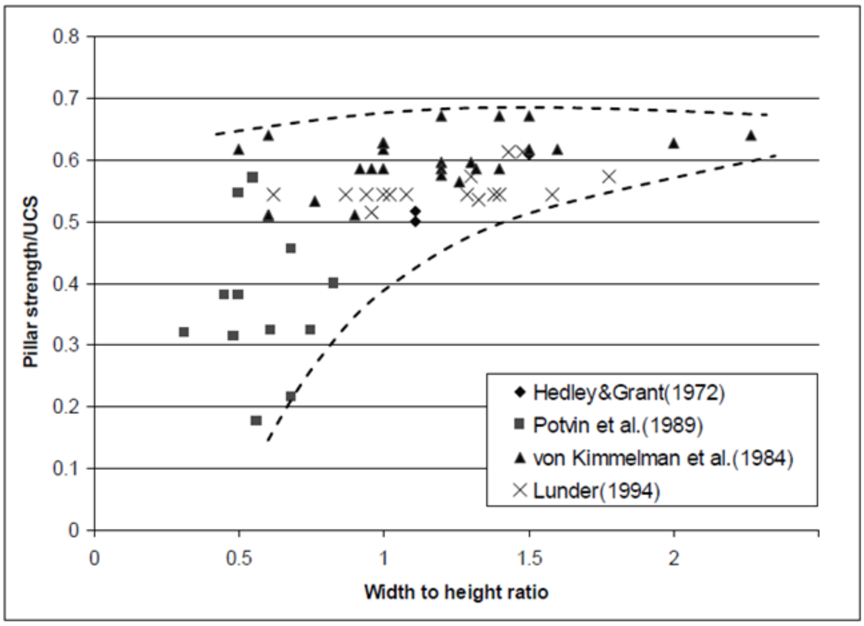


**Figure B19. Pillar stability graph showing examples of failed pillars from hard rock mines (Esterhuizen, 2006)**

One of the major criticisms of the database was the small range of pillar height. The data was collected from conventional stopes, because of the relatively high number of failed pillars available for investigation. The disadvantage of these sites was the uniformity of the stoping height, as the UG2 chromitite seams are relatively uniform in thickness across the Bushveld Complex. The differences in height were attributed to whether a siding was left adjacent to the pillars. Ninety-five per cent of the pillars were influenced by an adjacent gully, which affected the pillar heights on one side. An effective height was calculated using Equation 2 (Roberts et al. 2002) and was found to range between 1.9 m and 2.1 m. The remaining 5% with sidings had a height of 1.5 m. A final evaluation was done on the database excluding the 1.5 m high pillars. The standard deviation coefficient was calculated in every evaluation and used as a measure to determine the effectiveness of the equation. A lower standard deviation coefficient was considered to provide a more reliable strength law.

$h_e \approx [1+0.2692(w/h)^{0.08}]\ h \qquad [\text{if } Sd = 0 \text{ m}]$ (B2)

The maximum likelihood analysis of the data involved varying the exponents which yielded several sets of estimated safety factors (SF) for each pillar in the database. Further sensitivity analyses were done by comparing the SFs to observed pillar conditions in the database. The aim was to identify the scenario/s that best predicted the observed conditions. To facilitate the comparison, SFs and pillar condition codes were transformed into two classes, representing "Stable" and "Failed" conditions. The scenarios analysed only included four of the power formula equations as follows:

- Scenario 1: (i) Use the PlatMine formula parameters ($\alpha$=0.67, $\beta$=0.32 and K = 0.67) to estimate SF1.
- Scenario 2: (i) Make $\alpha$=0.5 and $\beta$=0.75 exponents (Hedley & Grant, 1972), and then estimate K. (ii.) Use the new parameters to estimate SF2.

- Scenario 3: (i) $\alpha$=0.71 and $\beta$=0.71, ($\alpha$=$\beta$) and then estimate K. (ii.) Use the new parameters to estimate SF3.
- Scenario 4: (i) Remove data points where h ≈1.5 m, and fix $\alpha$=0.64 and $\beta$=0.64, and then estimate K. (ii.) Use the new parameters to estimate SF4.

After running the maximum likelihood analysis for the above scenarios, the estimated SF data (SF1-SF4) was transformed such that values greater than 1 were classified and coded as "Stable" and those values less than 1 as "Failed":

- SF > 1 = "Stable".
- SF < 1 = "Failed".

The pillar conditions scale as illustrated by Watson, et al. (2021) was also re-classified, and coded as follows:

- "Stable": If the pillar condition code is less than 3.
- "Failed": If the pillar conditions code is greater than 3.

The resultant outputs were such that the database and the four scenarios would now have a new data field with two classes, i.e. "Stable" or "Failed". The observed pillar conditions data ("Stable" or "Failed") from the database was compared to the estimated data from the four scenarios. The comparison allowed for the determination of the performance of the four formulae (i.e. scenarios) used in classifying whether a pillar would "Fail" or be "Stable" based on the input parameters of its width and height. The analysis of the performance of the formulae and the varying parameters was evaluated based on established metrics for classification models, i.e. accuracy, precision, and recall. The terms are described as:

- Accuracy: measures how the model correctly predicts the failure of pillars. In other words, the rate at which the model predicts a pillar to be "Stable" and the pillar is indeed stable (or has been observed to be stable). It also measures the rate at which a pillar was predicted to have failed and is found to be failing. It is the overall correctness of the predictions. Careful consideration must be taken when using accuracy to evaluate how well a model classifies between failure and stability. This is especially true when dealing with unbalanced data as is the case in this database. Only 25% of the samples in the database show instances of failure while 75% are stable conditions. It is therefore important to evaluate accuracy together with other measures such as precision and recall.

- Precision is the ratio of true positive predictions to the total number predictions (true positives + false positives). Note that in this case, a positive prediction is set to be the "Stability" classification. Precision answers What proportion of "Stability" estimates was correct? That is, it reports on how many of the pillars which were predicted to be stable are stable. Precision is useful in the cases where a false positive (i.e. a pillar being predicted to be "Stable", and it is found NOT to be stable) is of higher concern than a false negative (i.e. a pillar predicted to have "Failed" and found to be rather "Stable). The cost of the false positives is that the pillars would be under-designed, and the consequence will cost lives, which is a higher price to pay than an overdesign that could be more conservative. As a result, precision would be looked at very carefully in the study.

- Recall (Sensitivity): explains how many of the actual positive (i.e. "Stable" predictions) cases were predicted correctly. It is the ratio of true positives predicted divided by the total number of actual positives. What proportion of actual "Stable" pillars was identified correctly?

## 10.5 *Research findings*

### 10.5.1 Re-evaluation of the PlatMine database

The analyses performed on the PlatMine database included a standard deviation coefficient (s) which was used to compare the virtuousness of the results. The standard deviation ($\mathbf{10^{\pm s}}$) needs to be evaluated about unity (Ryder et al., 2005). The original Platmine formula for UG2 pillar strength (Watson et al., 2021) is:

$$\sigma_p = 67\frac{w_e^{0.67}}{h_e^{0.32}} \qquad \text{(B2)}$$

Where $\boldsymbol{\sigma_p}$ is the pillar strength, $\boldsymbol{w_e}$ and $\boldsymbol{h_e}$ refer to the effective pillar width and height, respectively. The $\boldsymbol{w_e}$ was determined using the Wagner (1974) formula for rectangular pillars:

$$w_e \approx 2\ w\ L\ /(w+L) \qquad \text{(B4)}$$

where L is the pillar length.

The first re-analysis performed on the database was the application of the linear formula as shown in (B1. The back-fitted parameters from the database are shown in Table B2.

**Table B2. Back-fit values for Linear Equation B1**

| Parameter | Value |
|---|---|
| $K_i$ (*In situ* cube strength) | 85 MPa |
| a (Length parameter) | 0.58 |
| b (Linear $w/h_e$ parameter) | 0.43 |

Triaxial laboratory tests conducted on UG2 chromitite material (Maphosa, 2022) show non-linear behaviour at fairly low confinements (Figure B20). It is therefore suspected that the UG2 pillars will also behave in a non-linear fashion. Further analysis was therefore done using the power formula. To eliminate the volumetric effects, the analysis was forced to provide the same exponents for both w and h. The results are provided in Table B3 and (B3.

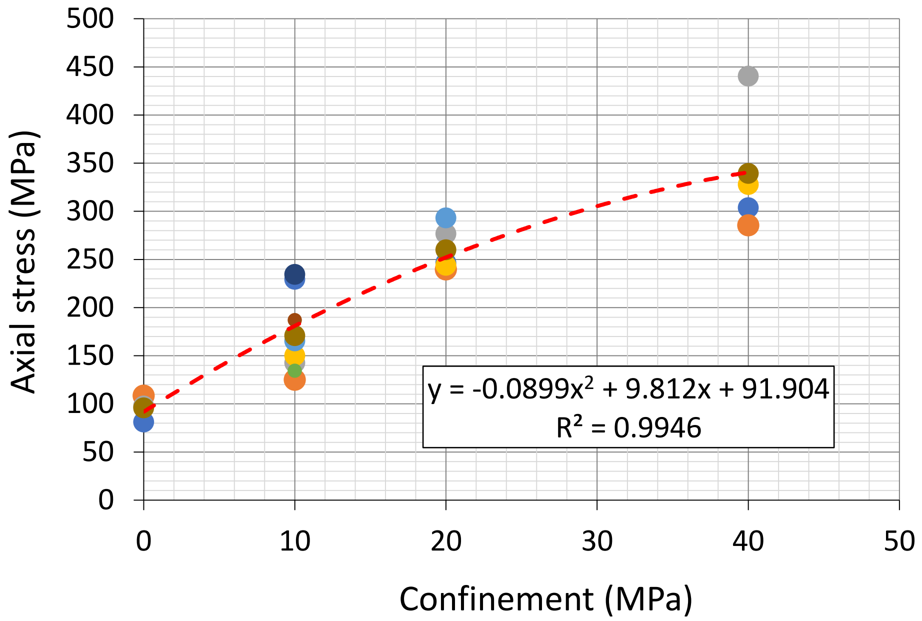


**Figure B20. Triaxial laboratory tests performed on UG2 chromitite material.**

**Table B3. Back-fit values for a power formula with equivalent exponents for w and h**

| Parameter | Value |
|---|---|
| K | 82 MPa |
| α (Effective width parameter) | 0.71 |
| β (Effective height parameter) | 0.71 |

$$\sigma_p = 82\left(\frac{w_e}{h_e}\right)^{0.71} \quad \text{(B3)}$$

A comparison between the original PlatMine formula, the linear formula and a power formula with equal exponents for width and height is provided in Table B4. Note the improved standard deviation coefficient for the latter analysis. However, the value for K' in (B3 appears to be a bit high, if it is considered to be the rock mass strength. The improvement of the standard deviation coefficient for the latter two evaluations over the original formula, suggests that the volumetric effect on strength provided by the original power formula may not be real.

**Table B4. Comparison between three formulae**

| Comment | Equation | S (Standard deviation coefficient) |
|---|---|---|
| Original PlatMine formula | $\sigma_p = 67 \frac{w_e^{0.67}}{h_e^{0.32}}$ | 0.0679 |
| Linear formula | $\sigma_p = 85 \left[\frac{1.58}{1 + (0.58 \times w/l)}\right] \left[0.43 + 0.57 \frac{w}{h_e}\right]$ | 0.0676 |
| Equal exponents for width and height | $\sigma_p = 82 \frac{w_e^{0.71}}{h_e^{0.71}}$ | 0.0671 |

Further analyses were conducted on databases where the slender pillars were removed and where the pillar heights of about 1.5 m were excluded. In both instances, the power formula was used, and the exponents were forced to be the same. Finally, the database was evaluated using the exponents suggested by Hedley & Grant (1972) and the analysis was only allowed to determine the K' value from the database. The results of the investigations are provided in Table B5.

**Table B5. Effects of removing data from the database**

| Comment | Equation | S (Standard deviation coefficient) |
|---|---|---|
| Slender pillars removed | $\sigma_p = 88 \frac{w_e^{0.63}}{h_e^{0.63}}$ | 0.0691 |
| The database consisting of pillars with h≈ 2.9 m | $\sigma_p = 88 \frac{w_e^{0.64}}{h_e^{0.64}}$ | 0.0724 |
| Exponents suggested by Hedley & Grant (1972) | $\sigma_p = 115 \frac{w_e^{0.5}}{h_e^{0.75}}$ | 0.0710 |

The results in Table B5 clearly show that the removal of data from the database did not improve the standard deviation coefficient (a larger value suggests a poorer fit). Similarly, the Hedley & Grant (1972) exponents show a poorer fit to the data in the database. The best fit for the data in the database, as shown in Table B3, are the results provided by (B3. In general, the results suggest a non-linear strengthening effect with w/h ratio, in agreement with the behaviour of the laboratory tests. The results of all the equations are plotted against w/h ratio for the range of data in the database in Figure B21. The analyses show that similar curves are shown by all the formulae within the boundaries of the database. Of note is the small difference between the original formula and (B3 (Equal α & β).

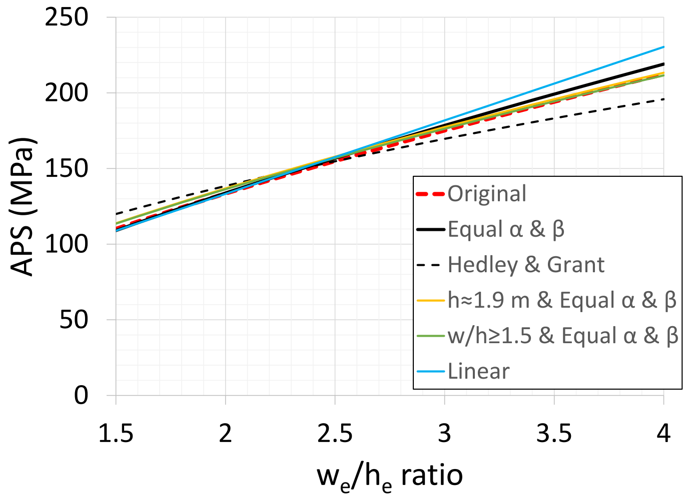


**Figure B21. Database analyses using various forms of the power and linear formulae**

### 10.5.2 Prediction Performance Metrics

Table B6 shows that both Scenario 1, which is rooted in the PlatMine formula, and Scenario 3, which is based on α = β, exhibit identical levels of accuracy, precision, and recall. In comparison to the other alternatives, these two models demonstrate superior performance. Precision is the most crucial metric in this report, as described in Section 2.2. Notably, for both scenarios, the models achieve a 97.8% precision rate when predicting a "Stable" pillar.

**Table B6: Prediction performance metrics for classifying between "Stable" and "Failed" pillars**

| Metric | Scenario 1 | Scenario 2 | Scenario 3 | Scenario 4 |
|---|---|---|---|---|
| | PlatMine | Hedley and Grant | α = β | Remove h = 1.5 m, α = β |
| Accuracy | 0.964 | 0.952 | 0.964 | 0.962 |
| Precision | 0.978 | 0.97 | 0.978 | 0.977 |
| Recall | 0.978 | 0.97 | 0.978 | 0.977 |

### 10.5.3 Confusion Matrix

Figure B22 provides a confusion matrix, showing the True Positives (TP), False Positives (FP), True Negatives (TN) and False Negatives (FN) found in the four scenarios:

- TP: When the model predicts the "Stability" of a pillar, and it is true.
- TN: When the model predicts a "Failed" pillar and it is true.
- FP (Type 1 Error): When the model predicts the "Stability" of a pillar, but it is false (i.e. the pillar has failed).

- **FN (Type 2 Error): When the model predicts a "Failed" pillar, but it is false (i.e. the pillar is stable)**

| | | Observed Values | |
|---|---|---|---|
| | | Positive (Stable) | Negative (Failed) |
| Predicted Values | Positive (Stable) | TP | FP |
| | Negative (Failed) | FN | TN |

| | |
|---|---|
| TP | True Positive |
| TN | True Negative |
| FP | False Positive |
| FN | False Negative |

**Scenario 1: PlatMine**

| | | Observed Values | |
|---|---|---|---|
| | | Positive (Stable) | Negative (Failed) |
| Predicted Values | Positive (Stable) | 30 | 3 |
| | Negative (Failed) | 3 | 131 |

**Scenario 3: α = β**

| | | Observed Values | |
|---|---|---|---|
| | | Positive (Stable) | Negative (Failed) |
| Predicted Values | Positive (Stable) | 30 | 3 |
| | Negative (Failed) | 3 | 131 |

**Scenario 2: Hedley and Grant**

| | | Observed Values | |
|---|---|---|---|
| | | Positive (Stable) | Negative (Failed) |
| Predicted Values | Positive (Stable) | 29 | 4 |
| | Negative (Failed) | 4 | 130 |

**Scenario 4: Remove h = 1.5 m, α = β**

| | | Observed Values | |
|---|---|---|---|
| | | Positive (Stable) | Negative (Failed) |
| Predicted Values | Positive (Stable) | 25 | 3 |
| | Negative (Failed) | 3 | 129 |

**Figure B22. Confusion matrix for classification between "Stable" and "Failed" pillars**

The performance matrices of Scenario 1 (based on the PlatMine formula) and Scenario 3 (based on α = β) show similar results in correctly classifying the pillars' stability and failure. Moreover, the models from both scenarios outperformed the alternatives. Out of 167 predictions, the pillars were classified accurately 161 times. However, it is concerning that there were instances where the pillars were classified as stable when they were not (i.e. false positives), which poses a risk to human lives due to the potential pillar designs based on false positives. This occurred 1.80% of the time when using models from scenarios 1 and 3. FP rates for scenario 4 (whereby h = 1.5 m is removed, α = β) and scenario 2 (based on Hedley and Grant's pillar strength exponent values) are 1.88% and 2.24%, respectively.

## 10.6 *Conclusions*

All the analyses of the PlatMine database for UG2 pillars (including the Prediction Performance Metrics) suggest that the most appropriate formula for the data in the database is provided in (B3. The results of the investigation suggest that the volumetric strengthening effect of pillars may not be true. In addition, it should be noted that the prediction of pillar strength by Equation 5 is not significantly different to the original PlatMine formula, within the range of w/h ratios in the database. One of the worst-performing formulae on the database was the Hedley & Grant (1972) formula with an altered K-value. It should be noted that there was a limited range of pillar heights in the database.

## 10.7 *References*

Bieniawski, Z.T. and Van Heerden, W.L. (1975). The significance of in situ tests on large rock specimens. Int. j. Rock Mech. Min. Sa'. & Georneeh. Abstr. .Vol. 12,pp. 101-113.

Esterhuizen, G.S. (2006). An evaluation of the strength of slender pillars, SME Annual Meeting, St. Louis, Missouri.

Hedley, D.G.F. and Grant, F. (1972). Stope pillar design for the Elliot Lake uranium mines. Bull. Can. Inst. Min. Metal., 65.

Lunder, P.J. (1994). Hard rock pillar strength estimation an applied approach. MSc thesis, University of British Columbia.

Maphosa, T.J. (2022). Optimum depth for the introduction of crush pillars at Impala platinum mine. MSc dissertation, School of Mining Engineering, University of Witwatersrand, Johannesburg, RSA.

Oates, T.E. and Malan, D.F. (2023). A study of UG2 pillar strength using a new pillar database. J. S. Afr. Inst. Min. Metall., vol. 123, no. 5. pp. 265–274

Oke, J. and Esterhuizen G.S. (2017). Improving Hard Rock Pillar Design by Including Rock Mass Classification and Failure Mechanisms. Proceedings of 51st US Rock Mechanics/Geomechanics Symposium held in San Francisco, California, USA.

Potvin, Y, Hudyma, M., and Miller, H.D.S. (1989). "Rib pillar design in open stoping," Can. Inst. Min. Metall. Bull. Vol. 82, pp. 31-36.

Roberts, D.P., Canbulat, I., and Ryder, J.A. (2002). Design parameters for mine pillars: strength of pillars adjacent to gullies; design of stable pillars with w/h ratio greater than 6; optimum depth for crush pillars. SIMRAC GAP617 Final Report. Safety in Mines Research Advisory Committee. Johannesburg.

Ryder, JA; Watson, BP & Kataka, MO. (2005). Pillar strength back-analyses. PlatMine 1.2, Johannesburg.

Salamon, MDG & Munro, AH. (1967). A study of the strength of coal pillars. JSAIMM, Vol.68.

Von Kimmelman, M.R., Hyde, B., and Madgwick, R.J., (1984), "The use of computer applications at BCL Limited in planning pillar extraction and the design of mining layouts," In Design and Performance of Underground Excavations, Int. Soc. Rock Mech. Symposium, Brown and Hudson, eds., Brit. Geotech. Soc., London, pp. 53-63.

Wagner, H. (1974). Determination of the complete load-deformation characteristics of coal pillars. Proceedings of 3rd International Congress on Rock Mechanics, ISRM, Denver, Vol. 2B, pp 1076-1082.

Watson, BP, Ryder, J A, Kataka, M O, Kuijpers, J S and Leteane, F P, (2008), Merensky pillar strength formulae based on back analysis of pillar failures at Impala Platinum, J. S. Afr. Inst. Min. Metall., vol 108, pp 449 – 461.

Watson, B.P., Lamos, R.A., and Roberts, D.P. (2021). PlatMine pillar strength formula for the UG2 Reef. Journal of the Southern African Institute of Mining and Metallurgy, vol.121, no. 8.

York G. and Canbulat I. (1998). The scale effect, critical rock mass strength and pillar system design, J. S. Afr. Inst. Min. Metall., pp 23 – 37.

Zipf, R.K., (2001). Toward pillar design to prevent collapse in room-and-pillar mines. 108th Annual Exhibit and Meeting, Society for Mining, Metallurgy and Exploration, Denver.